SINGLE-CELL SCREENING OF EXOSOME SECRETION IN BREAST CANCER

by
Mohsen Fathi

A thesis submitted to the William A. Brookshire Department of Chemical and Biomolecular Engineering,
Cullen Collage of Engineering
in partial fulfillment of the requirements for the degree of

DOCTOR OF PHILOSOPHY

in Chemical Engineering

Chair of Committee: Dr. Navin Varadarajan

Committee Member: Dr. Peter Vekilov

Committee Member: Dr. Richard C. Willson

Committee Member: Dr. Sendurai Mani

Committee Member: Dr. Katy Rezvani

University of Houston
December 2020

DEDICATION

This thesis is dedicated to my father, Professor Ghodratollah Fathi who was always the source of inspiration in my life. He was always dedicated to his family and his love was endless. A father who was committed to his research and never stopped his passion for the science until the last moment that he was fighting with cancer.

ACKNOWLEDGMENTS

I would like to gratefully acknowledge people without their effort this thesis would have not been successfully written. I wish to thank, first and foremost, my advisor, Dr. Navin Varadarajan whose guidance was so important during my Ph.D. program. He always encouraged me for a successful career and his tremendous supports was limitless.

I would like to thank Dr. Sendurai Mani for his valuable advice and supports during my Ph.D. career and for providing brilliant suggestions in the route of my research.

I would like to share the credit of my work with Dr. Peter Vekilov, Dr. Richard C. Willson, and Dr. Katy Rezvani for their constructive suggestions as a member of my Ph.D. committee during my qualifier, proposal, and defense.

I wish to thank Dr. Robiya Joseph for her amazing collaboration and help in performing the mice models.

I wish to express my sincere to Dr. Konrad Gabrusiewicz for introducing and guiding me in the field of exosome during my Ph.D. program.

I am indebted to my many colleagues, Dr. Jay R. T. Adolacion, Dr. Melisa Martinez-Paniagua, Dr. Xingyue An. Dr. Ankit Mahendra, Dr. Gabrielle Romain supported me in the training, performing experiments, and helping in the analysis.

Last but not least, to my dear family, Fariba and, Mehdi, my best friends, Rajat, Mehrdad, Mohammad, Alireza, and Ali, and all my friends at UH cycling club who made my Ph.D. wonderful with their spiritual and moral supports.

ABSTRACT

Exosomes mediate intercellular communication in health and disease. Conventional assays are limited in profiling exosomes secreted from large populations of cells and are unsuitable for studying the functional consequences of individual cells exhibiting varying propensity for exosome secretion. Here, we developed a high throughput single-cell technique that enabled the mapping of exosome secretion dynamics. By utilizing clinically relevant models of breast cancer, we established that non-metastatic cancer cells secrete more exosomes than metastatic cancer cells. We established isogenic clonal cell lines from non-metastatic cells with differing propensities for exosome secretion and showed that exosome secretion is an inheritable property preserved during cell division. Combined in vitro and in vivo studies with these cell lines suggested that exosome secretion can impede tumor formation. In human non-metastatic breast tumors, tumors with the higher secretion of exosomes have a better prognosis compared to tumors with the lower secretion of exosomes. As another application for our technique and to identify markers relevant to exosome secretion in metastatic cell lines, we profiled the cellular transcriptome of isogenic metastatic cell lines with varied exosome secretion rates established with our method. The genes identified with the highest expression and correlation in the high secretor clone were significantly associated with poor survival and low CD8 T cell infiltration in breast cancer patients. Our single-cell methodology can become an essential tool that enables the direct integration of exosome secretion with multiple cellular functions.

TABLE OF CONTENTS

LIST OF TABLES

LIST OF FIGURES

Chapter 1: Introduction

Extracellular vesicles (EVs) are lipid-bound vesicles secreted from most cell types and responsible for cellular communication in the extracellular spaces. Exosomes are one of the main subtypes of extracellular vesicles (EVs) that arise from the membrane of multivesicular bodies (MVBs) [1]. Exosomes, initially, were thought to be a cellular mechanism for the cells to get rid of unneeded materials, however, the improvement of technologies in characterizing the exosomes showed that exosomes contain bioactive molecules such as proteins, nucleic acids, and lipids which can regulate the cell-cell communication and cancer development [2,3]. Exosomes are found in bodily fluids such as blood and urine, and despite the invasive biopsy methods, the exosomes have shown outstanding application in clinical settings as carriers of biomarkers for cancer diagnosis and provide a non-invasive liquid biopsy method [4]. Exosomes can also act as an antigen-presenting vesicle and stimulate an immune response [5]. The unique characteristic of exosomes in providing a wide range of potential applications emphasizes the importance of exosome characterization and analysis.

1.1. Exosome biogenesis

Formation and release of exosomes consist of several biological pathways occurring inside the cells. The first step maturation of early endosomes which forms the multivesicular bodies (MVB). During the formation of MVB, its membrane goes under invagination and the intraluminal vesicles (ILVs) get formed, which would be called exosomes upon release to the extracellular environment. Two primary paths are known for the MVB, either its fusion with the plasma membrane

or fusion with the lysosome and autophagosome. The first leads to the release of ILVs or exosomes and the second one cause the degradation of MVB content and ILVs. Understanding the underlying pathways involved in the biogenesis might provide new options for therapeutic application. Following, I will describe the mechanisms have been discovered in different steps of exosomes release (Figure 1, reproduced from [6]).

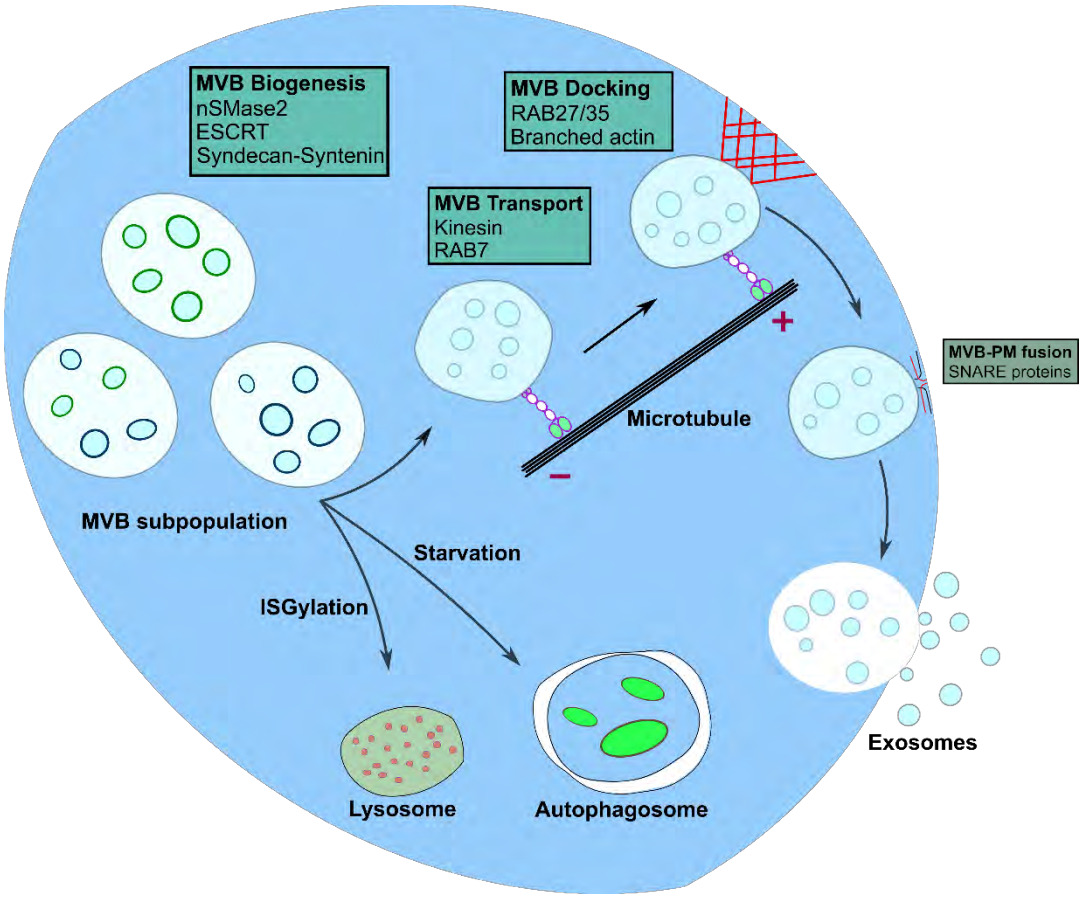

Figure 1. The pathways and process involved in formation and release of exosomes

1.1.1. Intraluminal vesicle formation and MVB maturation:

The invagination of late endosomes and forming the ILVs in the MVB is a critical step in the formation of exosomes. Several mechanisms have been identified in which the ESRCT is the most described pathway of MVB biogenesis. This process

is a membrane-scission machinery that is responsible for the sorting of ubiquitinated proteins into ILVs. It is initiated by ESCRT-0 which recognizes the ubiquitinated proteins on the surface of the late endosome. Then, a strong complex of cytoplasmic proteins and ESCRT-I/II and ESCRT-III forms. Later, the ESCRT-III mediates the membrane deformation and scission [7]. Several additional components are involved in this process such as ATPase VPS4 which regulates the membrane scission along with ESCRT-III. Also, Biaetti and et al., showed the key role of syndecan in ESCRT-mediated exosome formation. They showed that the syndecan is connected to the ESCRT-III associated protein ALIX mediated by adaptor protein syntenin.

Apart from ESCRT machinery, other mechanisms have been shown to regulates to the formation of ILVs. In 2008, Trajkovic and et al., showed that the ceramide, which is generated through sphingomyelin hydrolysis by neutral sphingomyelinase 2 (nSMase2) can induce a negative membrane curvature leading to the ILVs budding into MVBs [8]. Later, the Kajimoto and et al., showed the inhibitory G protein (Gi)- coupled sphingosine 1-phosphate (S1P) receptors can regulate the MVB maturation [9]. Moreover, the small GTPase ADP ribosylation factor 6 (ARF6) and its effector protein phospholipase D2 (PLD2) can control the syntenin-mediated CD63 ILV budding [10].

1.1.2. MVB trafficking and docking:

Once the MVB is formed, it can either fuse with the plasma membrane and secrete its exosomes or degrade its cargo by fusing with the lysosomes and autophagosomes. Although it has been shown that the balance between these two

processes is shifted towards the exosomal release, the mechanisms which derive the MVB fusion or MVB degradation are still unexplored [11]. In both cases, two steps are involved, the transport of MBV and later the fusion, however, the underlying effectors in these processes are distinct.

The intracellular transport of MVBs destined to the plasma membrane involves the molecular motors (dynein, kinesins, and myosins), the cytoskeleton (actin and microtubules), and molecular switches (small GTPases). It is shown that anterograde (towards microtubules positive ends) trafficking of MVB can be mediated by multiple kinesin isoforms [12], and RAB7 protein complexes [13]. Also, the mechanisms of trafficking MVBs to the plasma membrane can be cell type dependent. For example, activation of RAB35 mediates the MVB docking in oligodendroglia [14], while the RAB11 induces the release of exosomes in the K562 cell line [15]. On the other hand, despite the crucial role of RAB11 in K562, it appears to be replaceable in HeLa cells, and the silencing of RAB27A and RAB27B showed the highest impact in the reduction of exosome release. However, despite the effect of RAB27 isoforms in the secretion of exosomes from multiple cancer cell lines, they are not expressed in all cell type, which implies that each cell type may adopt its own secretory machinery for the secretion of exosomes [16,17].

Degradation of MVBs through fusion with lysosome or autophagosome can reduce the secretion of exosomes and several components are involved to mediate this process. Recently, it was shown that ISGylation of the ESCRT-I component TSG101 can promote the fusion of MVB with lysosomes and decrease

the secretion of exosome [18]. The impairment of lysosomal activity by inhibition of endosomal proton pump V-ATPase increased the secretion of exosomes [19]. Also, the fate of MVB can be regulated by the cellular conditions such as starvation which lead the fusion of MVB with autophagosomes. In this context, it has been shown that inhibition of autophagosome formation through interaction of prion protein (PrP) with caveolin can promote the secretion of exosomes [20]. Despite the direct effect of autophagy in secretion of exosomes, the underlying components are still unclear and can be dependent on the cellular conditions. For example, RAB11 which is shown to induce the transport of MVBs to the plasma membrane in K562 cell line, it can be colocalized with autophagosome marker LC3 and reduce the secretion of exosomes [15].

1.1.3. MVB fusion with plasma membrane:

At the final step, the MVB loaded with ILVs fuses with plasma membrane and release the exosomes to the extracellular matrix. Among the components involved in this exocytosis process, soluble N-ethylmaleimide-sensitive component attachment protein receptor (SNARE) proteins are the known complexes which localize to the intracellular membranes and mediate the fusion of MVB with the plasma membrane [21,22]. Several SNARE proteins such as SNAP23, Syntaxin-4, and VAMP7 have been shown to regulate the secretion of exosomes [23–25]. The formation of SNARE complex can be controlled by several regulators such as phosphorylation of SNARE proteins. For example, phosphorylation of SNAP23 at Ser95 and Ser110 showed increase in the exosome release [24,25]. There are

additional SNARE proteins such as YKT6, Syntaxin-1a, and Syntaxin-5 which modulate the exosome secretion in different cell types and organisms [26–28].

1.2. Exosome in cancer development

Exosomes as one of the mechanisms in the intracellular communication can regulate the development of cancer in various stages. The content of exosomes such as mRNA, miRNA, DNA, and proteins can affect the function of recipient cells. This signaling pathway can be autocrine or paracrine. The autocrine pathways will change the fate of exosome-releasing cells themselves and mediate the survival and growth of the cells. For example, the leukemia cells secrete exosomes containing TGFβ1 which can promote the tumor growth by binding to TGFβ1 receptor on the leukemia cells and activate the ERK, AKT, and anti-apoptotic pathways in the producer cells [29]. Also, Exosomes showed to contain the double-stranded DNA which their accumulation in the cells could cause the cell cycle arrest and apoptosis in the cells. Thus, the secretion of exosomes inhibited the accumulation of harmful cytoplasmic DNA and supported the cell survival [30] (Figure 2, reproduced from [31]).

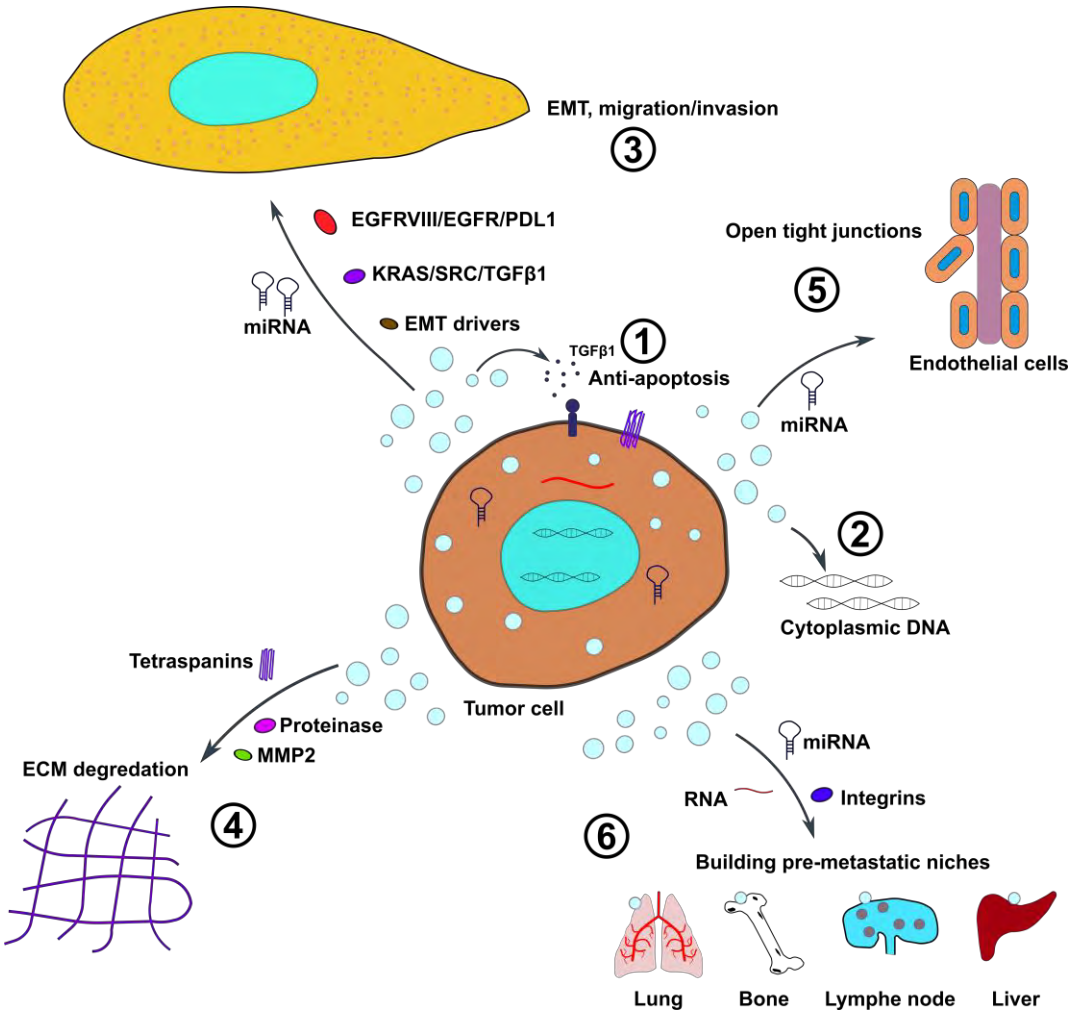

Figure 2. Function of tumor derived exosomes in cancer development by (1) apoptosis inhibition, (2) cytoplasmic DNA removal, (3) EMT induction, (4) ECM degradation, (5) endothelial modulation, (6) pre-metastatic niche preparation.

The paracrine pathways induced by exosomes can regulate the neighboring cells in the tumor microenvironment and modulate the intercellular communication. This can be mediated by transfer of the exosome cargo to the recipient cells, changing the miRNA and RNA expression, activating receptors, and finally altering their biological phenotypes. For example, transfer of EGFRvIII to cells lacking this receptor can activate AKT pathway and enhance the cell growth [32]. In addition, the exosomes of breast cancer cells can transfer PD-L1 to the cells with low level

of this protein and, thus promote the immune rejection [33]. Also, the colon cancer with wild-type KRAS can receive the mutant KRAS from exosomes secreted by other neighboring cells which lead them to an invasive phenotype [34].

1.3. Exosome in metastatic

Metastatic is circulation and spread of primary tumor to the other organs and several steps are involved in this process. First, the primary tumor starts the circulation via the blood vessel or the lymphatic system in a process called intravasation. Once circulated, they cancer cells should survive and exit the circulation (extravasation) to enter the distant organ. The exosomes can regulate this process at different steps.

1.3.1. Exosomes in cancer cell migration and invasion

Exosomes secreted by cancer cells can regulate the extracellular matrix (ECM) and promote the invasion and metastasis. For example, the exosomes secreted by breast cancer cells highly expressed in RAB27B contained activated matrix metallopeptidase 2 (MMP2) which degrades the ECM [35]. The CD151/TSPAN8-expressing exosomes secreted by rat pancreatic adenocarcinoma cell line (ASML) modify the ECM by degrading collagen and fibronectin through integrins and proteases [36]. Epithelial-mesenchymal transition (EMT) is another essential step in the tumor invasion which can be promoted by exosomes. Exosomes can deliver many EMT factors such as casein kinase II α (CKIIA), annexin A2, HIF1α, matrix metalloproteinase 13 (MMP13), and latent membrane protein 1 (LMP1) to contribute in the metastasis of tumor cells [37–40]. Also, exosomes can enhance the tumor cell intravasation by unlocking the tight junctions. The exosomes

secreted by breast cancer cells expressing miR-105 reduced the ZO1 expression in endothelial cells and broke up the tight junctions between endothelial cells [41]. Lastly, the exosomes showed to contain anti-metastasis factors such as miR-23b which its low expression due to loading in the exosomes promoted the metastasis [42].

1.3.2. Exosomes in pre-metastatic niches

Preparing the metastatic site for accepting the tumor cells and providing a suitable environment for their growth is an essential step in metastasis. The exosomes have been shown to manipulate the metastatic site and assist in tumor growth. For example, the pancreatic-derived exosomes downregulated cadherin-17 and increased proteases and adhesion molecules to prepare the pre-metastatic niche for entrance of tumor cells [43]. Also, the exosomes secreted by melanoma cells prepared lymph nodes for tumor metastasis by modulating ECM deposition and vascular proliferation [44]. Exosomes showed to predetermine the metastasis organ in breast cancer cells as the high expression of integrins $\alpha_6\beta_4$ and $\alpha_6\beta_1$ in exosomes primed for lung metastasis, while the high expression of integrin $\alpha_v\beta_5$ in exosomes primed for liver metastasis [45]. Also, the Exosomes containing snRNAs derived from lung cancer cells prepared the lung pre-metastatic niche by recruiting neutrophils into lung through activating TLR3 and release of cytokines [46].

Alternatively, exosomes from poorly metastatic cells showed to lack the capability to promote the metastasis. For example, the exosomes secreted by non-metastatic melanoma cells induced an immune response in the bone marrow. These exosomes expressed pigment epithelium-derived factor (PEDF) on their

surface and induced the recruiting the monocytes, natural killers, and macrophages in the pre-metastatic niche [47]. Also, the lung cancer cell derived exosomes containing miR-192 inhibited the interleukin 8 (IL8), intercellular adhesion molecules, and CXCL1 in the endothelial precursor cells of the bone microenvironment and prevent the successful angiogenesis and colonization [48].

1.4. Exosome isolation and characterization

Exosomes are small vesicles and their visualization is not feasible with traditional microscopy techniques. Also, Exosomes are specific subtype of vesicles ranging from 50-150 nm in diameter and distinguishing them from the other vesicle subtypes is challenging. This includes the purification and characterization of the exosomes. Therefore, in the last few decades, many researchers have tried to overcome this challenge and develop novel techniques which can target, specifically, the exosomes and not the other vesicles. These techniques include the isolation of exosomes such as ultracentrifugation, density-gradient centrifugation, immunoaffinity-based assays, and microfluidics devices. Also, several methods have been developed to characterize and validate the exosomes including the nanoparticle tracking analysis (NTA), and transmission electron microscopy (TEM).

1.4.1. Ultracentrifugation

Ultracentrifugation was the first method offered for isolation of exosomes and yet it is the most preferred method among researchers [49,50]. The method depends on the density and size of particles and several centrifugation steps are involved to increase the purity of exosomes (Figure 3). Initially, the cellular debris

and large particles are removed by a slow speed of 500xg. Then a 0.22 μm filter is used to remove the remaining large particles or EVs and apoptotic bodies. Finally, by two steps of high-speed centrifugation up to 100,000xg the exosomes can be isolated. Although the longer time during centrifugation can increase the yield, it can mechanically damage the exosomes and increase the soluble protein contamination in the final preparation [51,52]. Also, this method is not suitable for complete separation of exosomes from other components in extracellular spaces [1]. In addition, the method is very time consuming and can only work with large samples (100s of mLs) which makes it inapplicable for processing small clinical samples in a short amount of time [1]. However, no pretreatment is required for this method and a little technical expertise is sufficient for isolation of exosomes [53].

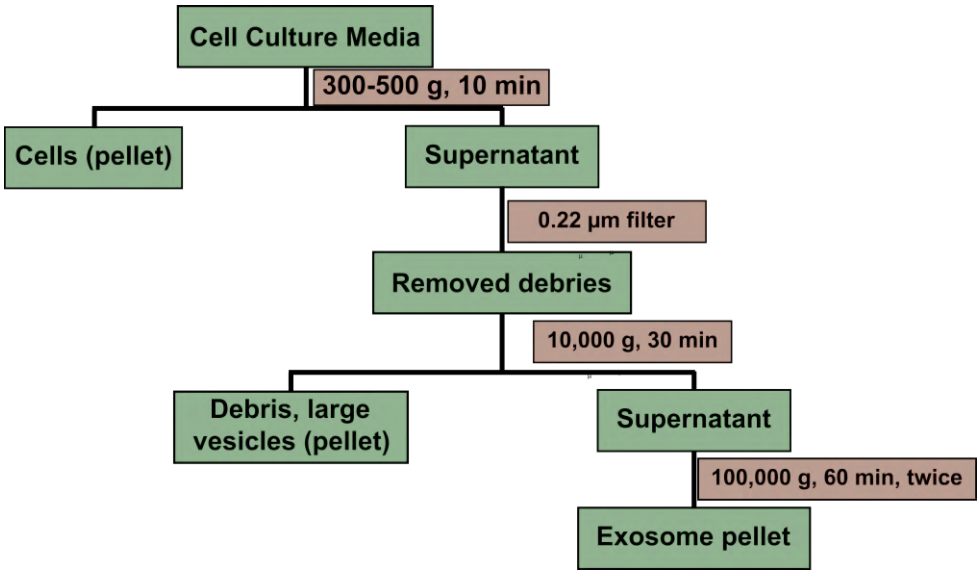

Figure 3. Workflow of exosome isolation by ultracentrifugation

1.4.2. Density gradient centrifugation

Density gradient centrifugation is another ultracentrifugation technique that similar to ultracentrifugation separates the particle by their size and density.

However, the separation occurs in the presence of a preconstructed density gradient, typically made of iodoxinol and sucrose [53,54]. First, the sample is placed at the top of the gradient and due to the centrifugation, the sample passes through the high-to-low density gradient medium. Then, the exosomes can be collected based on their density which is in the range of 1.1-1.2 g/mL. Even though the density gradient is effective in separating exosomes from other EVs, similar to ultracentrifugation, it has a very low exosome recovery [55,56].

1.4.3. Immunoaffinity based techniques

This method relies on the surface marker present on the surface of exosomes. It applies antibodies targeting the antigens on the surface of exosomes to capture them. The antibodies can be attached to a plate (ex. ELISA), or magnetic beads, resins, and microfluidic devices. Since the isolation is based on the antigen on the surface of exosomes, it allows the capture of exosomes derived from a specific source [57,58]. For example, the in hepatocyte derived exosomes express the Asialoglycoprotein receptor 1 (ASGR1) which can be targeted to isolate the liver derived exosomes [59]. Also, targeting specific markers for exosomes enables the separation of exosomes from other types of EVs [52]. However, the technique is limited to the antigen and lack of its expression disables the capture of exosomes. Besides, depends on the antibody, only specific exosomes can be collected. Unsimilar to ultracentrifugation, the immunoaffinity based assays results in higher purity and lower yield [60]. Despite the high purity in isolation of exosomes, this technique is often used exosomal enrichment by ultracentrifugation technique [57]. ELISA is one of the immunoaffinity based assays in which the antibodies are

immobilized on the surface of a plate. Exposing the exosome sample to the wells containing immobilized antibodies results in antibody-antigen interaction and capture of exosomes in the well. Later, the un-captured exosomes are washed away and using a detection antibody the exosomes can be tagged. ELISA has been used for testing the patient's blood for antibodies against different infections such as HIV, and Lyme disease [61], however, due to the time-consuming ultracentrifugation steps before exosome capture, it is not yet applicable in clinical settings.

1.4.4. Microfluidic devices

The conventional methods for exosome isolation face many challenges in the clinical settings, therefore, new techniques are required to provide the high-purity exosomes from small clinical samples. The use of microfluidic devices in the isolation, detection and analysis of exosomes have become important since these devices can detect exosomes based on their physical and biochemical properties. Beside applying the common properties of exosomes such as size, density and immunoaffinity, novel mechanisms have been used in microfluidic devices to detect the exosomes such as acoustic, electrophoretic, and electromagnetic properties of the exosomes [62,63]. The immune-based microfluidic devices are very similar to ELISA. The antibodies are immobilized on a microfluidic chip and the interaction of these antibodies with the surface proteins of exosomes enables their collection. The advantage of microfluidic devices over ELISA is isolation of exosomes from small amount of serum in short time in compare to ELISA which requires pre-enrichment of exosomes from serum [64,65]. However, similar to

ELISA, the assay is limited by the specific antibodies. Several microfluidic devices are commercially available such as ExoChip which uses the anti-CD63 antibody to capture exosomes expressing CD63 since CD63 is found to be in exosomes from many cell types [66]. Since the microfluidic devices require small amount of sample, their development has been very applicable in clinical setting for bringing the diagnostic, therapeutic, and prognosis applications (Figure 4, reproduced from [67]).

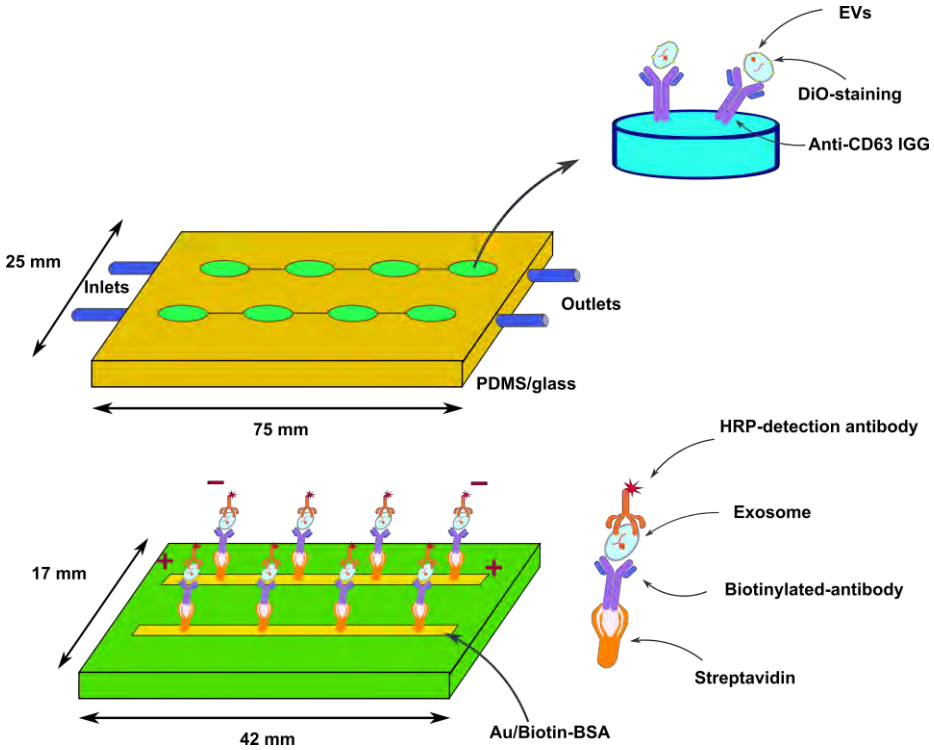

Figure 4. The schematic of ExoChip method operation for capturing and analyzing exosomes

1.4.5. Nanoparticle Tracking Analysis (NTA)

The evaluation of exosomes isolated by conventional technique is essential to determine the biological interactions of isolated exosomes. The characterization can be done based on the physicochemical properties of exosomes such as size, shape, surface charge, density, and porosity. Nanoparticle tracking analysis is one

of the techniques that allow the measurement of size distribution and concentration from the isolated exosomes (Figure 5, reproduced without modification from [68]). The technique follows the Stoke-Einstein equation, where the diffusion coefficient is based on the Brownian motion of particles [68]. In NTA , a laser light is scattered upon interaction with particles which can be collected by a microscope equipped with a camera and allows the tracking of the particles. By tracking the movement of each particle and measuring its velocity, the particle size is estimated and collected for all the particles. NTA allows the measurement of particle in the range of 10 nm to 1000 nm in diameter, which is in the range of exosome size [69]. The advantage of NTA is the easy sample preparation which makes it suitable for measuring the exosome size and concentration in few minutes. Also, it can be applied by fluorescently labeled antibodies to detect the presence of antigens on exosomes [68]. The NTA includes challenges such as correction of dilution factor, optimization of data collection and analysis parameters [70].

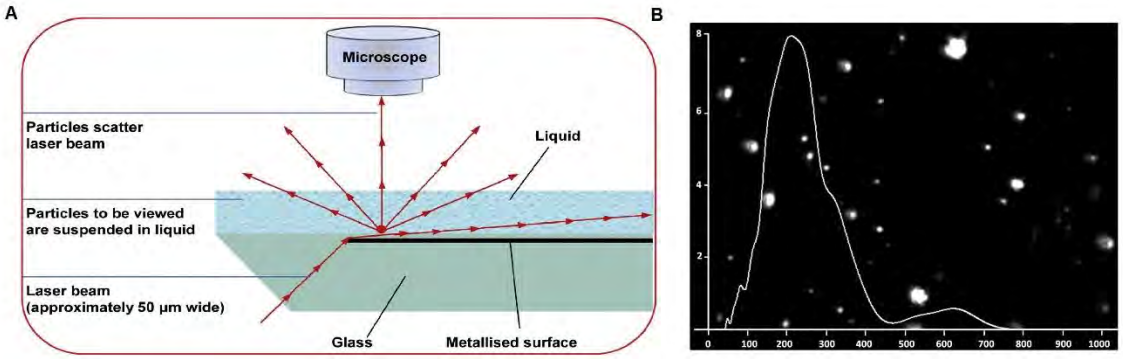

Figure 5. (A) Nanoparticle Tracking Analysis (NTA) instrument configuration. (B) Screenshot of video and size distribution of particles analyzed by NTA.

1.4.6. Transmission Electron Microscopy (TEM)

TEM is a widely used technique for characterization of the structure, morphology, and size of biological components such as exosomes. The technique

presents the image created by electron beams passing through the sample, where the scattered electrons are detected. TEM along with scanning electron microscopy (SEM) are both used to assess the morphology of exosomes, where in SEM, electrons are scattered when they interact with the particles, while in TEM, the electrons that do not interact with the particles are detected [71]. There two types of electron microscopy which are widely used for biological samples, TEM and cryo-electron microscopy (cryo-EM). The cryo-EM is applied on the samples under the liquid nitrogen and keep the morphology of particles intact. However, the TEM requires extensive sample preparation involving multiple steps such as glutaraldehyde fixation which can change the morphology of exosomes. For example, exosomes imaged by TEM showed a cup-shaped morphology, while the frozen exosomes analyzed by cryo-EM showed a round shape morphology [3]. Cryo-EM is also considered the best method for visualizing the nanoparticles and proteins and suitable for capturing images of exosomes. Tracing the proteins inside the exosomes is an important aspect of their biological function. Generally, the fluorescent dyes are used to visualize the proteins, however, depending on the size and shape of exosomes , creation of an exaggerated fluorescence signals disable distinguishing the exosomal proteins [1]. Therefore, an alternative method such as immunogold EM can be applicable to determines the function of specific proteins in exosomes.

1.5. Dynamic screening of exosome

The studies into secretion of exosomes and its mechanisms show that it is a tightly controlled process and multiple factors can modulate it (Section 1.2). The

secretion rate varies according to the cellular origin, the extracellular environment [72], the cell age [73], and metabolic status [74]. It is, also, likely that the release of exosomes is a dynamic process in which cells in response to internal and external stimuli adjust the secretion of various exosome subpopulations. Thus, the exosomes contain a heterogenous population in size, content, and functional impact. Different steps in exosome formation such as the invagination of membrane can induce the differences in size [6,75]. This wide range of size distribution results in different amount of exosomal content. For example, it was shown that for a given miRNA cargo, not all the exosomes had a similar abundance of the cargo [76]. Also, the inherent biology of cells and external factors can influence the content of exosomes and its biological function. This implies that subpopulations of exosomes can results in different biological outcomes such as induction of cell survival, or apoptosis, or immuno-modulation. The heterogeneity can also depend on the tissue source of release whether it is from cancerous tissue or normal tissue. Altogether, these factors result in a complex heterogeneity in the exosomes population (Figure 6, reproduced without modification from [77]).

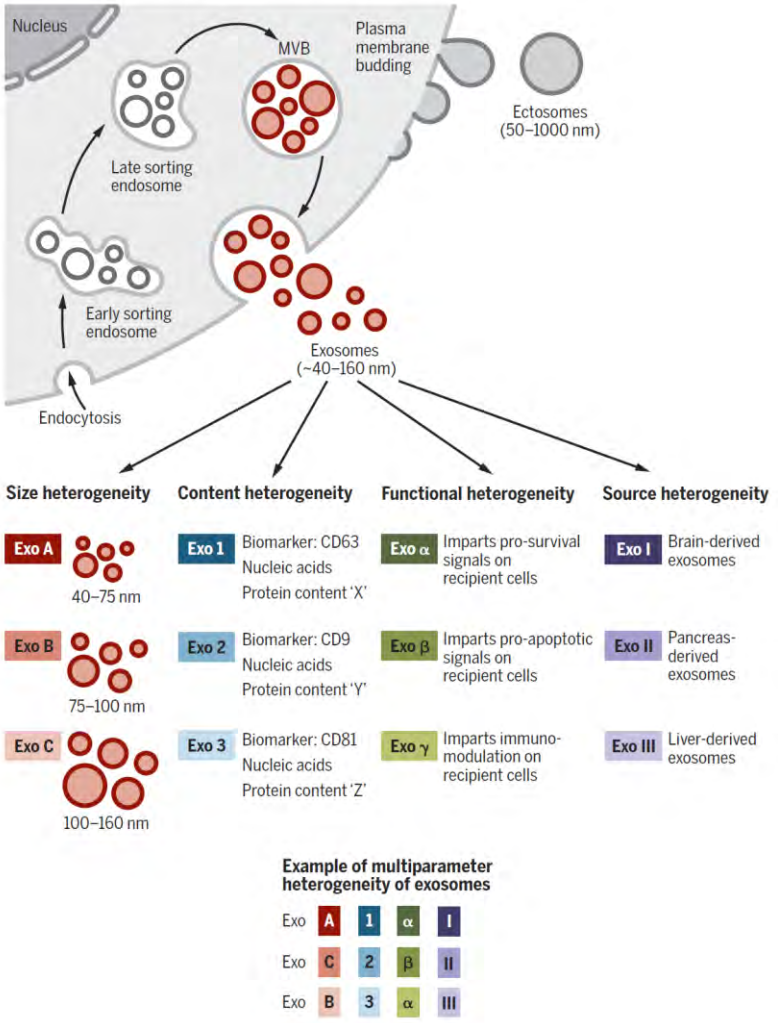

Figure 6. The complex heterogeneity of exosomes derived from differences in size, content, function, and source of release.

The biological function of exosomes which is reflected in their content can be mapped to their cell of origin. For example, the proteomic analysis of breast cancer cells and their exosomes can predict if the cell of origin is an epithelial like or mesenchymal like cell [78]. However, since the current studies on the exosomes is performed on a large pool of exosomes, these conventional methods fail to map these connections. Recently, the development of novel reporter allowed the real time monitoring of steps involved in secretion of exosomes [79]. Verweji and et al., showed that using a tetraspanin-based pH-sensitive reporter the fusion of MVB

with the plasma membrane can be monitored in the single cell level (Figure 7, reproduced without modification from [79]). Applying these novel reporters can further provide information on the dynamic secretion of exosomes and various steps.

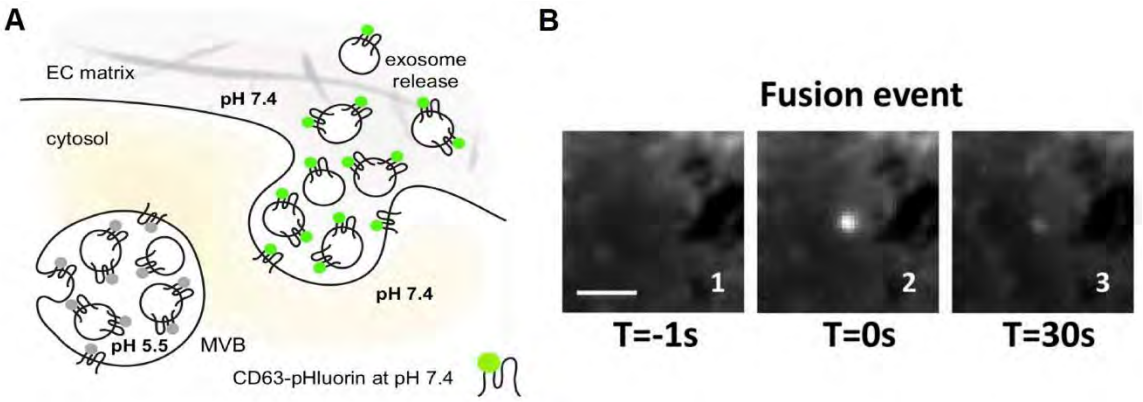

Figure 7. Real-time tracking of MVB-plasma membrane fusion. (A) the proposal model using reporter which scatter fluorescent signal upon change of pH. (B) real-time tracking of reporter (1) before, (2) during fusion, and (3) after fusion.

Despite the development of technologies in the exosome field, the direct connection of exosomes to the single cell is yet challenging and under development. A few microfluidic devices have been developed in which they showed the heterogeneity of exosomes secreted from single cells. Chiu and et al., applied an immunoaffinity-based method to screen the secretion of exosomes from single cells in a high-throughput manner. Their results showed that exosomes are heterogenous in expression of surface markers and single cells can secrete different number of exosomes depending on the targeted antibody [80]. Also, Son and et al., applied a microfluidic device to monitor the real time secretion of exosomes from single cell [81]. However, these techniques fail to map the

biological function of exosomes secreted form single cells to their cell of origin (Figure 8, reproduced without modification from [80,81]).

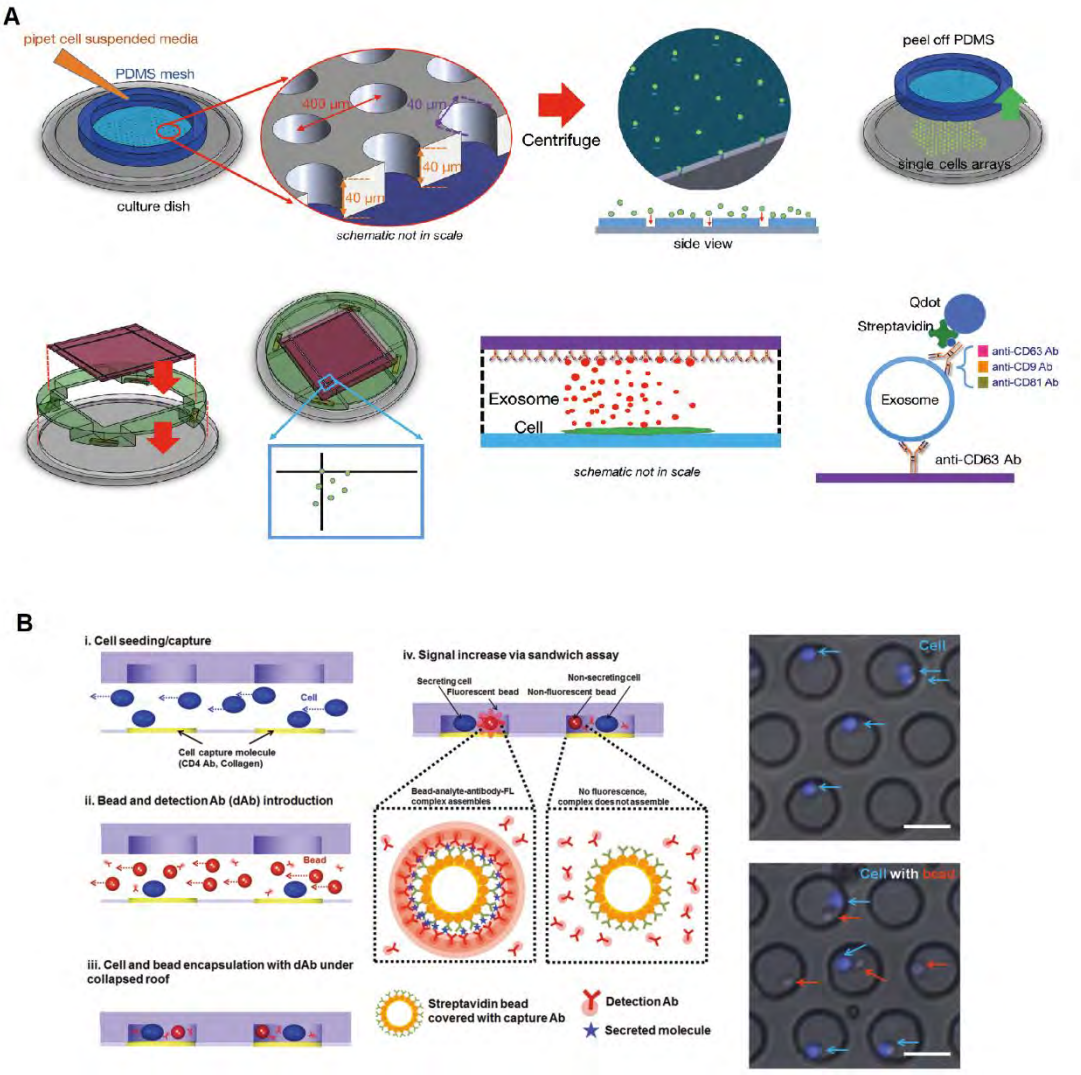

Figure 8. Immunoaffinity-based microfluidic devices for real time monitoring of exosome secretion from single cells designed by (A) Chiu et al, and (B) Son et al.

In my Ph.D. work, I aimed to overcome the challenges in mapping the direct correlation of exosome secretion and its biological function. First, using an immunoaffinity-based technique and applying that on a microfluidic device, I was able to develop a high-throughput technique which can monitor and quantify the

differences in the secretion rate between single cells. Later, applying a micromanipulator device, I retrieved selected single cells which showed diversity in the secretion rate. Finally, I utilized this technique to address the function of heterogenous exosomes in different steps of cancer development.

My Ph.D. research showed that the secretion of exosomes can impact the tumor microenvironment differently in breast cancers depending on the metastatic stage of the cells. The increase in the secretion of exosomes induced an immune response in primary tumor cells which was shown by a decrease in the tumor growth. As another application of the developed technique, I was able to profile the cell lines with different capacity in secretion of exosomes using single-cell RNA sequencing. The results showed that cell profiling can be helpful in discovery of new biomarkers involved in secretion of exosomes. Altogether, I developed a technique in my Ph.D. which can be applicable in directing the function of exosomes secreted by single cells to their biological functions.

Chapter 2: Functional single-cell profiling identifies that exosomes are associated with increased immune cell infiltration in non-metastatic breast cancer

2.1. Introduction

Exosomes, a subset of extracellular vesicles (EV), comprise a fundamental mechanism of intercellular communication across distant cells and serve to transport biological molecules such as lipid, nucleic acids, and proteins. Encapsulation of molecules into exosomes fundamentally alters their stability, transport, and trafficking, and characterizing the secretion of exosomal cargo from cells is of great interest in fundamental cell biology and for targeted drug delivery [3,11,77,82–84].

In the context of cancer, exosomes are known to affect a variety of biological events that promote tumor progression such as angiogenesis [85,86], invasion [87], evasion of immune surveillance [88,89], and drug resistance [90]. Exosomes from highly metastatic melanoma tumors promoted vascular permeability and contributed to the formation of the pre-metastatic niche [91]. Also, exosomes can transfer antigens and enhance the immune response by activating T cells and NK cells [5,92]. Due to their stability, they have great potential in cancer diagnosis [93,94] and treatment [95]. Mapping the dynamic secretion of exosomes at the cellular level can significantly advance our understanding of the role of exosomes in cancer.

From an analytical standpoint, the size of exosomes (40-150 nm) is in between the size of proteins and cells. A number of analytical methods including nanoparticle tracking analysis (NTA) [96], electron microscopy [97], flow cytometry

[97,98], microfluidic devices [99], and western blotting [100] have been widely used for characterization of exosomes, some even with the sensitivity of detecting individual exosomes. Unfortunately, however, these exosomes are derived from culturing billions of cancer cells and thus represent an averaging of exosomes secreted by all cells. From the standpoint of disease biology, this is suboptimal since these might reflect supra-physiological concentrations of these exosomes. Second, since tumors are heterogeneous populations, these approaches mask the inherent differences in exosome secretion between individual cells and mapping the direct relationship between exosome secretion and tumorigenic potential is not feasible. Not surprisingly, recent advances in microfabrication have revealed that the rate of exosome secretion from single cells can be very different [79–81]. Despite this progress, however, technological hurdles have prevented us from answering a number questions at the single-cell level including (1) heterogeneity of the short-term dynamics of secretion of exosomes, (2) whether exosome secretion is an inheritable property preserved upon cell division, and (3) whether there is a difference in tumorigenic potential between isogenic tumor cells with differences in the rate of exosome secretion.

Here we report a high-throughput single-cell technique for the dynamic quantification of exosome secretion from single cells. We utilized the 4T1 and 67NR syngeneic mouse mammary tumor models since these are well-validated, clinically relevant models with vastly different potential for metastasis. 4T1 spontaneously metastasizes to multiple sites, whereas 67NR is incapable of metastases and is restricted to the formation of the primary tumor [101]. By

tracking the dynamics of exosome secretion, we demonstrate that in both cell lines, the dominant secretor cells are capable of continuous secretion over short time intervals (6-24 hours). Surprisingly, the non-metastatic 67NR cells secreted more exosomes per cell than 4T1 cells, and this result was consistent with scRNA-seq of the same cells, showing an enrichment of the ALIX-Syndecan-Sytenin pathway. Although the secretion of exosomes from highly secreting 67NR clones caused an increase in proliferation and migration in vitro, the tumor growth was inhibited in vivo. Analysis of The Cancer Genome Atlas (TCGA) data illustrated that the secretion of exosomes is associated with better overall survival of non-metastatic patients, which was induced by higher secretion of IFN-γ, higher infiltration of Th1 cells, the polarization of M1 macrophages, and suppression of the IL6ST/STAT3 pathway. More broadly, the exosome secretion signatures are associated with better prognosis in non-metastatic melanoma but worse prognosis in non-metastatic lung cancers.

2.2. Material and Methods

2.2.1. Cell culture

4T1 and 67NR cells were purchased from ATCC. We cultured cells in RPMI 1640 supplemented with 10% FBS, 1% L-glutamine, HEPES, and penicillin-streptomycin. We cultured GSC20 cells in 50/50 mixture of Dulbecco's Modified Eagle's Medium (DMEM) and Ham's F-12 medium supplemented with 1% penicillin-streptomycin, B-27 supplement, and epidermal growth factor. We tested all cells for mycoplasma contamination using real-time PCR.

2.2.2. Exosome isolation and measurement

We used ultracentrifugation to isolate exosomes from GSC20 stem cells. Starting with 250 ml of culture media, we centrifuged the conditioned media at 300 × g for 4 minutes, filtered with 0.22 μm filters, and centrifuged at 10,000 × g for 30 minutes followed by ultracentrifugation at 100,000 × g for 70 minutes to pellet the exosomes. We washed the exosome pellet with PBS twice and centrifuged for another 100,000 × g for 70 minutes to purify the exosomes. We resuspended the exosomes in PBS and measured the exosome size distribution using the nanoparticle tracking analyzer (NTA). We stored the isolated exosomes at 4°C for one week or at -80°C for long term use.

2.2.3. Bulk exosome detection assay

We performed immunoassays utilizing LumAvidin beads (Luminex, catalog number L100-L115-01) to capture exosomes with different protein markers. First, we centrifuged 10^5 beads and resuspended in PBS with 1% BSA. We next incubated them with 3.5 μg/ml biotinylated CD81 or CD63 antibody (BioLegend, clone 5A6, and H5C6) for 30 minutes at room temperature, and washed them twice in PBS with 1% BSA. We added the exosomes at a 10^9 particle/ml concentration and mixed on a rotator for 2 hours at room temperature, followed by washing in PBS with 1% BSA twice. We mixed the beads with 4 μg/ml PE anti-CD63 antibody (BioLegend, clone H5C6) and rotated for 45 minutes at room temperature. Finally, after two washes, we resuspended the pellet in PBS with 1% BSA and imaged using A1/TiE inverted confocal microscope (Nikon) equipped with 20x/0.75 NA objective. We measured the fluorescent intensity of CD63 on the beads using ImageJ.

2.2.4. Functionalization of beads with anti-CD81 coating

We washed 10^5 LumAvidin beads (Luminex, catalog number L100-L115-01) in PBS with 1% BSA and incubated the beads with 3.5 µg/ml biotinylated anti-CD81 antibody (BioLegend, clone Eat-2) at the room temperature for 40 minutes. Then, after washing beads thrice in PBS with 1% BSA, we resuspended them in 120 µl of PBS with 1% BSA.

2.2.5. Exosome quantification using transwell assay

We utilized a Transwell insert with 3 µm pore membrane and loaded functionalized beads at the lower compartment, and cells on the upper compartment of the insert. For the GW4869 treatment assay, we used exosome-free complete media containing either 10 µM GW4869 or 10% DMSO. After 48 hours of incubation at 37°C, we collected the beads and labeled them with 4 µg/ml PE anti-CD63 antibody (BioLegend, clone NVG-2) for 45 minutes at 37°C. We subsequently washed the beads three times in PBS with 1% BSA and performed imaging using a Zeiss Axio Observer Z1 microscope equipped with 20x/0.8 NA objectives. Using ImageJ, we segmented and measured the fluorescent intensity of CD63 on the beads.

2.2.6. Transmission Electron Microscopy (TEM)

Via exosome quantification using a transwell assay, and after 48 hours incubation at 37°C, we collected the beads and fixed with 2% glutaraldehyde (Ladd research, catalog number 20215). We placed the samples on 100-mesh carbon-coated, formvar-coated copper grids treated with poly-L-lysine for approximately 1 hour. We then negatively stained the samples with Millipore-filtered aqueous 1% uranyl acetate for 1 minute. The stain was blotted dry from the grids with filter

paper, and samples were allowed to dry. We examined the samples in a JEM 1010 transmission electron microscope (JEOL, USA, Inc., Peabody, MA) at an accelerating voltage of 80 kV. We obtained the digital images were using the AMT Imaging System (Advanced Microscopy Techniques Corp., Danvers, MA).

2.2.7. PDMS nanowell array fabrication and preparation

Applying standard soft lithography techniques, we fabricated the PDMS nanowell array as previously described [102]. Before loading cells on the nanowell, we re-oxidized the array with air plasma and incubated with 1.5 ml PLL-g-PEG (SuSoS, Switzerland) solution dissolved in 10 mM HEPES buffer for 20 minutes at 37°C. After incubation, we rinsed the array with complete media before loading the cells.

2.2.8. Single-cell exosome detection assay

To perform the single-cell assay for the detection of exosomes, we prepared the nanowell array and functionalized beads, as described above. We labeled 67NR or 4T1 cells with PKH67 dye (Sigma-Aldrich, catalog number PKH67GL-1KT) as directed by the manufacturer. We loaded labeled cells and functionalized beads, sequentially on the nanowell array. We covered the nanowell with exosome-free complete media and imaged at its initial time point, incubating at 37°C. Every two hours, we incubated the nanowell array with 4 μg/ml PE anti-CD63 antibody (BioLegend, clone NVG-2) for 45 minutes at 37°C. We subsequently washed the nanowell array three times in PBS with 1% BSA and performed imaging using microscopy. After each imaging, we returned the nanowell to the incubator at 37°C.

We acquired all images by Zeiss Axio Observer Z1 microscope equipped with 20x/0.8 NA objectives and a Hamamatsu Orca Flash v2 camera.

2.2.9. Secretion analysis of single-cell exosome detection assay

We analyzed the TIFF images from microscopy, as outlined in Figure 9. Briefly, (1) TIFF images of 256 field of views (blocks) containing 36 wells were extracted and merged for the initial time point (0 hour) and the detection time points (2, 4, 6 hours). Block 100 is shown as an example for workflow. (2) The numbers of beads and cells in each well were identified for each block at all the time points. (3) Wells with a single bead and a single cell were identified. (4) The wells which didn't maintained bead:cell = 1:1 ratio in the entire experiment were excluded from the further analysis. (5) The CD63 pixel values on the surface of cell and bead were collected. These values were corrected using background subtractions. To calculate background intensity, average of CD63 pixel values not localized on the beads and cells in the entire block was calculated. Well 1000506 is shown as an example for workflow. (6) The overlap pixels between bead and cell were removed from pixel value sets of cell. This created an annulus shape for the pixels on the surface of cell. (7) Two-tailed t-test was applied on two set of pixel values, on bead and on the cell annulus, to identify the secretor cells in which the CD63 intensity for beads was significantly ($p < 0.01$) higher than cell annulus intensity.

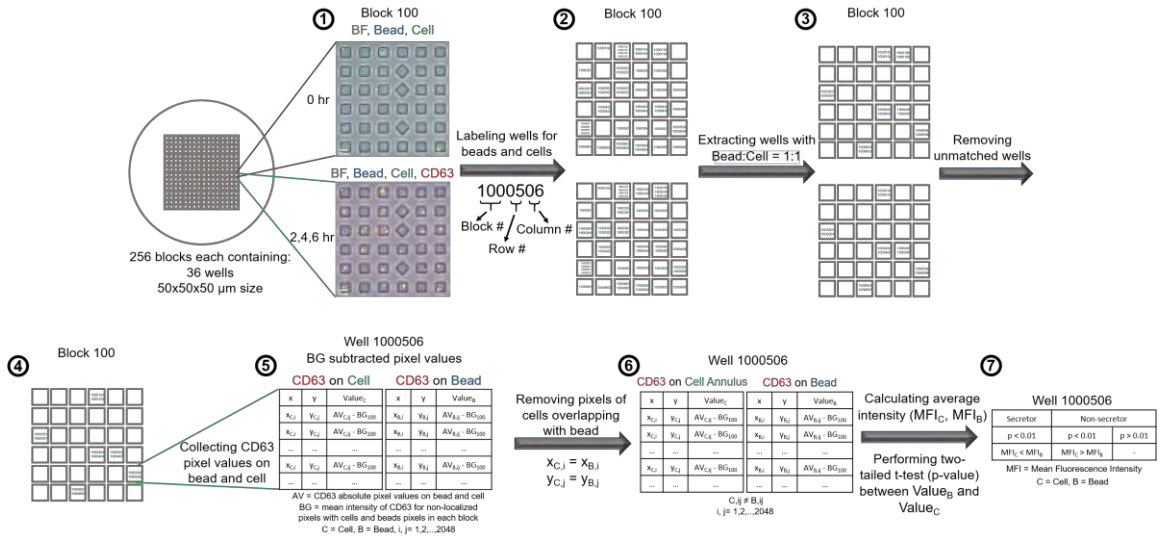

Figure 9. Overall workflow of the automate image-analysis for identification of secretor and non-secretor cells

2.2.10. Kinetic analysis of single-cell exosome detection assay

Using the wells containing a single bead and a single cell identified in the secretion analysis of single-cell exosome detection assay, we selected the wells which were detected in all the time points for the kinetic analysis. To determine the behavior of the cells between time points, we performed a two-tailed t-test on the CD63 pixel values of the bead between two consecutive time points. We chose an increase in intensity with a p-value below 0.01 as the criterion for a significant change in the secretion behavior of the cell.

2.2.11. Establishment of clonal cell lines.

We retrieved the secretor and non-secretor single cells using a micromanipulator (ALS, CellCelector) equipped with 50 µm glass capillaries. We transferred single cells to a 96-well plate containing complete media. We monitored the single cells and cultured them in complete media until they proliferated to 24 population doublings.

2.2.12. Wound healing assay

We cultured 67NR-S and 67NR-NS cells in a 12-well plate to 90% confluency with 10% FBS complete media. We subsequently replaced the media with 0.5% exosome-free FBS complete media for 12 hours. After starvation, we scratched the cells with 10 µl pipette tips and washed twice with PBS to remove the detached cells. We cultured the cells with 0.5% exosome-free FBS complete media during the assay to slow down cell proliferation. We obtained the images from six different areas per well with Zeiss Axio Observer Z1 microscope equipped with 20x/0.5 NA objectives at several time points. We analyzed the images with TScratch tool [103].

2.2.13. Soft agar colony formation assay

Performing an anchorage-independent growth assay using SeaPlaque agarose (Lonza, catalog number 50101), we assessed the transformation capacity of the 67NR-S and 67NR-NS cells in vitro. We used three different conditions in triplicates to determine the ability of these cells to form soft agar colonies: no treatment, 10% DMSO, and 10 µM GW4869 (Cayman Chemical, catalog number 13127). We suspended 2.5×10^3 cells in 0.7% top agar in exosome-free complete media containing the appropriate treatment conditions and placed on top of solidified 0.8% bottom agar in 6-well plates (Fisher, catalog number 353046). Upon setting of the top agar with cells, we added 500 µl of fresh exosome-free complete media containing the appropriate treatment conditions to the wells and incubated the plates for 14 days at 37°C. We fed the cells with exosome-free complete media with the appropriate treatments, twice per week. We counted the colonies from ten different areas per well and acquired the representative 20x images microscopically using Zeiss Axio Observer A1 microscope.

2.2.14. Mouse modeling assay

We injected 1×10^4 67NR-S and 67NR-NS cells subcutaneously into the fourth left mammary fat pad of five BALB/c mice (Jackson laboratory, strain 0000651 BALB/cJ) for each clone. We monitored the size of the tumor with caliper measurements weekly and calculated using formula $(L \times W^2) \times 0.5$, where L and W are the length and the width of the tumor, respectively. We sacrificed the mice and harvested the tumors before the onset of necrosis.

2.2.15. Single-cell RNA-sequencing

Following the Illumina Bio-Rad SureCell WTA 3' library prep reference guide, we prepared the scRNA-seq library. Briefly, we mixed an equal number of the mouse cell lines in cold PBS with 0.1% BSA in a concentration of 2,500 cells/µl, then filtered to achieve single-cell suspension. Using a ddSEQ Single-Cell Isolator, we co-encapsulated with oil the single cells and barcodes into droplets. After reverse transcribing and breaking the emulsion, we purified the first-strand products using purification beads, followed by cDNA synthesis and tagmentation. We PCR-amplified the cDNA and cleaned it up to remove short library fragments. Later, we sequenced the cDNA library in a NextSeq 500 sequencing system. Using Illumina BaseSpace Sequence Hub, we analyzed the sequencing data and created a count matrix containing the number of transcriptomes for every single cell. We imported these matrices into R and combined them into a single matrix, which was then cleaned, normalized, and analyzed using the Seurat (v3.1.4) package [104]. We ranked the differentially expressed genes of 4T1 and 67NR cell lines and transformed into human orthologous using the BiomaRt (v2.38.0) package

[105,106], and imported to GSEA software [107,108] provided by UC San Diego and Broad Institute for gene set enrichment analysis.

2.2.16. Bulk RNA sequencing dataset analysis

We downloaded the raw counts of RNA-seq dataset published by Kim et al., from GEO (GSE104765) [109]. We filtered the table for three replicates of 4T1 and 67NR cells. To obtain the differentially expressed genes, we used the DESeq2 (v1.22.2) package [110] in R.

2.2.17. Tumor Cancer Genome Atlas (TCGA) analysis

We downloaded all the TCGA data, including raw counts, RSEM gene normalized expression, and clinical data from the Broad Institute FireBrowse Data Portal (www.firebrowse.org). To collect the non-metastatic patients without lymph node metastasis, we used the TNM staging information and selected the patients with N0 and M0 for analysis. To perform hierarchal clustering on the breast cancer dataset, first, we filtered out genes with average RSEM expression < 5 to remove their effects in the data analysis. Next, we used hclust function in R to identify two clusters using ward.D2 as the linkage method with manhattan as the distance measure. Using the DESeq2 (v1.22.2) package, we identified CD63 and CD81 upregulated in cluster 1. Using a set of genes associated with exosome secretion (Table 1), we identified 13 genes with more than 1.2-fold change in cluster 1 as exosome signature genes for further analysis. For gene set enrichment analysis, we used the pre-ranked gene list of genes with a significant fold change of < 0.05 in GSEA software provided by UC San Diego and Broad Institute. For survival analysis, we used the Kaplan-Meier method to compare the overall survival of

patients divided by the median expression of 13 exosome signature genes. We tested the statistical significance of survival curves using the log-rank test. We calculated the cytolytic activity (Cyt) as the geometric mean of PRF1 and GZMA as previously described [111]. We performed CIBERSORTx [112] analysis on the RSEM gene expression of breast cancer patients to estimate the relative fraction of 22 immune cell types using 1000 permutations. We calculated the ssGSEA scores via the GSVA (v1.30.0) package [113] using gene signatures collected from a previously described signature [114]. We calculated in R the Spearman's rank correlation coefficient between the median expression of 13 exosome signature genes and a single gene of interest.

2.3. Results

2.3.1. Establishing a single-cell method for quantifying exosome secretion

We sought to establish a method based on nanowell arrays for identifying the secretion of exosomes at the single-cell level. We have previously demonstrated that functionalized beads can serve as biosensors to enable the efficient capture of analytes from single cells within nanowell arrays [102]. Accordingly, we wanted to investigate whether beads can serve to capture exosomes secreted by single cells within nanowell arrays.

The expression of transmembrane proteins, CD63 and CD81 on the surface of exosomes, has been widely used for isolation and detection of exosomes [115]. We sought to compare the use of either a single marker (CD63) or two markers (CD63 and CD81) for the capture of exosomes. Accordingly, we isolated exosomes from GSC20 cancer cell line, using a standard ultracentrifugation

procedure. Nanoparticle tracking analyses (NTA) confirmed that the exosomes had a median diameter of (132 ± 6) nm (Figure 10A). Quantitative analyses of the capture of purified exosomes onto either anti-CD63 or anti-CD81 antibody-coated beads demonstrated a specific increase in fluorescence when detected using a fluorescent anti-CD63 antibody (Ab). The beads coated with the anti-CD81 Ab showed lower background fluorescence in comparison to the anti-CD63-coated beads in the absence of exosomes (Figure 10B), which resulted in an increased area under the curve (AUC) (Figure 10C). Moving forward, we thus implemented the use of antibodies targeting CD81 (for capture) and CD63 (for detection).

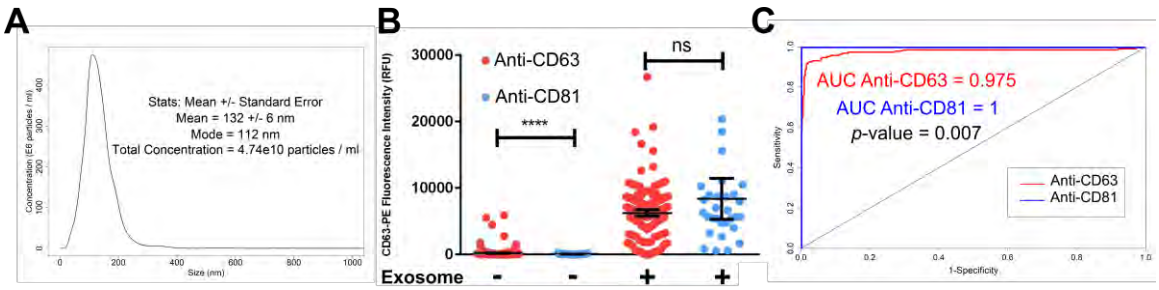

Figure 10. (A) Nanosight analysis of exosomes isolated from GSC20 cells. (B) CD63 (exosome) intensity of beads functionalized with either anti-CD63 or anti-CD81 for the capture of exosomes. PBS was used as negative control. Two-tailed t-test was applied. (C) ROC curve comparing both capture antibody. DeLong's test was applied for two ROC curves. Significance levels are shown as **** $p < 0.0001$.

To determine whether the immunoassay can capture exosomes secreted directly from cells, we modified the widely utilized transwell assay to harvest exosomes directly from cells [116–118]. We chose to work with a pair of syngeneic, isogenic mouse breast cancer cell lines, with differing metastatic potential, 4T1 and 67NR. We incubated the non-metastatic 67NR mouse breast cells in the upper chamber with anti-CD81-coated beads in the lower chamber of a transwell assay for 48 hours (Figure 11A). The exosomes isolated using this procedure displayed

the expected morphology and size as observed by Transmission Electron Microscopy (TEM) (Figure 11B). Collectively, these results suggest that the bead-based immunosandwich utilizing anti-CD81 and anti-CD63 Abs can be used to capture exosomes from cells and could be used for single-cell assays (Figure 11C).

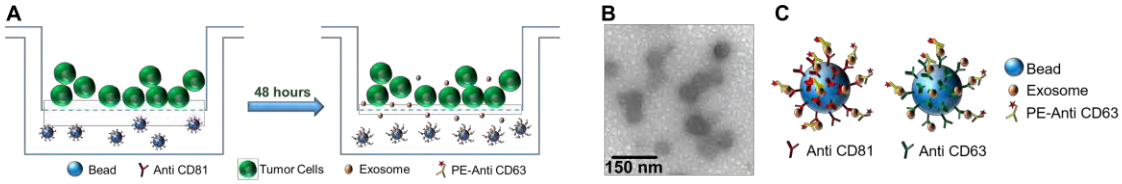

Figure 11. (A) Overall workflow of transwell assay for capturing exosomes for TEM visualization. (B) TEM images of exosomes isolated using the transwell assay. (C) Overall representative schematic of immunoassay showing higher efficiency of anti CD81 for capturing exosomes.

To analyze the secretion of exosomes from single cells, we utilized a custom nanowell array containing 9216 wells, and co-incubated beads and breast cancer cells (Figure 12).

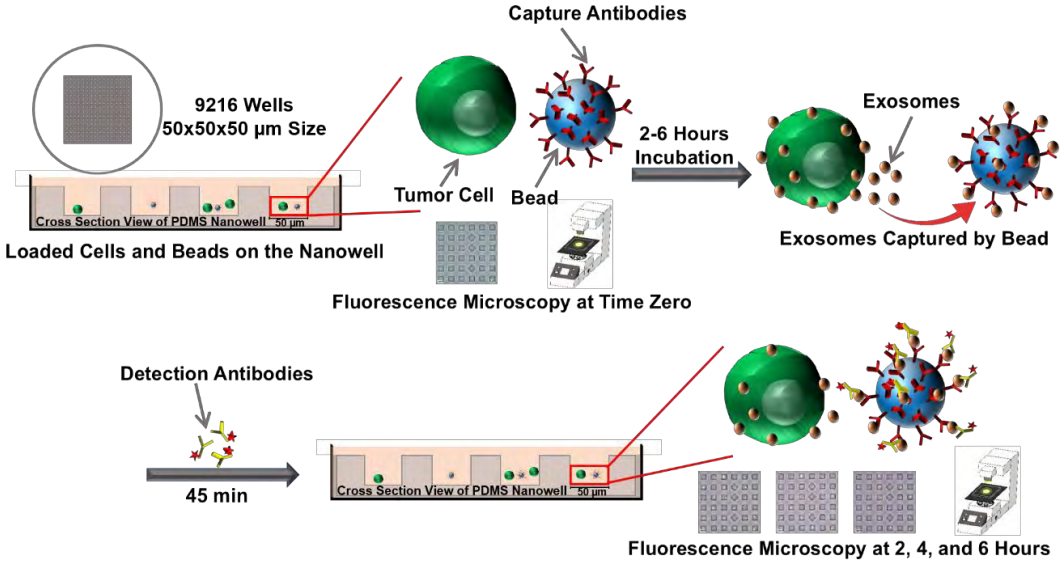

Figure 12. The overall workflow of the single-cell assay. Cells and anti-CD81 conjugated beads are loaded on the nanowell and incubated for 2-6 hours. The entire array is incubated with fluorescently-labeled antibody against CD63 and imaged using microscopy.

At two-hour intervals, we added the fluorescently tagged anti-CD63 Ab and imaged the entire nanowell array. As expected, individual cells demonstrated heterogeneity in exosome secretion (Figure 13A). We compared the frequency of single-cell secreting exosomes between 67NR, and the isogeneic, metastatic breast cancer cell line, 4T1. To quantify heterogeneity in secretory behavior and to estimate the relative rate of secretion between individual cells and across the cell lines, we restricted analyses to nanowells containing a single cell and a single bead. Within these nanowells, we used a combination of image segmentation, thresholding, and normalized fluorescent intensities to identify if individual cells were classified as secretors or non-secretors (detailed description in Figure 9). At each of the time points tested—two, four, and six hours—there was no difference in the frequency of single cells secreting exosomes, comparing 4T1 and 67NR (Figure 13B). Within all cells that secreted exosomes, we also compared the number of exosomes secreted per cell across 4T1 and 67NR single cells. Somewhat surprisingly, the non-metastatic cell line 67NR single cells secreted more exosomes per cell at each of the time points profiled (Figure 13C).

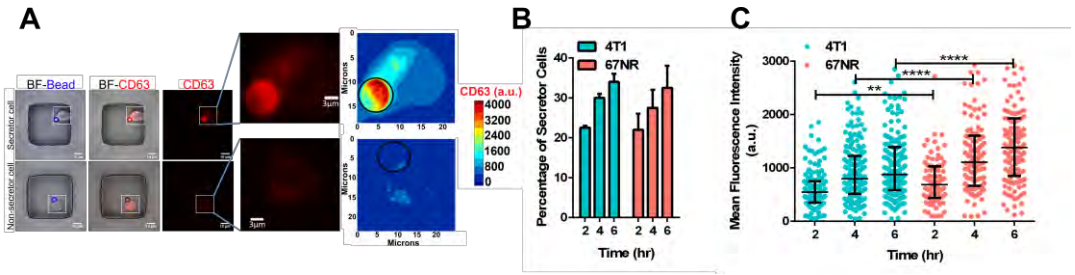

Figure 13. (A) Representative images of individual nanowells containing 67NR cells with different exosome secretion capacity. Comparison of the frequency of exosome secreting cells (B) and the rate of secretion (C) between 67NR (non-metastatic) and 4T1 (metastatic) breast cancer cells. Each dot represents a single cell with the median and quantiles. T-tests were used for comparison. Significance levels are shown as ** $p < 0.001$ and **** $p < 0.00001$.

Tracking the kinetics of exosome secretion in individual 4T1 and 67NR cells during a six-hour period revealed three major classifications for the cells: (1) a major subpopulation of cells which showed continuous secretion, (2) a subpopulation of cells that showed burst secretion at two hours, then subsequently stopped secreting, and (3) cells with burst secretion starting at four hours (Figure 14). Taken together, these results established that while the overall frequencies of cells secreting exosomes are not necessarily different between metastatic and non-metastatic cell lines, individual cells showed differences in secretory behavior. These results also indicate that non-metastatic 67NR cells can secrete more exosomes per cell in comparison with metastatic 4T1 cells, a characteristic that cannot be observed by routine ultracentrifugation procedures.

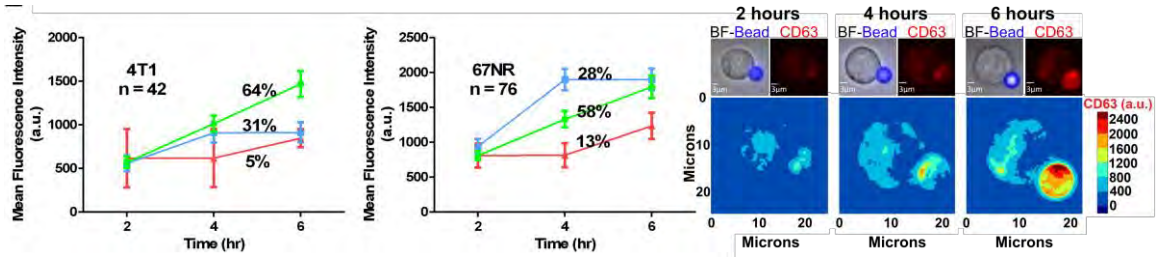

Figure 14. The kinetics of exosome secretion from single cells. The three subpopulations are shown as trend lines (mean ± SE). Representative images and contour maps of a single cell showing a continuous increase of CD63 intensity on the surface of the bead.

2.3.2. Single-cell RNA-sequencing illustrates that 67NR cells are enriched in exosome secretion pathways compared to 4T1 cells

To gain further mechanistic insights into the pathways that can support the increased exosome secretion capacity of 67NR cells in comparison to 4T1 cells, we performed single-cell RNA-sequencing (scRNA-seq). After data processing (see Methods), the final scRNA-seq dataset used for analyses had an average of 3,386 unique genes per cell and 35,604 transcripts (Figure 15A). Dimensionality

reduction using t-Distributed Stochastic Neighbor Embedding (t-SNE) showed a clear separation between the cells comprising each cell line (Figure 15B).

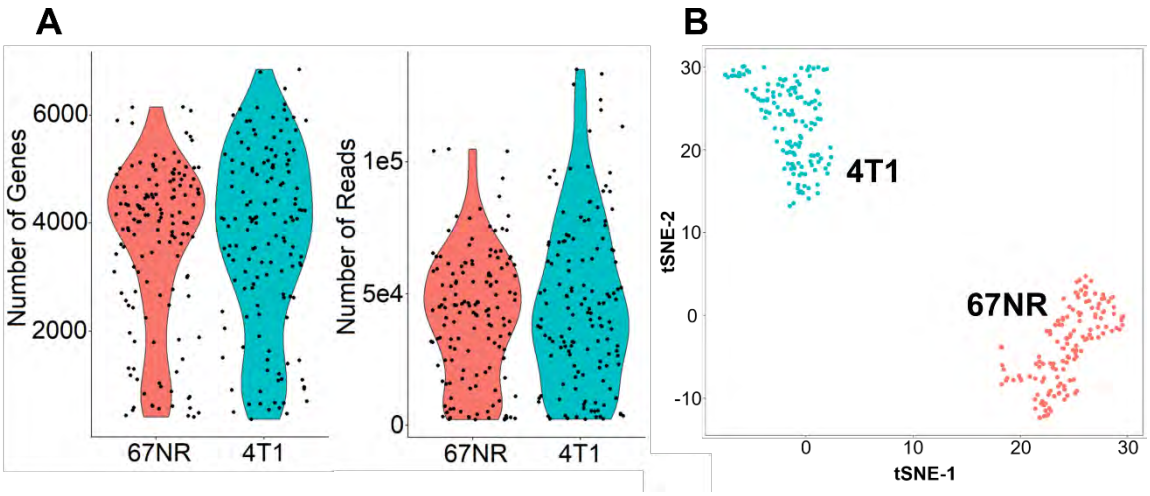

Figure 15. (A) Number of genes and reads detected in scRNA-seq for 67NR and 4T1 cells. (B) t-SNE plot of 67NR and 4T1 breast cancer cells clusters.

Hierarchical clustering indicates that a set of 1,647 differentially expressed genes (≥ 2-fold change) distinguishes the two cell types (Figure 16A). ScRNA-seq confirmed that a number of markers associated with epithelial-mesenchymal transition (EMT) including vimentin (Vim), fibronectin (Fn1), and Axl Receptor Tyrosine Kinase (Axl) were increased in 67NR cells (Figure 16B). In contrast, a number of matrix metalloproteinases associated with invasion, including Mmp9 and Mmp14, were increased in 4T1 cells (Figure 16C).

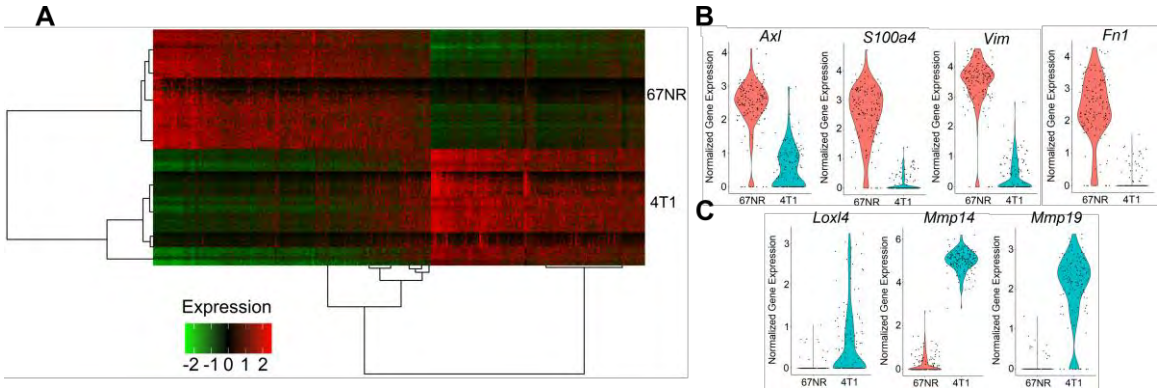

Figure 16. (A) Heat map comparing the expression of the differentially expressed genes in 67NR and 4T1 cells. Violin plot comparing the expression of (B) mesenchymal and (C) epithelia cell transcripts.

To test the correlation between the functional single-cell exosome secretion assay and the transcriptional signatures, we established a core gene signature using a previously described set of genes known to be involved in exosome secretion (Table 1) [119].

Table 1. Gene signature associated with exosome secretion

	Mouse symbol	Human Symbol	Ref.		Mouse symbol	Human Symbol	Ref.
1	*Hgs*	*HGS*	[120]	23	*Pkm*	*PKM*	[24]
2	*Stam*	*STAM*	[121]	24	*Snap23*	*SNAP23*	[24]
3	*Tsg101*	*TSG101*	[121]	25	*Rala*	*RALA*	[26]
4	*Chmp4c*	*CHMP4C*	[121]	26	*Ralb*	*RALB*	[26]
5	*Pdcd6ip*	*PDCD6IP*	[13]	27	*Rab2b*	*RAB2B*	[17]
6	*Vta1*	*VTA1*	[121]	28	*Rab5a*	*RAB5A*	[17]
7	*Vps4a*	*VPS4A*	[121]	29	*Rab9*	*RAB9A*	[17]
9	*Sdcbp*	*SDCBP*	[13]	30	*Rab7*	*RAB7A*	[122]
10	*Sdc1*	*SDC1*	[13]	31	*Rab11a*	*RAB11A*	[15]
11	*Sdc2*	*SDC2*	[13]	32	*Rab27a*	*RAB27A*	[123]
12	*Sdc3*	*SDC3*	[13]	33	*Rab27b*	*RAB27B*	[122]
13	*Sdc4*	*SDC4*	[13]	34	*Rab35*	*RAB35*	[14]
14	*Cd9*	*CD9*	[124]	35	*Cit*	*CIT*	[125]
15	*Cd82*	*CD82*	[124]	36	*Cttn*	*CTTN*	[126]
16	*Cd63*	*CD63*	[127]	37	*Smpd3*	*SMPD3*	[8]
17	*Lmp1*	*LMP1*	[128]	38	*Dgka*	*DGKA*	[129]
18	*Tspan8*	*TSPAN8*	[130]	39	*Pld2*	*PLD2*	[131]
19	*Syt7*	*SYT7*	[16]	40	*Arf6*	*ARF6*	[10]

Table 1 (continued)

20	*Vamp7*	*VAMP7*	[132]	41	*Bst2*	*BST2*	[133]
21	*Ykt6*	*YKT6*	[134]	42	*Atg12*	*ATG12*	[135]
22	*Stx1a*	*STX1A*	[136]	43	*Atg3*	*ATG3*	[135]

Gene set enrichment analysis (GSEA) comparing 4T1 and 67NR confirmed that 67NR cells were positively correlated with exosome secretion signatures (Figure 17A). The core set of genes in the GSEA that showed high discrimination between 4T1 and 67NR cells mapped to the known ALIX-Syndecan-Sytenin pathway (Figure 17B) [13]. The pathway genes consisting of tetraspanins (*Cd63*), *Rab7*, apoptosis-linked gene 2-interacting protein X (*Pdcd6ip*), syndecans (*Sdc2*, *Sdc4*), and syntenin (*Sdcbp*) were enriched in 67NR cells compared to 4T1 cells (Figure 17C). By contrast, two proteins that are known exosome secretion inhibitors, *Pikfyve* and *Isg15*, were significantly expressed in 4T1 cells but not in 67NR cells (Figure 17D) [18,137].

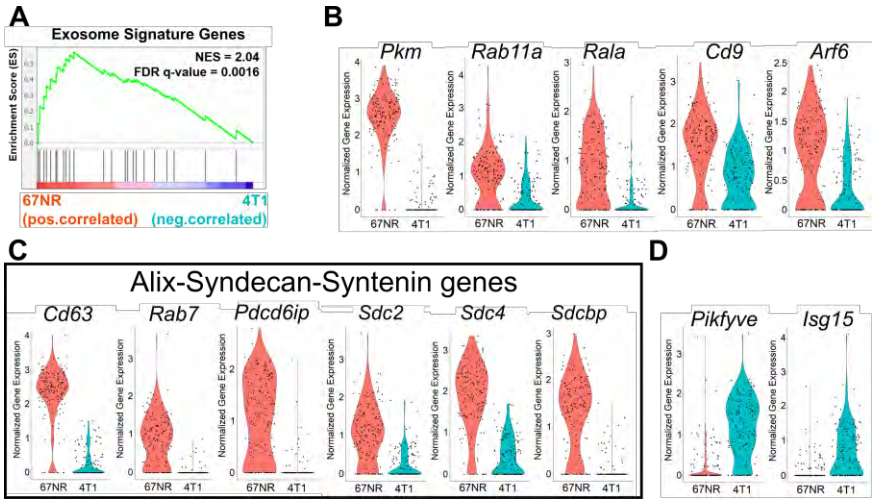

Figure 17. (A) Gene Set Enrichment Analysis (GSEA) analysis of the core exosome gene signature (Table 1) studies within 67NR cells compared to 4T1 cells. Violin plots of the (B) exosome-secretion genes, (C) genes associated with ALIX-Syndecan-Sytenin pathway, and (D) inhibitors of exosome secretion, *Pikfye* and *Isg15*.

We performed an independent verification of these results using reanalyzing population-level RNA-seq data on these same cell lines (GSE104765) [109]. These data also confirmed the higher expression of *Cd63*, *Rab7*, *Sdc2*, *Sdc3*, and *Sdcbp* in 67NR cells in comparison to 4T1 cells (Figure 18). Collectively, these results from transcriptional profiling further advanced our findings that non-metastatic breast cancer cells can secrete more exosomes than metastatic breast cancer cells and suggest that the ALIX-Syndecan-Sytenin pathway supports this function.

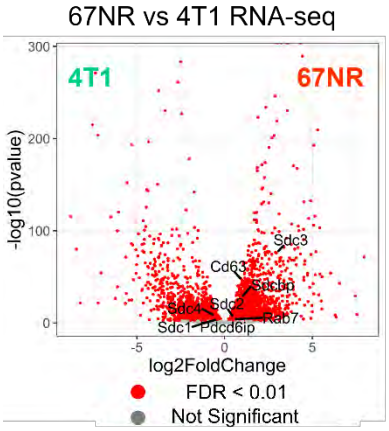

Figure 18. Expression of genes associate with Alix-Syndecan-Sytenin pathway in 67NR cells in comparison with 4T1 cells based on the bulk RNA sequencing.

2.3.3. Exosome secretion is an inheritable property during short-term culture of cancer cells

Our combined functional and transcriptional data illustrated that 67NR cells are proficient in exosome secretion. We next wanted to investigate the impact of exosome secretion on the functional properties of the 67NR tumor cells. We established a simple bioanalytical process to image cells secreting exosomes using nanowell arrays and microscopy, perform automated segmentation and

identification of secretor and non-secretor cells, and use an automated micromanipulator to retrieve single cells to establish clonal cell lines (Figure 19).

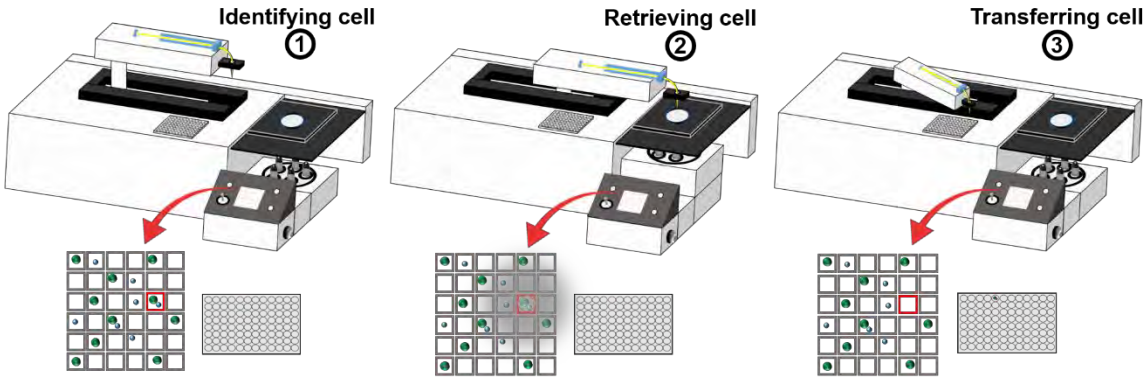

Figure 19. Schematic of the overall workflow for the imaging and retrieval exosome secreting single cells with the aid of an automated micromanipulator.

Since we want to ensure that long-term culture did not alter the properties of the cells, we grew the cells to no more than 24 population doublings. For the majority of the cells picked (20 out of 27), we were able to establish clonal cell lines, classified as secretor (cell population labeled as S, secretor, if the cell of origin was a secretor) and non-secretor (cell population labeled as NS, non-secretor, if the cell of origin was a non-secretor) (Figure 20A).

We tested the ability of single cells derived from these expanded populations to secrete exosomes using the single-cell assay. Consistently, across all six cell lines tested (three secretor lines and three non-secretor lines), the frequency of single cells secreting exosomes was higher among the 67NR-S cell lines in comparison to the 67NR-NS cell lines (Figure 20B). Within all cells that secreted exosomes, comparisons of the number of exosomes secreted per single cell as a function of time (two, four, and six hours) confirmed that the 67NR-S cell lines were composed of individual cells with high rates of exosome secretion (Figure 20C).

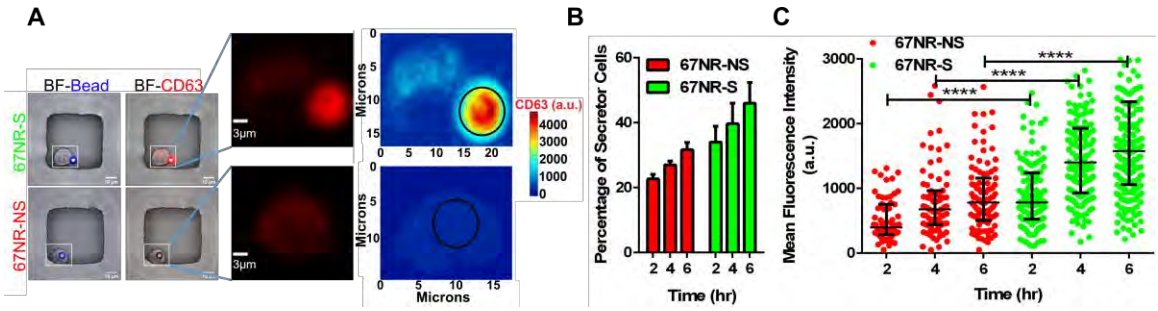

Figure 20. (A) Representative images of 67NR secretor and non-secretor single cells before retrieval. Comparison of the frequency of cells secreting exosomes (B) and (C) the rate of secretion of exosomes within 67NR-NS and 67NR-S cells. . Each dot represents a single cell with the median and quantiles. T-tests were used for comparison. Significance levels are shown as **** $p < 0.00001$.

Kinetic analyses of the dynamics of exosome secretion in these cell lines revealed two dominant subpopulations: (a) continuous secretors and (b) cells with burst secretion that stopped secretion after 4 hours (Figure 21). Taken together, these results establish that the secretion of exosomes is inheritable during cell division, and this allowed us to investigate the functional consequences of these exosome secreting cell lines.

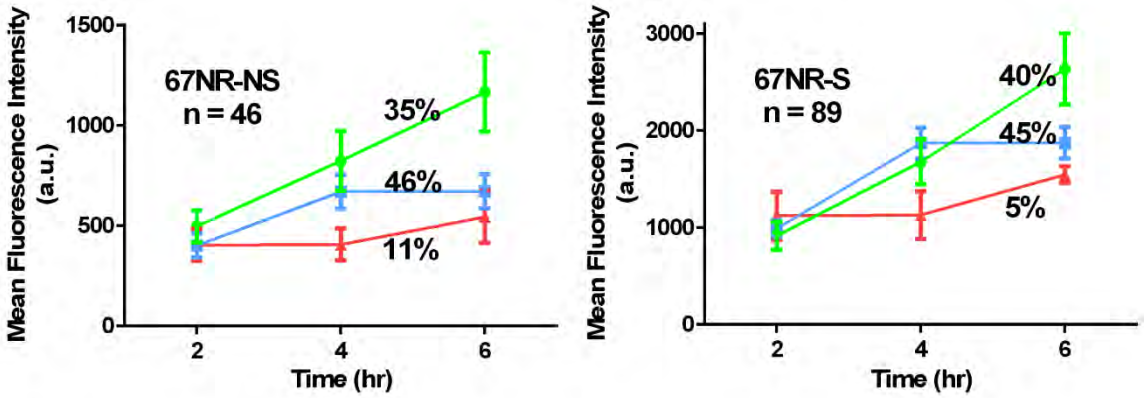

Figure 21. The kinetics of exosome secretion from individual cells that comprise the 67NR-NS and 67NR-S populations. The three subpopulations are shown as trend lines (mean ± SEM).

2.3.4. Secretion of exosomes prevents the tumor formation in non-metastatic cell lines

Since the expanded cell populations preserved the exosome secretion property of the cell of origin, we investigated in vitro functions of the 67NR-S and 67NR-NS cell lines. Phase-contrast microscopy revealed differences in the morphology with 67NR-S cells being more elongated than 67NR-NS cells (Figure 22A). Migration is a key characteristic of cancer cells essential for metastasis. To test the migratory behavior of the 67NR-S and 67NR-NS cell lines, we performed a scratch wound assay. 67NR-S cells were significantly more migratory than 67NR-NS cells (Figure 22B). To test the tumorigenicity potential of these cell lines, we used a soft agar formation assay [138]. 67NR-S cells formed 2-fold more colonies than the 67NR-NS cells in soft agar suspension cultures (Figure 22C). These in vitro data illustrate that the 67NR-S cells were more migratory and had enhanced tumorigenicity potential compared to 67NR-NS cells.

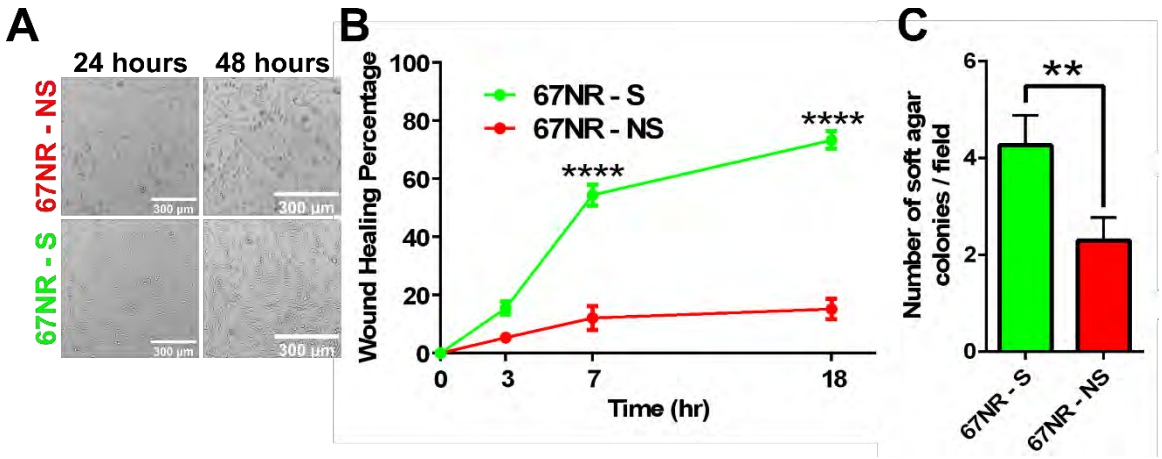

Figure 22. (A) The morphology of 67NR-NS and 67NR-S cell populations recorded using phase-contrast microscopy. (B) Wound healing assays illustrating the migration of 67NR-S and 67NR-NS clonal cells (mean ± SEM). A two-way ANOVA test was used (n= 6 for each cell line). (C) The colony formation assay for 67NR-S and 67NR-NS cell populations (mean ± SEM). The Mann Whitney t-test was used for comparison. Significance levels are shown as ** $p < 0.01$, and **** $p < 0.0001$.

We have utilized syngeneic models to be able to understand the impact of exosomes on both intrinsic growth potentials of the tumor and the impact of the host immune system. Parental 67NR cells are non-metastatic cells with a heterogeneous population and form primary tumors upon injection into mice. To determine the in vivo relevance of exosome secretion, we injected two 67NR-S and one 67NR-NS cell lines into the mammary fat pad of BALB/c mice and monitored the tumor growth for six weeks (Figure 23A). None of the mice that received the 67NR-S cells developed tumors (Figure 23B). By comparison, however, 80% of the mice that received 67NR-NS cells formed large tumors by week six (Figure 23C). Taken together, these results illustrate that despite having high tumorigenicity and migratory potential in vitro, the 67NR-S cells are rejected in vivo.

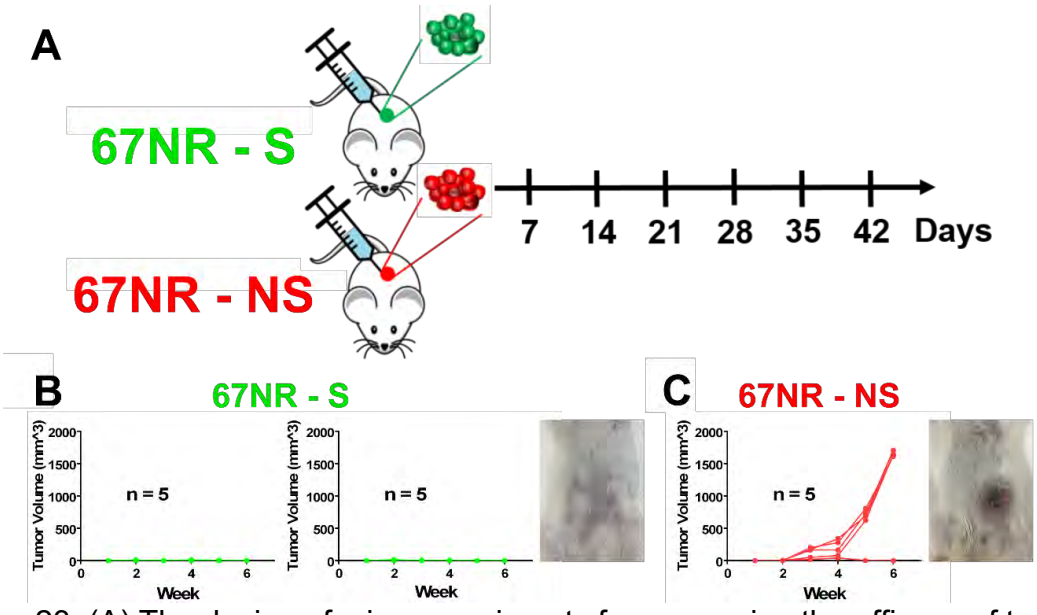

Figure 23. (A) The design of mice experiments for comparing the efficacy of tumor formation by 67NR-S and 67NR-NS cell lines. Tumor growth monitoring of BALB/c mice injected with (B) 67NR-S clones (two clonal cell populations, five mice each) and (C) 67NR-NS clone (single clonal cell population, five mice). A representative image of a single mouse is shown.

To directly link exosome secretion to the rejection of tumors in vivo, we investigated the use of GW4896, a chemical inhibitor of exosome biogenesis. Treatment of 67NR-S cells with GW4896 significantly inhibited exosome secretion when profiled using the transwell exosome capture assay (Figure 24A). Unfortunately, however, the treatment of 67NR-S cells with GW4896 almost completely abolished colony formation in a soft agar assay (Figure 24B), precluding its use in vivo. Collectively, studies with these non-metastatic breast cancer cells demonstrated that despite enhanced tumor-forming potential in vitro, exosome secreting cell lines are rejected in vivo presumably due to the host immune system.

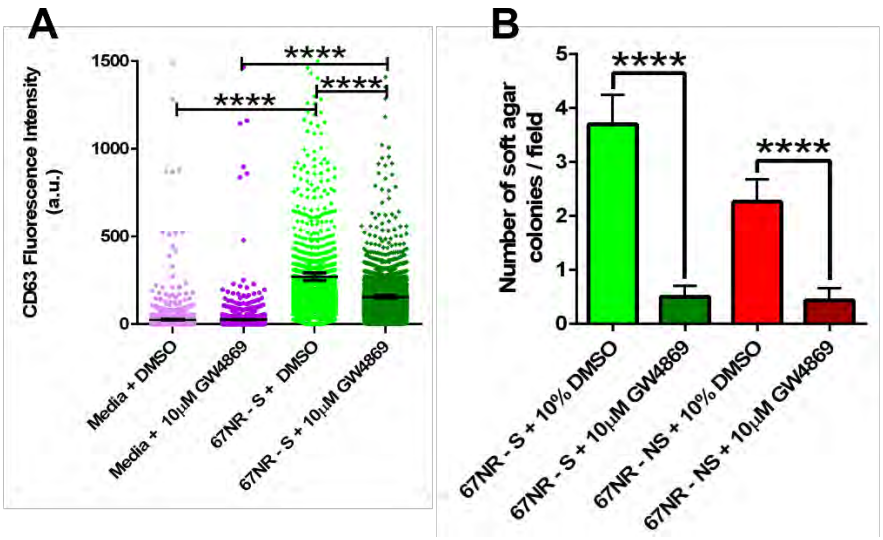

Figure 24. (A) Exosome secretion within 67NR-S clonal cell populations treated with GW4869 or DMSO. Each dot represents CD63 (exosomes) intensity on a single bead (mean ± SEM). (B) Colony formation in 67NR-S and 67NR-NS clonal cell populations upon treatment with GW4869 (mean ± SEM). The Mann Whitney t-test was used for comparison. Significance levels are shown as ** $p < 0.01$, and **** $p < 0.0001$.

2.3.5. Secretion of exosomes improves the survival in non-metastatic breast cancer patients

Based on the mice data, we sought to directly understand the impact of exosome secretion and the link to the immune system within human patients with breast cancer. We analyzed the correlation between gene expression and survival of non-metastatic breast cancer patients available within The Cancer Genomic Atlas (TCGA). Since our single-cell method utilizes CD63 and CD81 to detect the exosomes, we first compared the survival of patients with higher and lower expression of these markers. Since there was no difference in survival of patients stratified by CD63 or CD81, we conclude that these single markers are necessary but not sufficient to identify a complex property like exosome secretion (Figure 25).

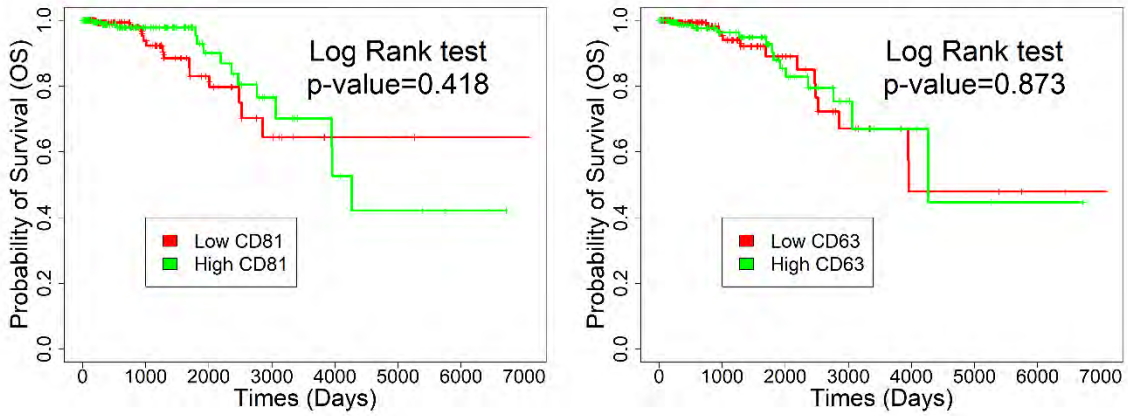

Figure 25. The overall survival of non-metastatic breast cancer patients (N0 and M0 in TNM staging system) divided by median CD81 and CD63 expression.

To identify signatures of exosome secretion, we applied unsupervised hierarchal clustering (no gene selection) to stratify non-metastatic breast cancer patients into two groups with 182 and 268 patients each (Figure 26).

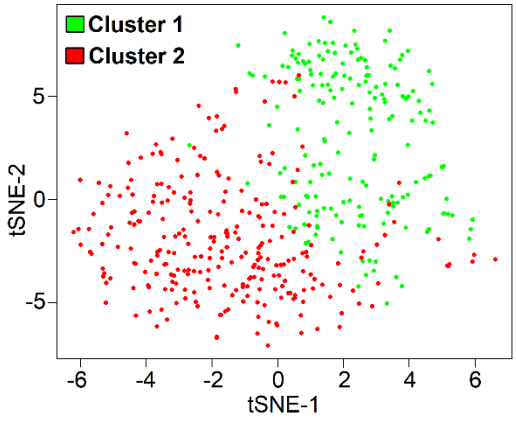

Figure 26. t-SNE plot of the clusters identified by unsupervised hierarchal clustering of non-metastatic breast cancer patients.

A set of 13 genes related to exosome secretion were identified as being differentially expressed between these two groups (Figure 27A). We therefore utilized the median expression of this 13-gene cluster to stratify patient tumors as exosome high (BRCA_Exo^{Hi}) and low (BRCA_Exo^{Lo}). Consistent with our scRNA-seq data on 4T1 and 67NR cells, the expression of genes in ALIX-Syndecan-Sytenin pathway was elevated in BRCA_Exo^{Hi} patients in comparison to the BRCA_Exo^{Lo} patients (Figure 27B).

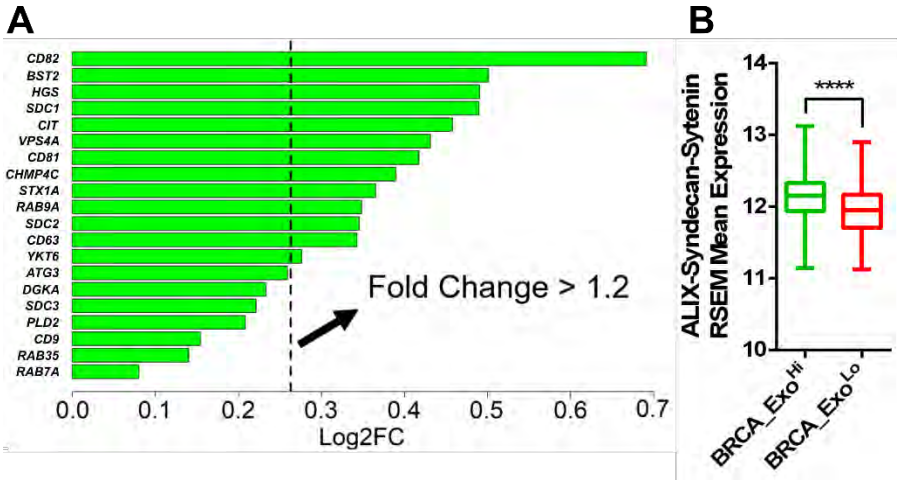

Figure 27. (A) Enrichment of the 13 genes with fold change > 1.2 associated with exosome secretion in the BRCA_Exo^{Hi} patients. (B) The average expression of genes in ALIX-Syndecam-Syntenin pathway within BRCA_Exo^{Hi} and BRCA_Exo^{Lo} patients. The median and quantiles are shown.

The overall survival was significantly higher for BRCA_Exo^{Hi} patients in comparison to the BRCA_Exo^{Lo} patients (median survival not reached vs. 10.8 years, HR: 0.4, 95% CI: 0.18-0.92), consistent with our findings in mice that non-metastatic cells secreting exosomes do not form tumors (Figure 28).

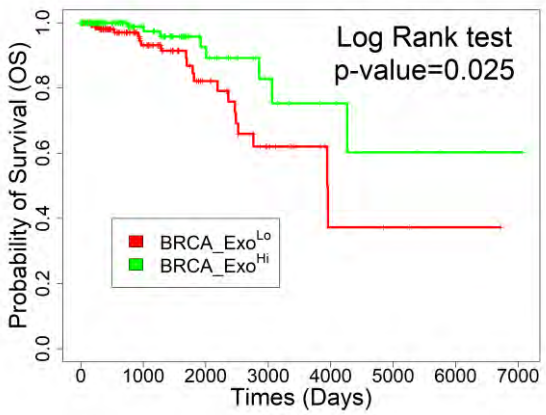

Figure 28. Differences in the survival of non-metastatic breast cancer patients stratified by the median expression of 13 exosome gene signature.

To identify if immune cell infiltration is associated with improved overall survival observed in patients with higher expression of exosomes, we used the previously published cytolytic score (based on the expression of *GZMA* and *PRF1*) as an in silico metric of immune cell cytolytic activity [111]. The cytolytic activity was significantly elevated in the BRCA_Exo^{Hi} cohort compared to the BRCA_Exo^{Lo} cohort (Figure 29A). To identify the immune cell type that was responsible for this signature, we used the normalized gene expression data to quantify the relative frequencies of the 22 different immune cell types using the CIBERSORTx algorithm. CD8 T cells were not significantly different between the two clusters (Figure 29B).

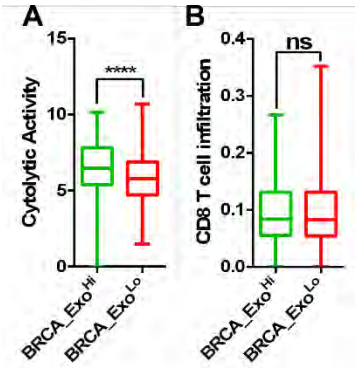

Figure 29. (A) Cytolytic activity score and (B) infiltration of CD8 T cells in non-metastatic breast tumors comparing the BRCA_Exo^{Hi} and BRCA_Exo^{Lo} patients. The median and quantiles are shown. two-tailed t-test was used. Significance levels are shown as ***** $p < 0.00001$.

The difference in cytolytic activity was reflected with significant differences in macrophage subsets: a higher frequency of M0 and pro-inflammatory M1 macrophages, and a decreased frequency of anti-inflammatory M2 macrophages were observed in the tumors of BRCA_Exo^{Hi} patients compared to the BRCA_Exo^{Lo} patients (Figure 30A). Similar to the macrophages, the frequency of intratumoral memory CD4 T cells was also significantly different between BRCA_Exo^{Hi} and BRCA_Exo^{Lo} patients. We utilized signatures of helper T cells within the previously described Immunome signature set [114], to identify that Th1 cells were significantly increased, and Th17 cells were significantly decreased in the BRCA_Exo^{Hi} patients compared to the BRCA_Exo^{Lo} patients (Figure 30B). Collectively, these results showed that tumors in BRCA_Exo^{Hi} patients harbor M0/M1 macrophages and Th1 cells.

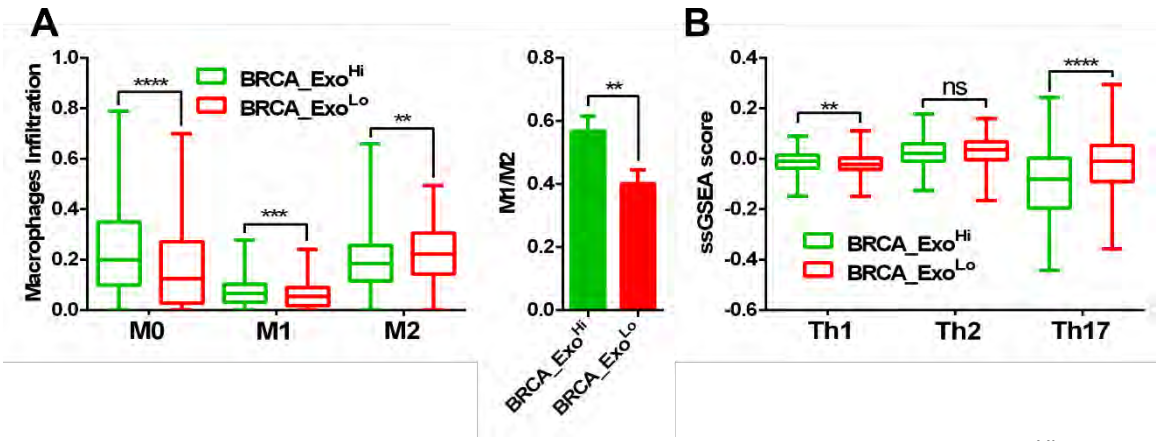

Figure 30. (A) Macrophage infiltration scores for the BRCA_Exo^{Hi} and BRCA_Exo^{Lo} tumor with the ratio of M1/M2 macrophages within these tumors (mean ± SEM). (B) The immune score of T helper cells for BRCA_Exo^{Hi} and BRCA_Exo^{Lo} tumors. The median and quantiles of the infiltration percentage are shown. A two-tailed t-test was used. Significance levels are shown ** p < 0.01, ***** p < 0.00001.

We utilized GSEA to identify soluble mediators of the immune cell polarization within the tumor microenvironment of these patients. Not surprisingly, several pathways associated with chemokine/cytokine receptor interactions were enriched in BRCA_Exo^{Hi} tumors (Figure 31A). Consistent with the high frequency of Th1 cells, interferon-gamma (IFN-γ) signaling was significantly elevated within the exosome high tumors (Figure 31B).

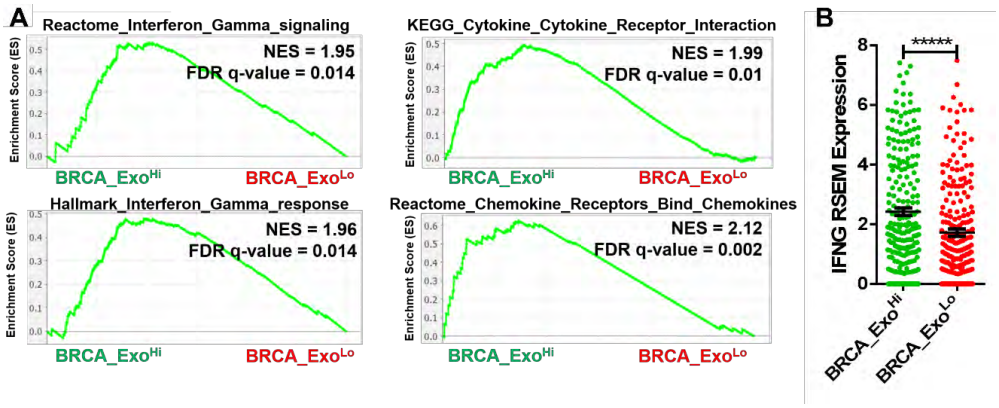

Figure 31. (A) GSEA of interferon-gamma, cytokines/chemokines receptor interaction pathways comparing BRCA_Exo^{Hi} and BRCA_Exo^{Lo} tumors. (B) Expression of IFNG in BRCA_Exo^{Hi} and BRCA_Exo^{Lo} patients (mean ± SEM). Two-tailed t-test was used. Significance levels are shown as **** p < 0.0001.

It is well known that the priming of macrophages in the presence of IFN-γ leads to the differentiation of pro-inflammatory M1 macrophages and downregulation of the IL6 signaling pathway. Although the expression of the IL6 receptor (*IL6R*) was not different, the expression of IL6 signal transducer (*IL6ST*) and the downstream signal transducer and activator of transcription 4 (*STAT3*) were significantly decreased in the BRCA_Exo^{Hi} tumors compared to the BRCA_Exo^{Lo} tumors (Figure 32).

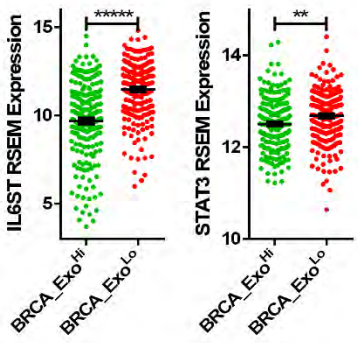

Figure 32. Normalized expression of *STAT3* and *IL6ST* in BRCA_Exo^{Hi} and BRCA_Exo^{Lo} tumors (mean ± SEM).

We also utilized the median expression score of the 13 exosome signature genes to confirm a significant inverse correlation between the exosome signature and *IL6R*, *IL6ST*, and *STAT3* within this entire cohort of patients (Figures 33). Taken together, the secretion of exosomes likely influences the infiltration of Th1 cells and a skewed ratio of M1/M2 macrophages through the crosstalk between IFN-γ and IL6/STAT3 pathways.

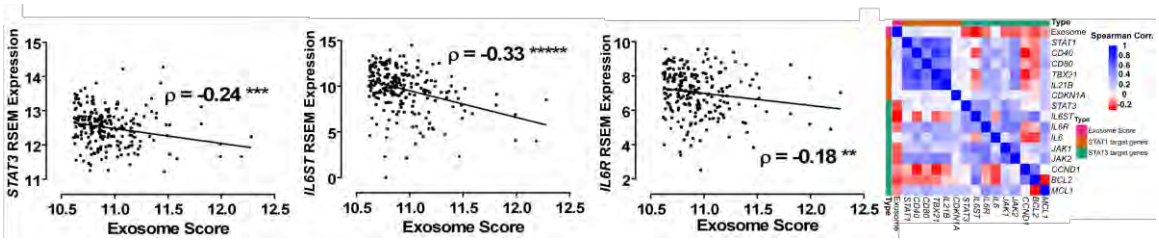

Figure 33. The anti-correlation of STAT3, IL6R, and IL6ST with exosome score within non-metastatic breast cancer patients (Spearman correlation). The heatmap showing the spearman correlation between selected genes and exosome score within non-metastatic breast cancer patients. two-tailed t-test was used. Significance levels are shown as * p < 0.05, ** p < 0.01, *** p < 0.001, **** p < 0.0001, ***** p < 0.00001.

We investigated the utility of the exosome secretion signature and its association with patient survival across pan-cancer datasets within the TCGA. Similar to breast cancer, exosome secretion signatures were associated with improved overall survival in melanoma (SKCM) patients (14.3 vs. 9.4 years, HR: 0.62, 95% CI: 0.39-0.97) (Figure 34A). By contrast, in both lung squamous cell carcinoma (LUSC) and stomach and esophageal carcinoma (STES), exosome secretion signature was associated with worse overall survival for patients (Figure 34B).

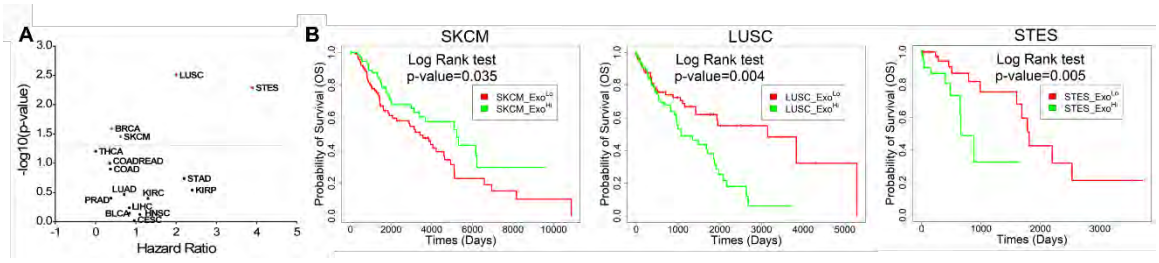

Figure 34. (A) Volcano plot of overall survival of pan-cancers divided by the median expression of exosome gene signatures. (B) Overall survival of non-metastatic SKCM, LUSC and STES patients divided by median expression of exosome gene signatures.

2.4. Discussion

Exosomes and EVs derived from tumors serve as long-distance messengers and hence play important roles in the metastatic cascade [139,140]. Exosomes

derived from metastatic cells have been shown to participate in a broad range of functions: remodel the extracellular matrix and the transformation of fibroblasts, promote angiogenesis, prepare the pre-metastatic niche, and alter the nature of the tumor microenvironment [45,141]. By contrast, the exosomes released by non-metastatic tumors has been relatively understudied. In both metastatic and non-metastatic tumors, studies that have aimed to investigate the role of exosomes have utilized exosomes purified from large numbers of cancer cells isolated from cell culture. This approach masks the heterogeneity in the secretion of the different cells that comprise the population. Comprehensive characterization of the heterogeneity of exosome secretion between the single cells within the same population has been restricted to only a few reports, and even in these studies, the ability to isolate and propagate cells with differences in exosome secretion capabilities is lacking [80,142]. We developed and validated a platform based on nanowell arrays for directly profiling exosome secretion from single cells and used these to establish cells derived from a clinically relevant mouse breast cancer model that have significant differences in the rate of exosome secretion. Our studies show that, surprisingly, the non-metastatic cell line, 67NR secretes more exosome per cell than its isogenic, metastatic counterpart, 4T1. Although prior studies from each of these cell lines have demonstrated that exosomes derived from 4T1 can facilitate metastasis, these studies utilized supraphysiological concentrations of purified exosomes [143]. Our results are consistent with studies in melanoma that showed that purified exosomes from poorly metastatic melanoma cells could inhibit metastasis [47]. ScRNA-seq suggested that the ALIX-

Syndecan-Sytenin pathway known to be important for exosome secretion was enriched in 67NR cells compared to 4T1 cells [13]. In vitro functional studies based on 67NR-S (high secretor) and 67NR-NS (low secretor) cells illustrated that the 67NR-S cells are more migratory and have enhanced tumorigenic potential; however, they are deficient at tumor formation in vivo.

To explore the relevance of our results in human breast cancers, we analyzed the signatures of exosomes with non-metastatic breast cancer patients within the TCGA. Our results demonstrate that patients with signatures of high exosome secretion (including the ALIX-Syndecan-Sytenin pathway) have improved survival compared to patients with signatures of low exosome secretion. To quantify if immune cells can help explain this difference in survival between the two cohorts of patients, we quantified the cellular composition in terms of the 22 subtypes of immune cells using the CIBERSORTx algorithm [112]. The cytolytic score, an in silico metric of inflammation, was significantly increased in tumors with high exosome secretion compared to tumors with low exosome secretion [111]. Surprisingly, the cytolytic score was not reflected by the high abundance of CD8 T cells but correlated with Th1 cells (secretion of IFN-γ) and M1 macrophages (suppression of IL6ST/STAT3 pathway). These results are consistent with studies using purified exosomes that revealed that breast cancer-derived exosomes alter macrophage polarization via IL6ST/STAT3 signaling [144].

Our platform has direct utility in single-cell studies of profiling the link between exosomes and function. In the current report, we have defined exosome secretion based only on abundances of CD63/CD81. This definition only marks a subset of

all exosomes, but the assay can be easily modified to include additional markers including CD9 and EpCAM [58]. Second, the ability to isolate cells based on differences in exosome secretion can be utilized to perform scRNA-seq on the retrieved cells directly. This method will have great utility to map the molecular players in the exosome secretion cascade directly. Furthermore, based on the differentially expressed transcripts, it will be possible to infer the proteins that are likely enriched in the exosomes secreted by these single cells. Third, the establishment of cell lines with differences in exosome secretion among metastatic cells will help map the functional impact of exosome secretion and their role in the biology of metastasis. We anticipate that our method can be broadly utilized to map the functional consequences of exosome secretion at the single-cell level.

Chapter 3: Integrated single-cell functional and molecular profiling identified a core signature of exosome secretion in metastatic breast cancer

3.1. Introduction

Exosomes are small extracellular vesicles secreted by all cell types and have been shown to be involved in cell-cell communication [3,145,146]. Exosomes are composed of a lipid bilayer and contain biological molecules such as nucleic acids and proteins [147,148]. They can transfer their content to the other cells in the tumor microenvironment which can lead to the genetic alteration in the target cell. This transformation is not limited to the site of secretion and exosomes can transfer their cargo to the cells in the other sites by spreading through body fluids [149,150].

The transformation of biological molecules can impact the development of cancer in different stages such as angiogenesis [151,152] , immune suppression [153–155], and metastasis [47]. For example, tumor-derived exosomes upregulate the angiogenesis-related genes and enhance the endothelial cell proliferation [130]. The secretion of tumor-derived exosomes containing PD-L1 upregulates the expression of PD-L1 in breast cancer cells and blocks the activation of T cells [33]. Exosomes can also trigger the invasion and migration of tumor cells as the exosomes from metastatic breast cancer cells contained matrix metallopeptidase 2 (MMP2) which degrades the extracellular matrix and promotes the invasion [35]. The exosomes of MDAMB231 cells carrying caveolin-1 can promote the migration and invasion capability in the recipient cells [156]. Also, primary tumors secrete exosomes to prepare the metastatic site by downregulating the cadherin-17 in lung [43]. Taking all together, understanding the function of exosomes and cells they

originate from can increase our knowledge of the complexity of the cancer microenvironment.

The formation and release of exosomes involve several steps starting with the inward budding of the plasma membrane and the formation of early endosomes. Then, the maturation of early endosomes results in the formation of multivesicular bodies (MVB) containing intraluminal vesicles which are also called exosomes. Finally, the MVB fuses with the plasma membrane, if not with the lysosome, and releases the exosomes. Several mechanisms have been reported in endosomal and MVB sorting including the endosomal sorting complex required for transport (ESCRT)-dependent [157,158], and ESCRT-independent machineries such as sphingolipid ceramide [8] and tetraspanins CD63 [159] which control the exosome formation. Also, the release of exosomes through the fusion of MVB with plasma membrane involves several proteins including the soluble N-ethylmaleimide-sensitive factor attachment protein receptors (SNAREs) [132,160] , and the RAB family members, RAB27A, RAB27B, and RAB7 [13,17]. Despite extensive research in the formation of exosomes, the pathways which regulate the secretion and packaging of exosomes are still unclear [6]. Also, although the content of exosome reflects to a large extent the biological state of its cell of origin, it does not necessarily demonstrate the intracellular interactions that lead to their formation [140]. In other words, the molecules involved in the formation and release of exosomes do not necessarily need to be incorporated into them [119]. Therefore, the identification of markers associated only with the formation and

secretion of exosomes in the cells can enhance our understanding of the exosome increase in the tumor microenvironment.

The current studies on the exosomes are mainly executed through the isolation of exosomes by techniques such as density gradient centrifugation or ultrafiltration [161]. Even though these techniques can be used for the identification of molecules carried by exosomes, they cannot identify the cellular components involved in the process of exosome formation. Therefore, to address the biological state of cells upon secretion, an integrated method for profiling the cellular components of cells upon an increase in the secretion of exosomes is essential.

The development of high-throughput single-cell RNA sequencing (scRNA-seq) in the last five years has enabled the characterization of heterogeneous tumor cells at the single-cell resolution [162,163]. In this study, we used the scRNA-seq technique to characterize the transcriptome of two monoclonal cell lines with different rates of secretion. To obtain the monoclonal cell lines, we applied a high-throughput single-cell technique to identify and retrieve single cells with different secretion capacity without any external perturbation. We utilized the MDAMB231 cell line which is a well-validated metastatic breast cell line and the secretion of exosomes from these cells has been reported to enhance the migration and invasion of cancer [164]. By performing the scRNA-seq analysis we identified 34 gene signatures which can be linked to the secretion and biogenesis of exosomes. Among these genes, four genes *HSP90AA1*, *HSPH1*, *EIF5*, and *DIAPH3* showed significant correlation and were recognized as core exosome gene sets. This gene signature was able to predict the secretion rate of exosomes from three different

breast cancer cell lines which was validated by *in vitro* analysis. Further, the higher expression of core exosome genes showed a strong correlation with poor survival and low CD8 T cell infiltration in breast cancer patients in The Cancer Genome Atlas (TCGA). Also, the expression of the core signature gene was associated with the basal-like subtype of breast cancer which is known as the invasive subtype of breast cancer. Taken together, we identified novel markers that can be associated with exosome secretion and poor prognosis in breast cancer patients.

3.2. Material and Methods

3.2.1. Cell culture

MDAMB231, HCC70, and MCF7 cells were purchased from ATCC. We cultured MDAMB231 and HCC70 cells in RPMI 1640 supplemented with 10% FBS, 1% L-glutamine, HEPES, and penicillin-streptomycin. We cultured MCF7 cells in Eagle's Minimum Essential Medium with 10% FBS, 1% HEPES, MEM Non-Essential Amino Acids, and penicillin-streptomycin. We tested all cells for mycoplasma contamination using real-time PCR.

3.2.2. Single-cell exosome detection assay

We analyze the secretion of exosomes from single cells as previously described. Briefly, we labeled cells with PKH67 dye (Sigma-Aldrich, catalog number PKH67GL-1KT) as directed by the manufacturer. For capturing the exosomes on the surface of LumAvidin beads (Luminex, catalog number L100-L115-01), we incubated the beads with 3.5 µg/ml biotinylated anti-CD81 (BioLegend, clone TAPA-1) antibody at the room temperature for 40 minutes, followed by three washes in PBS with 1% BSA. Then we loaded the labeled cells and functionalized beads on the PLL-g-PEG (SuSoS, Switzerland) treated

nanowell. 45 minutes before each detection time point, we covered the nanowell with 4 μg/ml PE anti-CD63 antibody (BioLegend, clone H5C6) at 37°C. We imaged the nanowell by Zeiss Axio Observer Z1 microscope equipped with 20x/0.8 NA objectives and a Hamamatsu Orca Flash v2 camera.

3.2.3. Secretion analysis of single-cell exosome detection assay

We analyzed the TIFF images exported from the microscope as previously described in chapter 2. Briefly, we segmented, quantified the cell:bead ratio, identified the cell:bead ratio of 1:1, and calculated the background-subtracted pixel values for identification of secretors and non-secretor single cells. To analyze the dynamic of secretion from single cells, the wells which maintained their 1:1 ratio during the experiment were detected. Then, based on a two-tailed t-test on the CD63 pixel values, we selected a significant increase with p-value < 0.01 as the criterion for a change in the secretion behavior of the cell.

3.2.4. Establishment of clonal cell lines.

As previously described in chapter 2, we used a micromanipulator (ALS, CellCelector) equipped with 50 μm glass capillaries to retrieve the detected secretor and non-secretor single cells. We transferred the retrieved cells to a 96 well plate containing complete media and cultured the cells up to 24 population doublings.

3.2.5. Wound healing assay

We cultured MDAMB231-S and MDAMB231-NS cells to 90% confluency in a 12-well plate with 10% FBS complete media. We then replaced the media with 0.5% exosome-free FBS complete media for 18 hours. After starvation, we

scratched the cells with 10 µl pipette tips and washed twice with PBS. During the assay, we incubated the cells with 0.5% exosome-free FBS complete media to slow down cell proliferation. We obtained the images from six different areas per well with the Zeiss Axio Observer Z1 microscope equipped with 20x/0.5 NA objectives at several time points. We analyzed the images with the TScratch tool [103].

3.2.6. Exosome quantification using transwell assay

We utilized a Transwell insert with 3 µm pore membrane and loaded functionalized beads at the lower compartment, and cells on the upper compartment of the insert. After 48 hours of incubation at 37°C, we collected the beads and labeled them with 4 µg/ml PE anti-CD63 antibody (BioLegend, clone H5C6) for 45 minutes at 37°C. We subsequently washed the beads three times in PBS with 1% BSA and performed imaging using a Zeiss Axio Observer Z1 microscope equipped with 20x/0.8 NA objectives. Using ImageJ, we segmented and measured the fluorescent intensity of CD63 on the beads.

3.2.7. Surface marker staining

To measure the expression of CD81, we coated the cells with 3.5 µg/ml biotinylated anti-CD81 (BioLegend, clone TAPA-1) antibody at the 37°C for 30 minutes. After one wash in PBS with 1% BSA, we stained the cells with 4 µg/ml PE-streptavidin (BioLegend) at the 37°C for 45 minutes. We used a Zeiss Axio Observer Z1 microscope equipped with 20x/0.8 NA objectives to image the cells and using ImageJ we measured the intensity of CD81 on the cells.

3.2.8. Single-cell RNA-sequencing

We labeled HCC70, MCF7, MDAMB231, MDAMB231-S, and MDAMB231-NS cells separately with the Sample-Tags from the BD Human Immune Single-Cell Multiplexing Kit (BD Biosciences, San Jose, CA), described in “Single Cell Labeling with the BD Single-Cell Multiplexing Kits” protocol. Then, we proceeded to library preparation with a mixture of ~5000 cells (approximately 1000 cells from each group). We prepared the whole transcriptome following the BD “mRNA Whole Transcriptome Analysis (WTA) and Sample Tag Library Preparation Protocol” using the BD Rhapsody System. We assessed the quality and quantity of the final library by Agilent 4200 TapeStation system using the Agilent High Sensitivity D5000 ScreenTape (Agilent Technologies, Santa Clara, CA) and a Qubit Fluorometer using the Qubit dsDNA HS Assay, respectively. We diluted the final library to 3 nM concentration and used a HiSeq PE150 sequencer (Illumina, San Diego, CA) to perform the sequencing.

3.2.9. Sequencing reads alignment

We analyzed the FASTQ files on the Seven Bridges website (https://www.sevenbridges.com/) by running the “BD Rhapsody WTA Analysis Pipeline” (BD Biosciences, San Jose, CA). After performing alignment, filtering, and sample tag detection, we downloaded the sample tag calls and molecule count information for further analysis in R (v 4.0.1) using Seurat Package [104] (v 3.0).

3.2.10. Data processing and differentially gene expression analysis

By following the standard processing workflow in Seurat Package, we performed the clustering. Briefly, we removed cells with < 8000 gene count and high mitochondrial gene expression (> 20% of the reads). Upon clustering, we

removed the cells in clusters that contained a mixture of sample tags, and we ended up with 3431 single-cell profiles (773 MDAMB231-S, 815 MDAMB231-NS, 971 MDAMB231, 645 MCF7, and 227 HCC70). Next, we identified the differentially expressed genes using *Findmarkers* function in Seurat. We selected the markers with > 1.2-fold change higher expression in MDAMB231-S in comparison to MDAMB231-NS as the gene signature for exosome secretion.

3.2.11. Gene correlation analysis and ExoCarta analysis

To calculate the spearman correlation between genes, we used *cor.test* function in R to calculate the significant correlations. Later, we plotted the heatmap of spearman coefficients with *pheatmap* package (v 1.0.12). We downloaded the list of proteins and mRNA in the ExoCarta dataset from their website (http://exocarta.org/download).

3.2.12. Gene set enrichment analysis for breast cancer cell lines

To perform pathway analysis between breast cancer cell lines, we pre-ranked the significant genes (p-value < 0.05) between each pair of cell lines calculated by *findmarkers* function in *Seurat* package. We ran the GSEA software provided by UC San Diego and Broad Institute using Broad Institute C2: curated gene sets.

3.2.13. Core signature identification and network analysis

We calculated the spearman correlation between the identified gene signature among the MDAMB231-S cells. We used *ward.D2* as a hierarchal clustering method along with *Euclidean* distance method to cluster the markers. Using the *pvclust* package (v 2.2-0) [165], we assessed the uncertainty in clustering analysis.

we used the approximately unbiased (AU) value > 95 as the criteria for a significant cluster. We plotted the heatmap using *pheatmap* package.

To build the network between markers, we used *igraph* package (v 1.2.5) [166]. First, we created an undirected network containing a list of links and nodes. The size of nodes represented the average gene expression of each marker and the links represented the spearman coefficient between each marker. Next, we removed the negative links, and to simplify the network, we removed the links which showed a smaller coefficient than the average of positive links. To visualize the network, we used the layout algorithm of layout_with_graphopt.

3.2.14. Cancer Cell Line Encyclopedia (CCLE) analysis

We downloaded the CCLE log2 transformed RNAseq TPM gene expression and the cell line information from the DepMap portal (https://depmap.org/portal/download/). To perform the correlation analysis, we filtered the gene expression matrix for the exosome gene signature and performed the spearman correlation among all 1304 cell line. For analyzing the correlation of gene signature with breast cancer subtype, first, we selected breast cancer cell lines using the *primary_disease* information of cell lines. Then, using the *lineage_molecular_subtype,* we grouped the cell lines into different subtypes.

3.2.15. Tumor Cancer Genome Atlas (TCGA) analysis

We downloaded all the TCGA data, including raw counts, RSEM gene normalized expression and clinical data from the Broad Institute FireBrowse Data Portal (www.firebrowse.org). For PAM50, tumor size, and stages analysis, we downloaded the *BRCA_clinicalMatrix* file from University of California Santa Cruz

Xena Hub Portal (https://xena.ucsc.edu/) and we used *PAM50_mRNA_nature2012*, *Tumor_nature2012*, and *AJCC_Stage_nature2012* for PAM50, tumor size and stages information, respectively. We calculated the spearman's rank correlation coefficient using *cor.test* function between the markers upregulated in MDAMB231-S and plotted using *pheatmap* package in R. For survival analysis, using the Kaplan-Meier method we compared the overall survival of patients divided by the median expression of four core exosome signature genes. Using the log-rank test We calculated the statistical significance of survival curves. To perform pathway analysis, first, we calculated the differentially expressed genes between patients divided by the median expression of four core signature genes using *DESeq2* (v 1.22.2) package [110]. We next used the pre-ranked gene list of genes with a significant *p*-value of < 0.05 to run GSEA software provided by UC San Diego and Broad Institute using Broad Institute C2: curated gene sets. We used the RSEM gene expression of breast cancer patients to estimate the relative fraction of 22 immune cell types using 1000 permutations in CIBERSORTx analytical tool. We calculated the cytolytic activity (Cyt) as the geometric mean of PRF1 and GZMA as previously described.

3.3. Results

3.3.1. Establishing monoclonal cell lines with divergent rates of exosome secretion.

To directly map the heterogeneity in exosome secretion rates within clonal cells, as I explained in chapter 2, we developed a high-throughput single-cell technique based on nanowell arrays that can detect the secretion of exosomes. The

exosomes are identified using a combination of two separate markers, CD63 and CD81 via the formation of an immunosandwich (Figure 35).

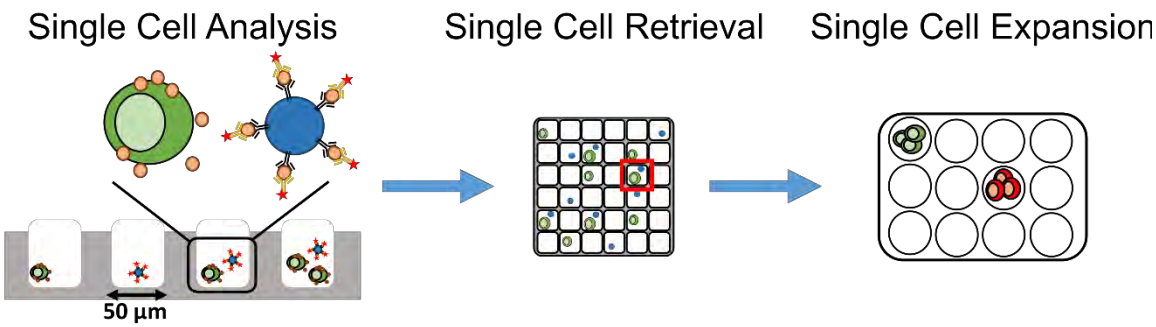

Figure 35. The workflow of single-cell analysis and monoclonal cell establishment.

We mapped the heterogeneity in exosome secretion within the metastatic triple-negative breast cancer cell line, MDAMB231. Not surprisingly, single-cell profiling identified individual cells with vastly different rates of exosome secretion within this population of MDAMB231 cells (Figure 36).

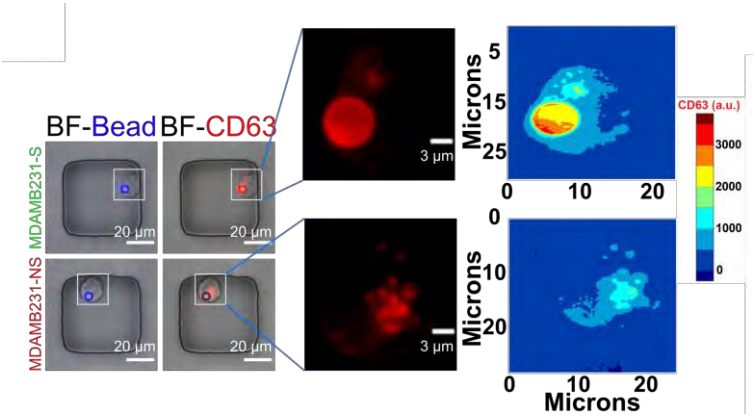

Figure 36. Representative images of MDAMB231-S and MDAMB231-NS single cells. The inserts show single cells and the contour map of CD63 (exosome) intensity.

To quantify if exosome secretion is a stably inheritable property of these single cells, we retrieved individual exosome secretor (labeled MDAMB231-S) and non-secretor cells (MDAMB231-NS) using an automated robot and expanded them to establish clonal populations. After limited expansion (<20 generations) we tested

the secretion rates of these clonal populations using our single assay and confirmed that individual cells from the MDAMB231-S population can secrete more exosomes compared to MDAMB231-NS cells. The differences in the exosome secretion capacity increased as a function of time (Figure 37).

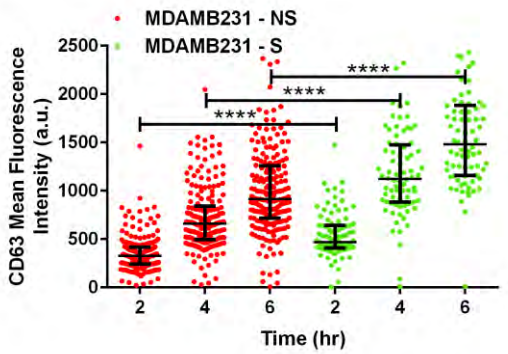

Figure 37. The rate of secretion of exosomes by cells within the MDAMB231-S and MDAMB231-NS population. Each dot represents a single cell with the median and quantiles. T-tests were used for comparison. Significance levels are shown as **** $p < 0.00001$.

Tracking the kinetics of exosome secretion, showed that more than 85% of MDAMB231-S cells secrete exosomes continuously over the six-hour period. By contrast, however, the MDAMB231-NS showed a higher percentage of cells with an initial burst secretion that stalled after four hours (Figure 38).

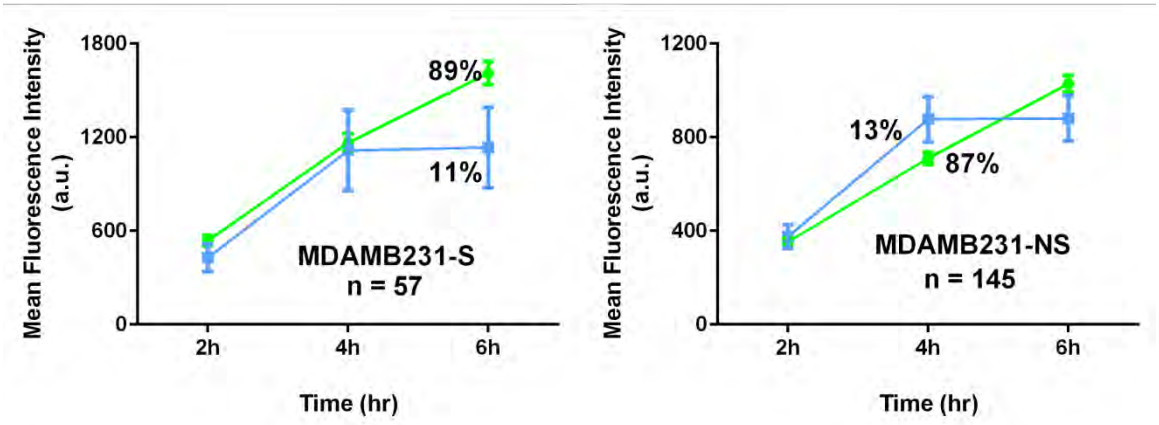

Figure 38. The kinetics of exosome secretion from individual cells that comprise the MDAMB231-S and MDAMB231-NS cell lines. The two subpopulations are shown as trend lines (mean ± SEM).

Since it has been previously shown that exosome secretion can be associated with increased migration in metastatic breast cancer cells, we compared the migratory potential of these clonal lines with divergent exosome secretion rates. To test the migratory capacity, we used a wound healing assay, and as expected MDAMB231-S cells were significantly more migratory than MDAMB231-NS cells (Figure 39). Taken together, these results showed that we can directly identify single cells with differences in rates of exosome secretion and that the exosome secretion property is maintained upon clonal expansion. The availability of the clonal populations allowed us to rapidly compare the transcriptional differences across thousands of single cells by scRNA-seq.

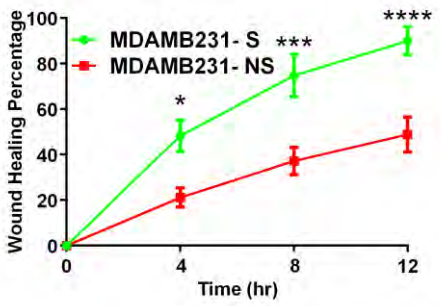

Figure 39. Wound healing assays showing the migration of MDAMB231-S and MDAMB231-NS cell lines (mean ± SEM). A two-way ANOVA test was used (n= 7 for each cell line). Significance levels are shown as * $p < 0.05$, *** $p < 0.001$, and**** $p < 0.0001$.

3.3.2. Identification of exosomes gene signature in breast cancer cells

To derive a genetic signature associated with exosome secretion, we performed scRNA-seq on cells from the MDAMB231-S and MDAMB231-NS populations using the Rhapsody platform (Figure 40).

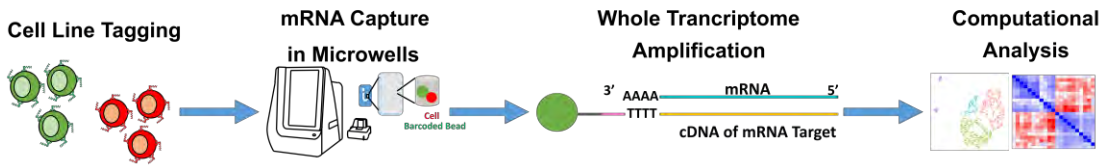

Figure 40. The workflow of single-cell RNA sequencing and whole transcriptome profiling for monoclonal cell lines.

After data processing and filtering, we identified 1970 single cells with an average of 4710 unique genes and 24,219 transcripts per cell (Figure 41A). Dimensionality reduction showed a clear separation between the two cell lines (Figure 41B).

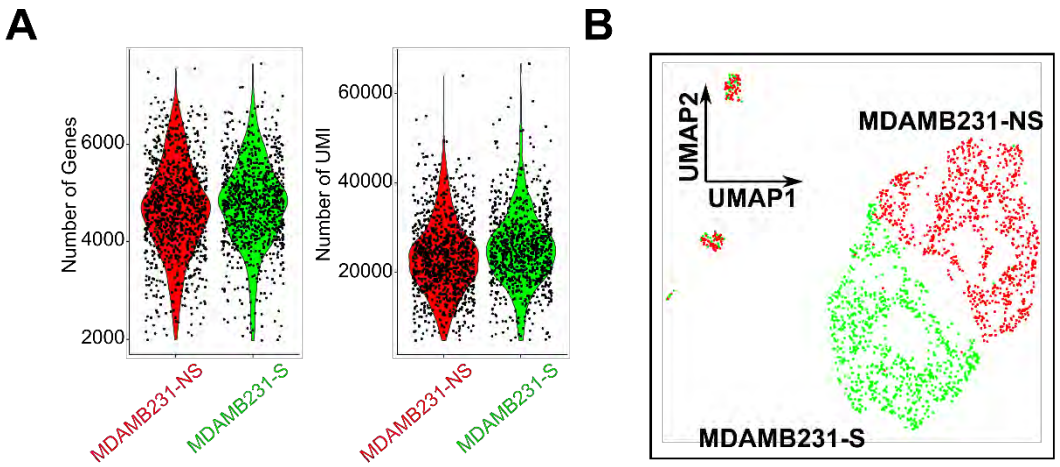

Figure 41. (A) The violin plot showing the number of genes and transcriptome per cells. (B) UMAP plot of the all detected single cells from MDAMB231-S and MDAMB231-NS cell lines.

By clustering the single cells, we were able to identify two clusters which solely consisted of the secretor and non-secretor clones (Figure 42).

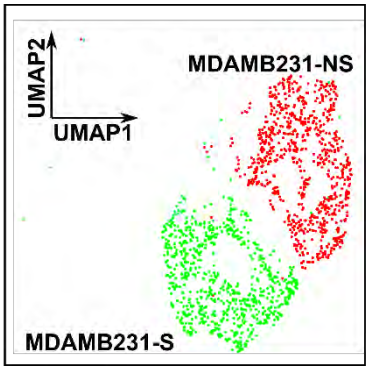

Figure 42. UMAP plot of MDAMB231-S and MDAMB231-NS cells clusters selected for further downstream analysis.

Differential gene expression analysis identified 322 genes were significantly (p-adjusted-value < 0.05) enriched in the MDAMB231-S cells compared to MDAMB231-NS cells (Supplementary table 2). To investigate if these differentially expressed genes (DEGs) are known to be associated with exosome secretion, we compared them to the molecules within the exosome database, ExoCarta [167–169]. Out of 322 DEGs, 211 DEGs were annotated within ExoCarta as mRNA, proteins, or both (Figure 43, Supplementary table 3).

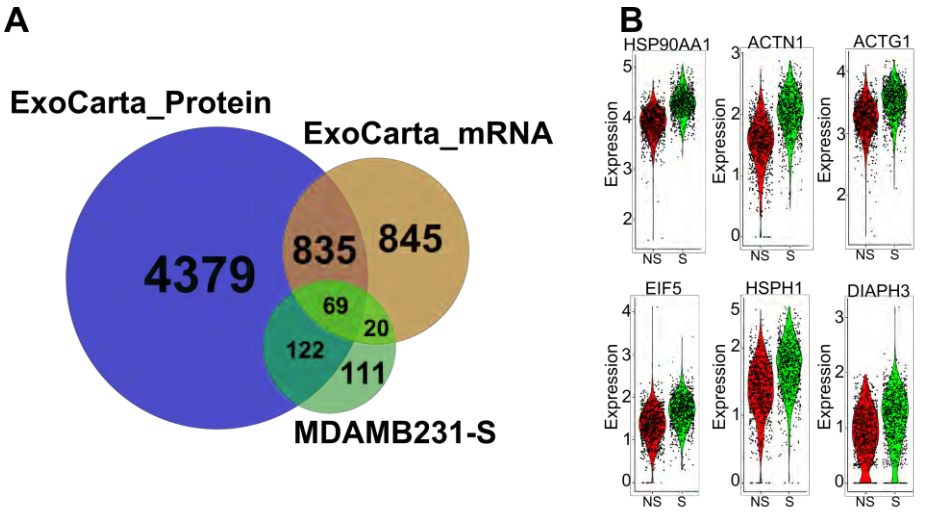

Figure 43. (A) Venn diagram of the overlap of differentially expressed genes between MDAMB231-S genes and mRNA and proteins in the ExoCarta dataset. (B) Violin plot of selected top genes upregulated in MDAMB231-S in comparison to MDAMB231-NS cells.

When we restricted the DEGs with > 1.2-fold change in the MDAMB231-S cells, we identified a set of 34 genes that are known to be associated with exosome secretion, metastasis and invasion (Figure 44). For example, exosomes expressing CAV1 have been show to transport adhesion proteins and promoted the invasion in breast cancer [156]. Similarly, FXYD5 is a glycoprotein known to reduce the cell adhesion and promote the metastasis in breast cancer cells [170], and SKA3 is a microtubule-binding subcomplex of the outer kinetochore and its expression is associated with breast cancer growth [171] and brain metastasis [172].

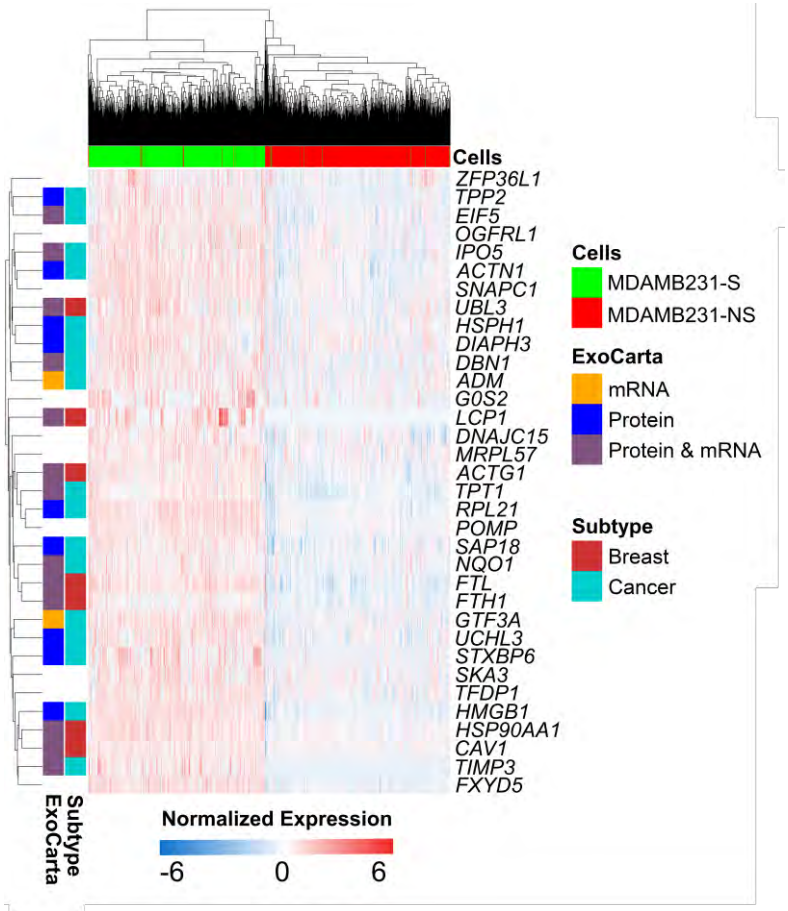

Figure 44. The heatmap of the top 34 genes upregulated in MDAMB231-S cells. The side colors represent the presence of genes in the ExoCarta dataset and previously linked to breast cancer or other cancer types.

To further refine the core gene signature, we posited that the genes associated with exosome secretion, or packaging within the exosomes, are regulated in a coordinated manner. Accordingly, we calculated the spearman coefficient between the DEGs and applied a hierarchical clustering to identify the cluster of genes that were significantly correlated with each other. By applying a multiscale bootstrap resampling method, we identified the clusters which showed the approximately unbiased (AU) value > 95. Among these clusters, *HSP90AA1* was significantly correlated with *HSPH1*, *EIF5*, and *DIAPH3* (Figure 45A, B), and these four genes were also significantly correlated with the exosome marker, CD81 (Figure 45C).

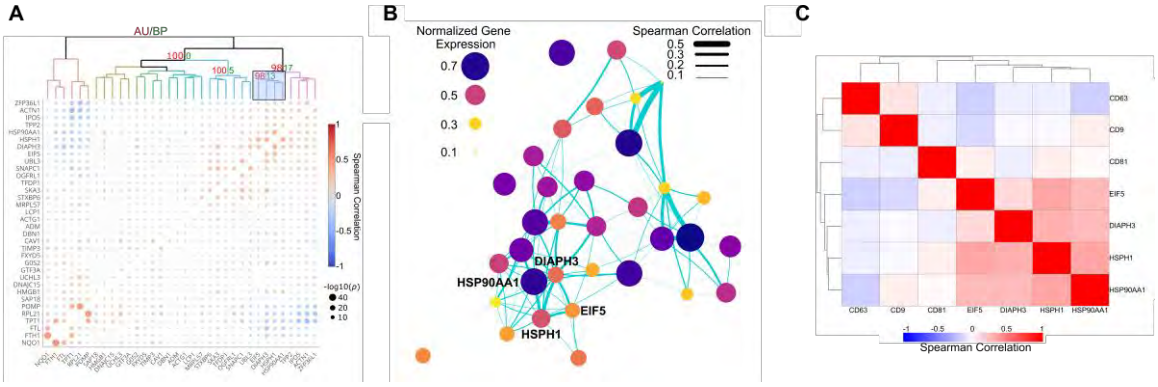

Figure 45. The heatmap of spearman coefficients correlation (A) and the connection network (B) between top genes in MDAMB231-S cells with four core exosome genes highlighted. (C) The spearman coefficient correlation between the four core exosome genes and surface markers CD63, CD81, and CD9 in MDAMB231-S cells.

Previously, it is shown that DIAPH3 can activate the beta-catenin/TCF signaling by binding to HSP90 which results in growth, migration, epithelial-mesenchymal transition, and metastasis in hepatocellular carcinoma cells [173]. Taken together, scRNA-seq on MDAMB231 secretor and non-secretor cells identified a core gene cellular signature (Exo-sig) of CD81-expressing exosomes.

3.3.3. Rate of exosome secretion in breast cancer cells

To validate whether Exo-sig can predict the secretion of exosomes we investigated three breast cancer cell lines, MDAMB231, MCF7, and HCC70 with differences in metastatic potential. MDAMB231 and HCC70 cell lines are both triple-negative cancer cells while the MCF7 is an estrogen-receptor (ER) and progesterone-receptor (PR) positive cancer cell line [174]. We performed scRNA-seq on MDAMB231, MCF7, and HCC70 cell lines, and we obtained an average of 4459 unique genes and 22,071 transcripts per cell (Figure 46A). After dimensionality reduction, all three cell lines clustered separately (Figure 46B), and a total of 2634 DEGs (> 1.2-fold change) were identified.

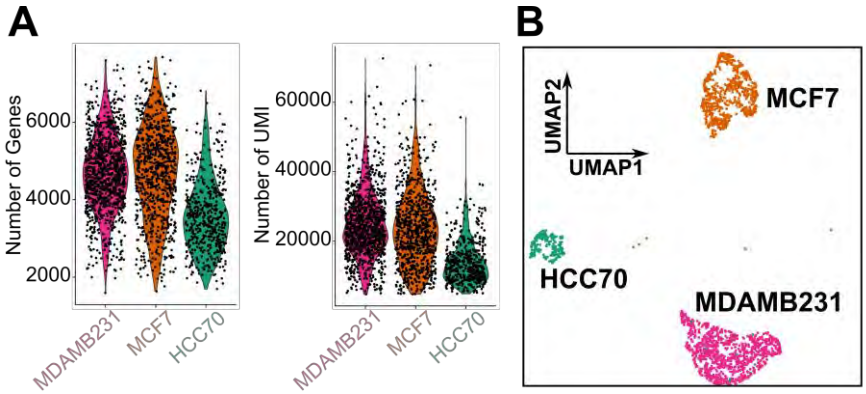

Figure 46. (A) The violin plot showing the number of genes and transcriptome per cells. (B) The UMAP plot of MDAMB231, MCF7, and HCC70 cells clusters analyzed by scRNA-seq.

To validate the phenotype of the cancer cell lines in the scRNA-seq data, we compared the expression of DEGs with known markers for breast cancer subtypes including luminal, basal-A, and basal-B [174]. The gene expression showed that markers for luminal (e.g. *GATA3*, *FOXA1*, *KRT18*, and *KRT19*), basal-A (e.g. *SLPI*, *KRT16*, and *KRT6B*) and basal-B (e.g. *AXL*, *CAV1*, *VIM*, and *SEPRINE1*) subtype

were, respectively, upregulated in MCF7, HCC70 and MDAMB231 cell lines (Figure 47).

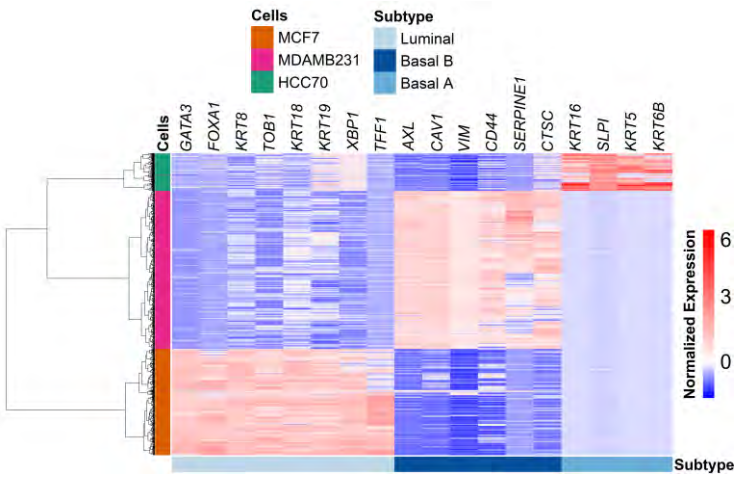

Figure 47. The heatmap of expression of genes associated with luminal, basal A and, basal B breast cancer subtypes in MDAMB231, MCF7, and HCC70 cell lines.

Similarly, pathway analysis confirmed that MDAMB231 and MCF7 cell lines are enriched for genes enriched in pathways corresponding to basal and luminal phenotype, respectively (Figure 48).

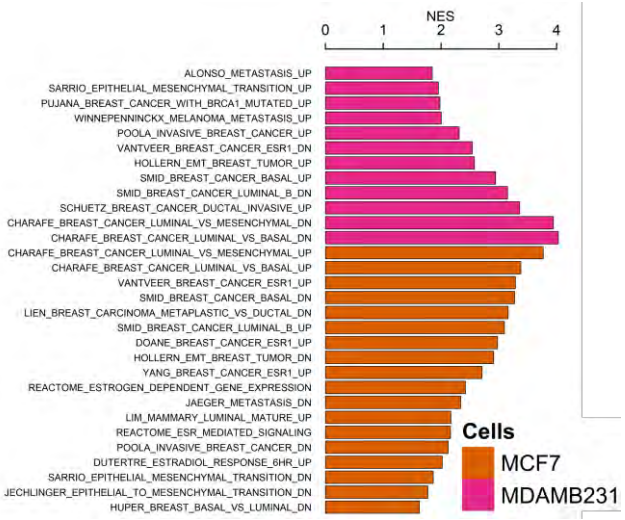

Figure 48. The normalized enrichment score (NES) of pathways associated with metastasis, luminal, and basal breast cancer subtypes by pairwise comparison between MDAMB231 and MCF7cell lines.

Consistent with the fact that HCC70 was derived from a primary tumor, pathway analysis showed a lower score for metastatic and epithelial-mesenchymal transition pathways in comparison to the MDAMB231 and MCF7 cell lines (Figure 49).

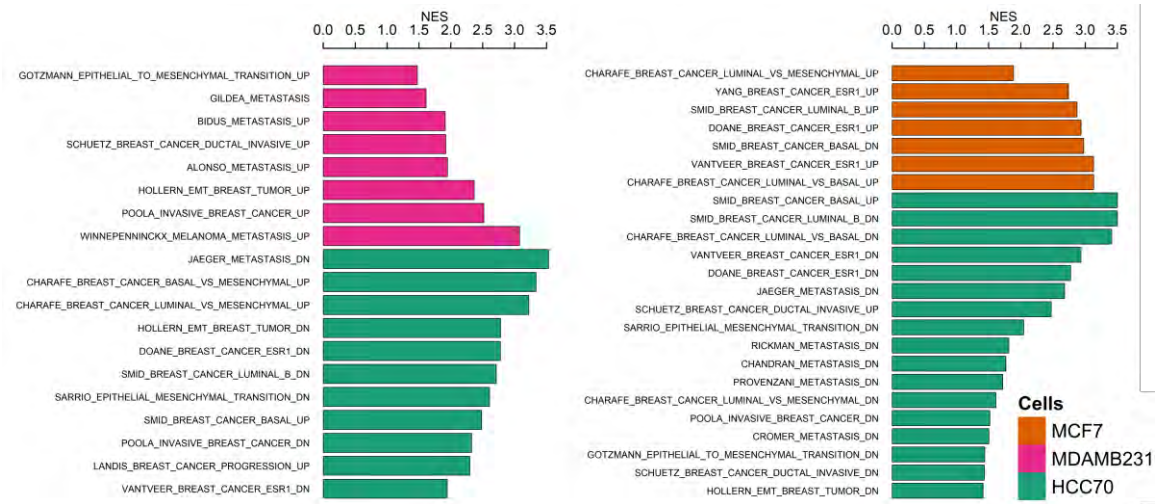

Figure 49. The normalized enrichment score (NES) of pathways associated with metastasis, luminal, and basal breast cancer subtypes by pairwise comparison between MDAMB231 vs HCC70, and MCF7 vs HCC70 cells.

To validate the invasion phenotype of cell lines, we used a wound healing assay, and as expected MDAMB231 cells the highest motility, while the HCC70 cell lines completely failed in migration and closing the wound (Figure 50).

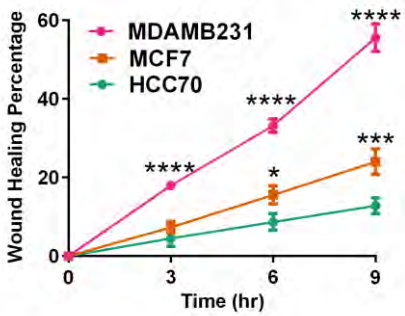

Figure 50. Wound healing assays showing the migration of MDAMB231, MCF7, and HCC70 cell lines (mean ± SEM). A two-way ANOVA test was used (n= 7 for each cell line). Significance levels are shown as * $p < 0.05$, *** $p < 0.001$, and **** $p < 0.0001$.

To predict the secretion of exosomes from these three cell lines, first, we compared the number of DEGs shared between HCC70, MCF7 and MDAMB231-S cells. The results showed that MCF7 and HCC70 shared 33 and 29 DEGs with the MDAMB231-S, respectively (Figure 51).

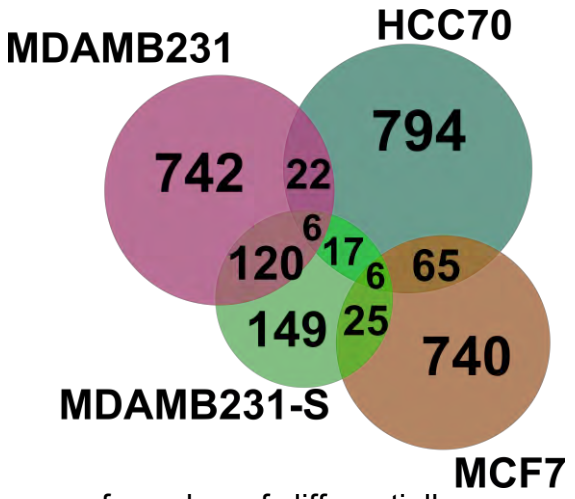

Figure 51. Venn diagram of overlap of differentially expressed genes between MDAMB231, MCF7, HCC70, and MDAMB231-S.

Comparing the average expression of Exo-sig showed ordered expression across the three cell lines: HCC70 has the lowest expression, MCF7 had an intermediate expression and MDAMB231 had the highest expression (Figure 52).

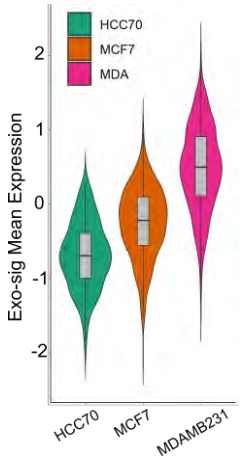

Figure 52. The violin plot showing the average expression of four core exosome genes in MDAMB231, MCF7, and HCC70 cell lines.

Consistent with this observation, the spearman correlation between these markers showed a significant correlation in the MDAMB231 cell line while these correlations were smaller in MCF7 and HCC70, respectively (Figure 53).

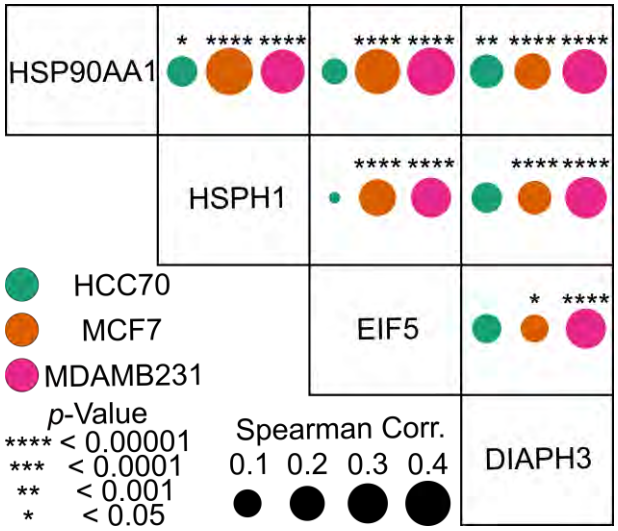

Figure 53. The spearman coefficient correlation of four core exosome genes in MDAMB231, MCF7, and HCC70 cell lines.

As shown above, since Exo-sig is associated with CD81/CD63 exosomes, we compared the expression of *CD63*/*CD81* within the scRNA-seq data. Not surprisingly, while both MDAMB231 and MCF7 showed expression of *CD63* and *CD81*, HCC70 cells showed low expression of *CD81* (Figure 54).

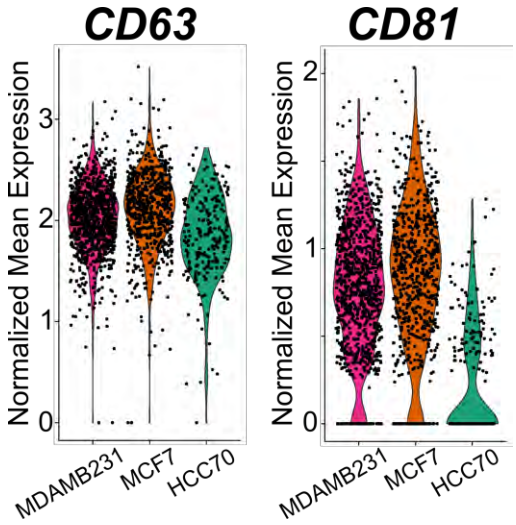

Figure 54. The violin plot showing the expression of exosome surface markers, *CD63* and *CD81* in MDAMB231, MCF7, and HCC70 cell lines.

Taken together, based on Exo-sig, scRNA-seq predicted that exosome secretion rate was likely to increase in an order manner from HCC70 (lowest) to MDAMB231 (highest) (Figure 52).

We utilized our single cell assay to directly profile the rates of exosome secretion from each of these three cell lines. As predicted, HCC70 cells had a very low rate of exosome secretion, MCF7 cells had an intermediate rate of secretion and MDAMB231 cells had a high rate of exosome secretion (Figure 55).

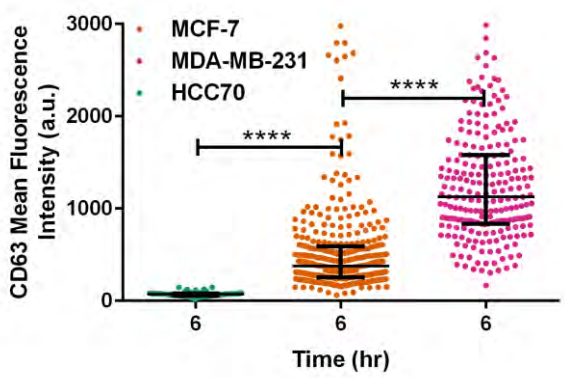

Figure 55. The rate of secretion of exosomes by cells within the MDAMB231, MCF7, and HCC70 cell lines at six hours. Each dot represents a single cell with the median and quantiles. T-tests were used for comparison. Significance levels are shown as **** $p < 0.00001$.

We also independently validated these results using a transwell assay to capture the exosome secreted from the entire population of cells (Figure 11A). These results again showed that HCC70 secreted fewer exosomes compared to MDAMB231 cells (Figure 56).

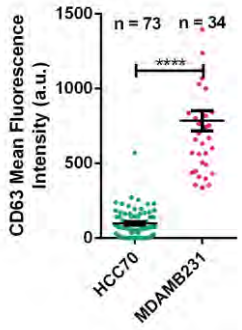

Figure 56. The rate of secretion of exosomes by cells in the culture media of the MDAMB231 and HCC70 cell lines at 48 hours. Each dot represents the CD63 (exosome) intensity on the bead (mean ± SEM). T-tests were used for comparison. Significance levels are shown as **** $p < 0.0001$.

To further understand the differences between MCF7 and MDAMB231 cells we quantified the kinetics of exosome secretion by imaging at two, four and six hours. Consistently at every time point, MDAMB231 cells showed increased rate of exosome secretion compared to MCF7 cells (Figure 57).

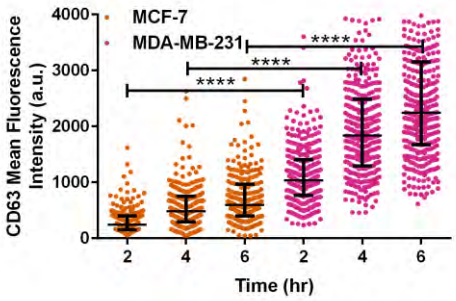

Figure 57. The rate of secretion of exosomes by cells within the MDAMB231 and MCF7 cell lines at two, four, and six hours. Each dot represents a single cell with the median and quantiles. T-tests were used for comparison. Significance levels are shown as **** $p < 0.00001$.

Tracking the kinetics of exosome secretion, cells secreting exosomes continuously was the dominant phenotype in both cell lines (Figure 58). In summary, these combined scRNA-seq and exosome profiling results show that the more invasive cells have a higher rate of exosome secretion and that Exo-sig can predict cells with different rates of exosome secretion.

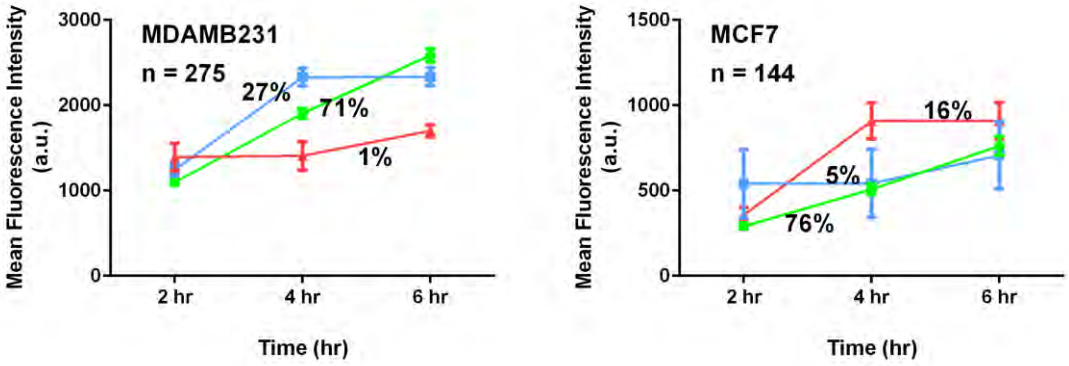

Figure 58. The kinetics of exosome secretion from individual cells that comprise the MDAMB231 and MCF7 cell lines. The three subpopulations are shown as trend lines (mean ± SEM).

To generalize the value of Exo-sig, we obtained the gene expression of 1304 cell lines available in the Broad Institute Cancer Cell Line Encyclopedia (CCLE). Even within this expanded dataset the Exo-sig genes showed high correlation with each other (Figure 59A). Focusing specifically on breast cancer, Exo-sig showed highest expression in basal-B phenotypes, followed by Basal-A, HER2-enriched, and luminal (Figure 59B). This is consistent with the known aggressiveness of each of these subtypes of breast cancer. The validation of Exo-sig as a core signature of exosome secretion within these cell lines allowed us to investigate exosome secretion within cancer patients.

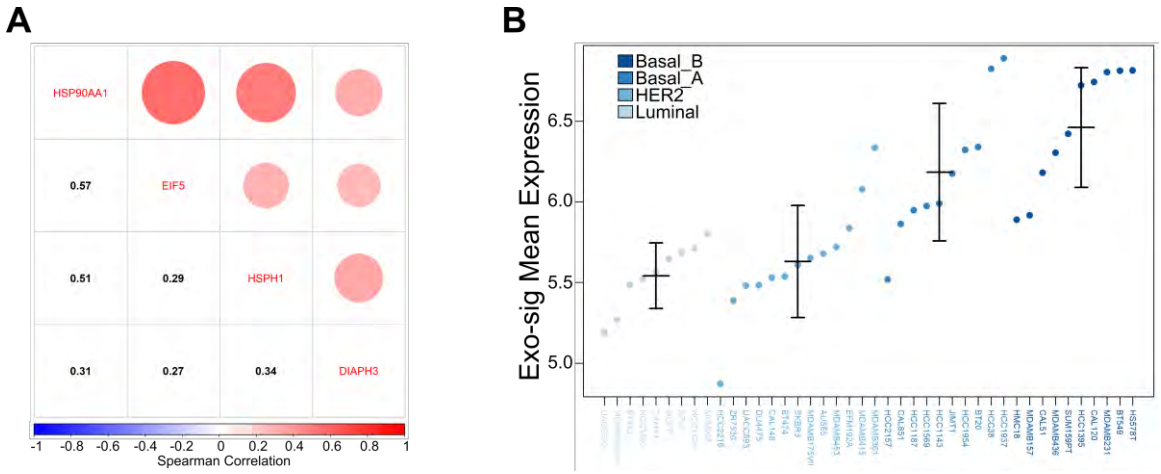

Figure 59. (A) The spearman coefficient correlation of four core exosome genes in the CCLE dataset cell lines. (B) The average expression of the top genes identified from MDAMB231-S cells in breast cancer cell lines available on the CCLE dataset.

3.3.4. Impact of Exo-sig on clinical breast cancer outcomes

To investigate the translational value of Exo-sig, we took advantage of the TCGA and interrogated the combined transcriptomic and clinical/pathological annotations for 1093 patients with breast cancer. We first confirmed using Spearman correlation that the four genes that comprised Exo-sig are also significantly correlated with each other within human breast cancers (Figure 60).

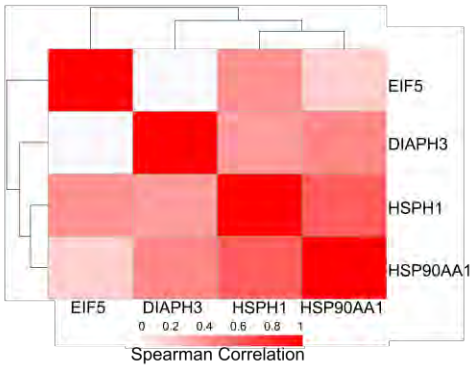

Figure 60. The spearman coefficient correlation of four core exosome genes in breast cancer patients available on the TCGA dataset.

We stratified the patients into two groups: high exosome expression (Exo^{Hi}) and low exosome expression (Exo^{Lo}) based on Exo-sig. The overall survival was

significantly lower for Exo^{Hi} patients in comparison to the Exo^{Lo} patients (median survival 10.8 vs 7.5 years, HR: 2.3, 95% CI: 1.53-3.45), suggesting that exosome secretion is associated with worse survival in breast cancers (Figure 61).

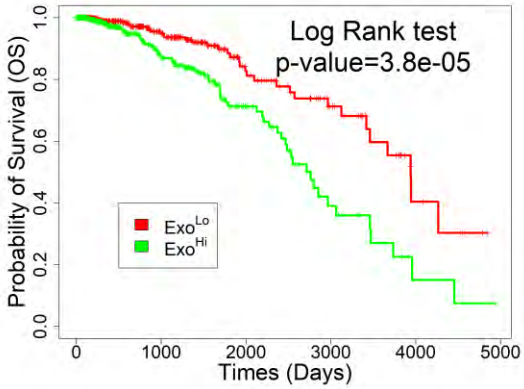

Figure 61. The overall survival of breast cancer patients divided by the median of the average expression of four core exosome genes, Exo^{Hi} and Exo^{Lo}.

Quantification of the pathology of the disease showed that Exo-sig was associated with increased tumor size and more advanced disease in patients (Figure 62A, B). This clinical data is consistent with our *in vitro* cell line data (Figure 50).

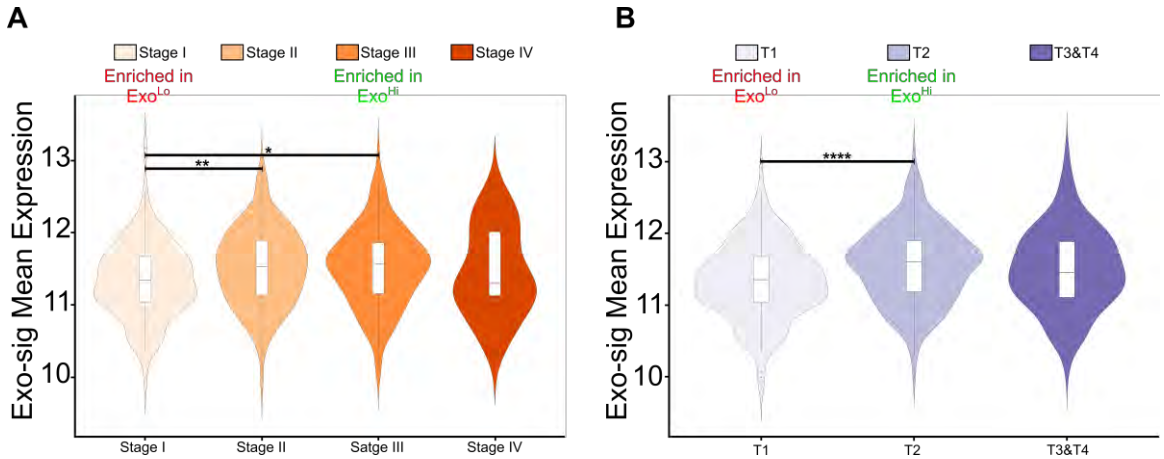

Figure 62. The violin plot showing the average expression of four core exosome genes grouped by (A) the breast cancer stages, stage I, stage II, stage III, and stage IV (B) the size of the tumor, T1, T2, and T3&T4. One-way Anova tests were used for comparison. Significance levels are shown as * $p < 0.05$, ** $p < 0.01$, *** $p < 0.001$, and **** $p < 0.0001$.

We next use Exo-sign and the transcriptomics to stratify the different subtypes of breast cancers. The Exo^{Lo} tumors were enriched in normal-like and luminal breast cancers whereas the Exo^{Hi} tumors were enriched in basal breast cancers (Figure 63).

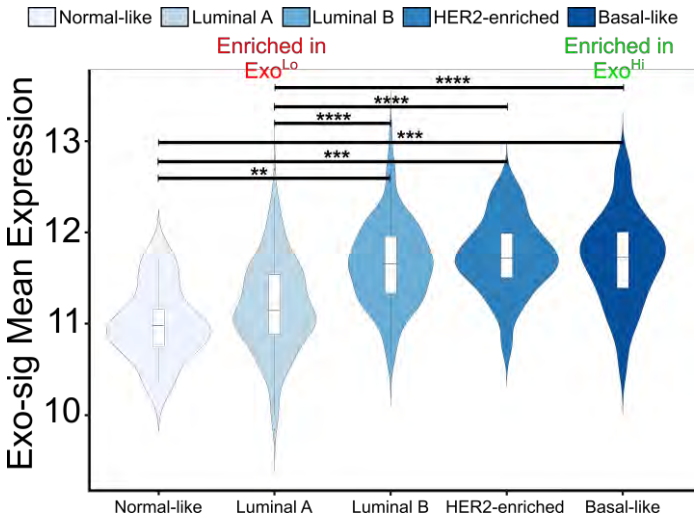

Figure 63. The violin plot showing the average expression of four core exosome genes grouped by the breast cancer subtypes, normal-like, luminal A, luminal B, HER2-enriched, and basal-like. One-way Anova tests were used for comparison. Significance levels are shown as * $p < 0.05$, ** $p < 0.01$, *** $p < 0.001$, and **** $p < 0.0001$.

Gene set enrichment analysis (GSEA) specifically focused on pathways associated with tumor cell functions illustrated that the Exo^{Hi} tumors are enriched in pathways associated with invasiveness, metastasis and epithelial to mesenchymal transition (EMT) in comparison to the Exo^{Lo} tumors (Figure 64). Taken together, the clinicopathological data are consistent with our in vitro observation that exosome secretion is associated with increased aggressiveness and invasion of tumor cells.

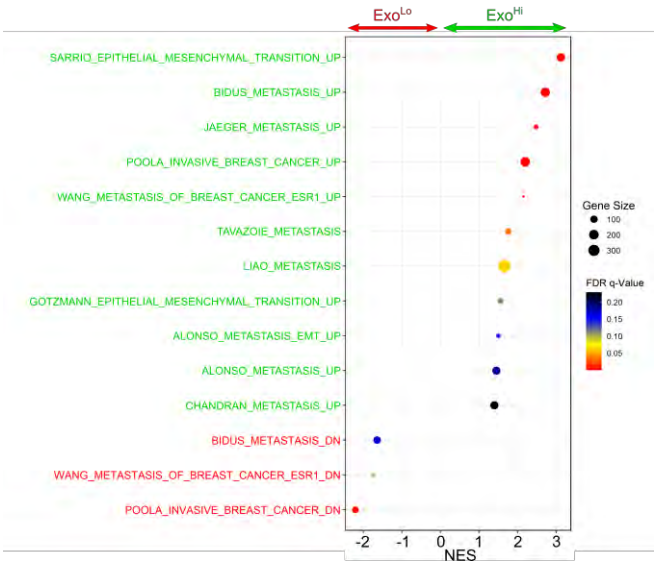

Figure 64. The normalized enrichment score (NES) of pathways associated with metastasis in the Exo^{Hi} and Exo^{Lo} patients.

To identify if the nature and frequency of the immune cell infiltrate is associated with the decreased overall survival observed in patients with higher expression of exosomes, we used the normalized gene expression data to quantify the relative frequencies of the 22 different immune cell types using the CIBERSORTx algorithm. Exo^{Lo} tumors had an increased frequency of CD8 T cells, increased cytolytic activity (associated with increased expression of both *PRF1* and *GZMA*), and increased frequency of *TBX21* expression in comparison to Exo^{Hi} tumors (Figure 65A-C). Collectively, these results suggest that increased exosome secretion within tumors is associated with decreased CD8+ T cell infiltration and this in turn can promote larger and more aggressive tumors.

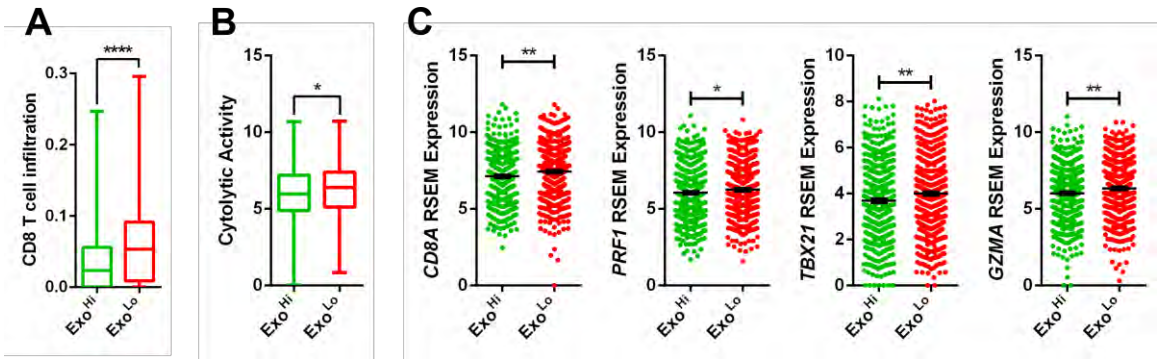

Figure 65. (A) CD8 T cells infiltration and (B) cytolytic activity score in the Exo^{Hi} and Exo^{Lo} patients. The median and quantiles of the scores are shown. (C) Normalized expression of CD8 T cells signature, *CD8A*, *PRF1*, *TBX21*, *GZMA* in the Exo^{Hi} and Exo^{Lo} patients (mean ± SEM). T-tests were used for comparison. Significance levels are shown as * $p < 0.05$, ** $p < 0.01$, *** $p < 0.001$, and **** $p < 0.0001$.

3.4. Discussion

Exosomes released from tumor cells contain biological molecules which can modulate the tumor microenvironment and play an essential role in metastasis and cancer therapy. Marleau and et al., showed that removing the exosomes can improve the response to trastuzumab in HER2+ breast cancer patients [175]. Delivery of let-7 miR by modified exosomes to EGFR+ breast cancer inhibited tumor development in mice [176]. Therefore, controlling exosome biogenesis or altering its content can open up opportunities for developing novel cancer therapy and drug delivery methods. However, despite our broad knowledge of mechanisms involved in the secretion of exosomes, there are still unknown machinery systems to be discovered. Isolation and profiling the exosomes by traditional techniques fail to map the source of exosomes in the cell of origin and not all the cellular signaling pathways can be identified. Also, several studies have profiled the exosome secretion in single cells and showed that single cells secrete diverse and heterogenous exosomes [80,142]. Therefore, to profile cells upon the secretion of

exosomes, an integrated technique is needed to simultaneously screen the secretion and profile the cellular components of cells.

Here, we sought to profile the metastatic MDAMB231 breast cancer monoclonal cells with different potential in the secretion of exosomes. First, we screened the single cells for their secretion by a high-throughput single-cell technique we previously described in chapter 2. Using the high-throughput technique we were able to distinguish and retrieve single cells for further analysis. Then, we used scRNA-seq to profile the transcriptome of the two cell lines established from single cells which showed high and low secretion. We identified several biomarkers were shown to be associated with exosomes secreted from breast cancer cells. For example, it was shown that Caveolin-1 (encoded by CAV1) containing exosomes can enhance the proliferation and invasion of metastatic cells [177]. It has been also shown that UBL3 can enhance the sorting of cargo in exosomes by acting as a post-translational modification factor [178]. Jenjaroenpun et al., showed that FTL and FTH1 are highly upregulated in exosomes isolated from MDAMB231 cell lines [179,180] and lymphocyte cytosolic protein 1 (encoded by LCP1) secreted from exosomes of metastatic breast and melanoma cells can mediate the tumor microenvironment [181,182].

We identified four genes *HSP90AA1*, *HSPH1*, *EIF5*, *DIAPH3* as core exosomes gene signature which can predict the secretion of exosomes. The results showed that these genes are highly correlated in both MDAMB231-S cells and 1304 cell lines available in CCLE. Also, all four genes have already been found in exosomes secreted by cancer cells. HSP90AA1 is one of the heat shock proteins (HSPs) its

extracellular role has been linked to the increased motility and invasion in cancer cells [183]. This protein can be secreted by breast cancer cells through exosomes and increase the migration and metastasis capability of tumor cells [184]. Recently, Hoshino and et al., showed that HSP90AA1 is expressed in exosomes of more than 80% of cell lines [185]. It has also been shown that HSPH1 is expressed in exosomes secreted by melanoma [186], ovarian [187], and colorectal cancer cells [188]. EIF5 has been associated with hepatocellular carcinoma exosomes [189] and DIAPH3 was found to be enriched in exosomes secreted by colorectal cancer cells [34]. Our results showed that the expression and correlation of these genes can predict the secretion of exosomes from breast cancer cell lines. As we tested the MDAMB231, MCF7, and HCC70 cell lines, we found that higher expression of these genes was reflected in the higher secretion of exosomes from the MDAMB231 cell line. MDAMB231 is a triple-negative breast cancer (basal-like) cell line and associated with tumor invasion and poor survival upon metastasis [190]. Our results showed that the gene expression of exosome markers can predict the higher secretion of exosomes from basal-like subtype cancer cells. Taken together, we identified markers that can predict the secretion of exosomes from breast cancer cells.

Further, we investigated the effect of the core exosome gene signature in the outcome of patients available on The Cancer Genome Atlas (TCGA). the results demonstrated a poor survival associated with the high expression of exosome markers. To explain the poor survival associated with high expression of markers, we quantified the infiltration of immune cells using the CIBERSORTx

deconvolution algorithm [112]. The results showed that poor survival is associated with a significant decrease in the CD8 T cell infiltration. Also, this result was observed in the low cytolytic score which is known as an index for cancer immunity [111]. We, further, evaluated whether the exosome markers can predict the cancer subtype and invasion of patients. The results showed that the expression of exosome markers was lower in patients with luminal subtype and their expression increased by more aggressive subtype such as basal-like and HER2-enriched subtypes. Also, the tumor size and stage of cancer increased as the average expression of exosomes markers increased, showing the correlation of identified genes with the invasiveness of cancer.

In conclusion, we aimed to identify the key cellular molecules involved in the formation and release of the exosome. In this study, we introduced the significance of exosome markers which are associated with tumor prognosis. Also, using the scRNA-seq we were able to identify several novel markers that might be associated with the secretion of exosomes. However, further functional explorations are required to investigate the functions of these markers in the secretion of exosomes.

Supplementary Tables

Supplementary Table 2. DEGs identified in MDAMB231-S cells

	p_val	avg_logFC	pct.1	pct.2	p_val_adj
FTL	3.25E-197	0.7202	1	1	6.81E-193
TIMP3	2.65E-189	0.684679	0.772	0.039	5.56E-185
SNAPC1	3.72E-105	0.618307	0.994	0.972	7.78E-101
FXYD5	4.54E-147	0.613699	0.997	0.988	9.50E-143
G0S2	8.52E-39	0.503925	0.864	0.679	1.78E-34
ACTN1	1.40E-111	0.473523	1	0.988	2.93E-107
RPL21	3.77E-168	0.456343	1	1	7.90E-164
LCP1	4.94E-106	0.450469	0.555	0.059	1.03E-101
HMGB1	6.96E-174	0.398048	1	1	1.46E-169
POMP	7.94E-134	0.384086	1	0.999	1.66E-129
OGFRL1	7.77E-64	0.383265	0.977	0.869	1.63E-59
HSP90AA1	3.66E-124	0.378335	1	1	7.65E-120
GTF3A	2.52E-84	0.370392	0.992	0.948	5.28E-80
TPP2	1.39E-78	0.370058	0.836	0.479	2.90E-74
NQO1	1.21E-43	0.365837	1	0.985	2.54E-39
IPO5	1.00E-66	0.361782	0.975	0.893	2.10E-62
ADM	2.34E-35	0.356058	0.984	0.946	4.91E-31
STXBP6	1.97E-73	0.349169	0.708	0.309	4.13E-69
UCHL3	9.50E-70	0.337897	0.995	0.957	1.99E-65
TFDP1	5.84E-65	0.330891	0.991	0.955	1.22E-60
TPT1	1.18E-130	0.323696	1	1	2.47E-126
HSPH1	1.06E-51	0.314137	0.995	0.985	2.21E-47
EIF5	1.50E-57	0.313741	1	0.987	3.14E-53
FTH1	2.09E-57	0.313198	1	1	4.39E-53
SAP18	1.90E-81	0.310996	1	0.995	3.98E-77
UBL3	2.45E-45	0.308859	0.887	0.72	5.12E-41
ZFP36L1	1.38E-19	0.3067	0.992	0.969	2.88E-15
DBN1	9.05E-57	0.304801	0.893	0.69	1.89E-52
CAV1	7.12E-65	0.294491	1	0.999	1.49E-60
SKA3	5.68E-38	0.293225	0.916	0.827	1.19E-33
DIAPH3	1.51E-26	0.281176	0.942	0.904	3.15E-22
DNAJC15	1.11E-49	0.273965	0.988	0.95	2.32E-45
ACTG1	4.12E-75	0.271669	1	1	8.63E-71
MRPL57	1.94E-53	0.269731	0.999	0.973	4.06E-49
SLIRP	5.01E-54	0.258274	0.999	1	1.05E-49
EMP2	2.55E-44	0.253305	0.843	0.596	5.35E-40
ZYX	3.52E-35	0.252229	0.978	0.892	7.36E-31

Supplementary table 2 (Continued)

EIF2S1	2.24E-42	0.250329	0.984	0.951	4.69E-38
TBC1D4	2.74E-30	0.249007	0.642	0.398	5.73E-26
PAPOLA	2.14E-34	0.245771	0.99	0.973	4.49E-30
KISS1	6.79E-32	0.244231	0.965	0.886	1.42E-27
SEC22B	6.92E-36	0.239924	0.966	0.91	1.45E-31
LY6E	2.25E-38	0.239817	0.885	0.707	4.70E-34
SLC9A3R2	1.69E-29	0.239474	0.931	0.831	3.53E-25
TXN	1.35E-52	0.238684	1	1	2.83E-48
CKAP2	1.35E-06	0.23578	0.829	0.773	0.028316
SLC7A1	1.75E-27	0.235318	0.735	0.521	3.66E-23
PHGDH	8.03E-81	0.233213	0.468	0.052	1.68E-76
MRPS31	3.78E-36	0.233093	0.925	0.793	7.92E-32
TFRC	3.02E-26	0.232459	0.97	0.934	6.33E-22
CDCA4	2.62E-19	0.227478	0.933	0.86	5.48E-15
ERH	1.19E-59	0.22687	1	0.998	2.49E-55
UFM1	1.03E-36	0.226475	0.974	0.894	2.17E-32
HMGA1	8.99E-58	0.225912	1	1	1.88E-53
ACAT2	1.62E-28	0.22555	0.951	0.853	3.39E-24
ASNS	1.37E-09	0.224951	0.701	0.616	2.87E-05
KRT18	2.70E-34	0.221779	0.995	0.977	5.66E-30
CTSD	6.36E-25	0.221328	0.886	0.74	1.33E-20
HNRNPA3	1.81E-38	0.217372	0.999	0.994	3.78E-34
ARGLU1	2.61E-27	0.216928	0.935	0.838	5.47E-23
EEF1A1	8.94E-101	0.21651	1	1	1.87E-96
MT1X	6.54E-09	0.216298	0.988	0.969	0.000137
MTMR6	6.83E-25	0.214403	0.801	0.623	1.43E-20
PDLIM7	1.15E-27	0.213086	0.966	0.883	2.40E-23
ATP5MPL	3.44E-39	0.212619	0.996	0.989	7.20E-35
CC2D2A	5.58E-49	0.211519	0.569	0.225	1.17E-44
RPS29	2.57E-57	0.210966	1	1	5.39E-53
PSMC1	5.53E-35	0.210714	0.997	0.989	1.16E-30
TEX30	1.71E-25	0.21063	0.841	0.654	3.58E-21
EXOSC8	1.13E-27	0.210583	0.977	0.94	2.37E-23
UBR4	7.70E-25	0.207756	0.987	0.941	1.61E-20
FCF1	1.31E-27	0.207344	0.944	0.853	2.74E-23
SNW1	1.47E-27	0.20647	0.984	0.925	3.07E-23
MDK	4.84E-36	0.204032	0.609	0.317	1.01E-31
KTN1	7.82E-19	0.202761	0.99	0.983	1.64E-14
HNRNPH1	3.81E-24	0.202434	0.991	0.96	7.98E-20
ITM2B	2.16E-30	0.202241	0.966	0.902	4.53E-26

Supplementary table 2 (Continued)

SRSF5	1.94E-27	0.200972	0.995	0.99	4.06E-23
KPNA3	1.68E-26	0.200566	0.97	0.917	3.51E-22
PLS3	7.70E-25	0.200289	0.975	0.918	1.61E-20
DIS3	2.59E-23	0.199927	0.841	0.685	5.41E-19
DYNC1H1	5.47E-18	0.199504	0.921	0.804	1.15E-13
STK24	1.14E-27	0.197317	0.934	0.815	2.40E-23
PSMA3	1.17E-34	0.196915	0.999	0.995	2.45E-30
TPM4	1.33E-30	0.195069	1	0.998	2.79E-26
NAMPT	7.41E-21	0.19264	0.955	0.893	1.55E-16
NCL	3.24E-33	0.19235	1	0.999	6.79E-29
TMED10	7.32E-27	0.191719	0.995	0.974	1.53E-22
TMX1	1.25E-21	0.191648	0.988	0.945	2.61E-17
MED4	1.26E-26	0.189841	0.893	0.731	2.64E-22
SET	5.53E-37	0.188472	1	0.998	1.16E-32
KRT8	1.34E-21	0.186775	0.969	0.924	2.80E-17
PLAC8	2.49E-21	0.186575	0.992	0.985	5.21E-17
DKC1	7.83E-22	0.186194	0.964	0.904	1.64E-17
ERG28	5.20E-28	0.185843	0.805	0.58	1.09E-23
GLIPR1	1.25E-18	0.18583	0.915	0.782	2.61E-14
TM9SF2	3.66E-22	0.18568	0.907	0.798	7.66E-18
RRP15	4.76E-23	0.185667	0.979	0.958	9.97E-19
PDS5B	1.90E-27	0.185606	0.664	0.425	3.98E-23
SUGT1	5.53E-24	0.183626	0.969	0.913	1.16E-19
CALM1	3.84E-57	0.181678	1	1	8.04E-53
IRS1	1.19E-19	0.180118	0.827	0.669	2.49E-15
BZW1	2.55E-32	0.177366	1	0.999	5.34E-28
CNN2	4.48E-22	0.177052	0.997	0.994	9.39E-18
LRR1	1.63E-22	0.175522	0.899	0.799	3.42E-18
FOSL1	6.13E-17	0.175207	0.994	0.974	1.28E-12
RCOR1	1.66E-17	0.174719	0.7	0.547	3.47E-13
C4BPB	3.66E-22	0.174205	0.505	0.28	7.67E-18
ALG5	1.50E-23	0.173949	0.904	0.775	3.15E-19
RFC3	3.22E-12	0.172084	0.882	0.811	6.74E-08
LBR	8.72E-12	0.171848	0.978	0.945	1.83E-07
GTF2F2	4.72E-17	0.171645	0.997	0.983	9.89E-13
NDUFB1	1.27E-22	0.171424	0.997	0.991	2.66E-18
IL11	1.67E-13	0.171315	0.612	0.443	3.50E-09
TOP1	8.14E-13	0.171231	0.968	0.929	1.70E-08
EFHD2	2.09E-18	0.171115	0.965	0.907	4.38E-14

Supplementary table 2 (Continued)

XRCC5	2.67E-33	0.170791	1	1	5.58E-29
RB1	3.72E-19	0.170415	0.89	0.788	7.79E-15
FRMD6	1.58E-14	0.169971	0.965	0.908	3.30E-10
MPP5	1.90E-14	0.169934	0.882	0.796	3.98E-10
RTRAF	7.14E-26	0.169075	0.986	0.974	1.50E-21
LASP1	3.28E-18	0.168883	0.97	0.95	6.86E-14
HNRNPD	3.23E-23	0.168063	0.997	0.994	6.77E-19
RAB4A	8.00E-22	0.167994	0.802	0.621	1.68E-17
PTMA	6.21E-61	0.164524	1	1	1.30E-56
NDUFAF2	4.44E-21	0.164135	0.974	0.941	9.29E-17
MZT1	6.69E-16	0.162046	0.911	0.834	1.40E-11
NDFIP2	2.55E-24	0.161714	0.713	0.491	5.34E-20
KRT81	1.46E-21	0.161391	0.308	0.119	3.05E-17
SLC1A5	9.14E-12	0.160861	0.99	0.979	1.91E-07
AKT1	4.71E-19	0.160267	0.924	0.823	9.87E-15
LAMP1	3.93E-15	0.159981	0.959	0.919	8.22E-11
GNPNAT1	1.66E-18	0.159433	0.974	0.948	3.49E-14
CDC20	3.66E-07	0.158434	0.854	0.805	0.007656
POLR1D	7.64E-19	0.157725	0.973	0.93	1.60E-14
WARS	2.86E-13	0.157059	0.763	0.656	5.99E-09
PABPC1	9.06E-35	0.156553	1	1	1.90E-30
WDR77	1.86E-19	0.156158	0.855	0.721	3.89E-15
EIF4H	7.46E-18	0.155909	0.984	0.955	1.56E-13
PPP2R5C	2.11E-15	0.155846	0.984	0.962	4.42E-11
COMMD6	4.47E-17	0.155602	0.981	0.962	9.37E-13
NUDT15	2.59E-19	0.154976	0.916	0.8	5.43E-15
MT2A	2.12E-17	0.154886	1	1	4.44E-13
CD55	1.23E-11	0.154848	0.926	0.86	2.58E-07
SIVA1	1.58E-16	0.153431	0.959	0.89	3.31E-12
RPL36AL	4.47E-23	0.153389	0.996	0.995	9.37E-19
P3H2	6.74E-17	0.152812	0.666	0.499	1.41E-12
RPSA	7.19E-32	0.151997	1	1	1.51E-27
SPRY4	7.36E-16	0.151958	0.611	0.416	1.54E-11
FLNA	2.80E-15	0.151524	0.909	0.804	5.85E-11
MAX	3.75E-17	0.151414	0.865	0.767	7.85E-13
OAF	2.33E-13	0.151394	0.922	0.826	4.88E-09
PPP4R3A	2.37E-19	0.150891	0.713	0.507	4.95E-15
ANP32A	9.69E-19	0.150738	0.996	0.984	2.03E-14
FBP1	4.75E-18	0.150156	0.675	0.483	9.95E-14
PARP4	9.56E-16	0.150129	0.805	0.654	2.00E-11

Supplementary table 2 (Continued)

HMGN1	7.43E-22	0.149949	0.999	0.996	1.56E-17
DDX24	5.91E-17	0.148872	0.992	0.98	1.24E-12
ARHGDIB	5.17E-19	0.148255	0.996	0.985	1.08E-14
FUS	9.89E-21	0.148002	0.999	0.996	2.07E-16
COPS6	3.46E-19	0.147952	0.983	0.962	7.24E-15
UPF3A	6.48E-17	0.147689	0.858	0.728	1.36E-12
TARS	6.40E-18	0.147545	0.999	0.991	1.34E-13
MTHFD1	1.10E-14	0.147185	0.939	0.871	2.30E-10
ATP5MC1	1.18E-17	0.146618	0.997	0.982	2.46E-13
IRS2	8.09E-20	0.146501	0.539	0.32	1.69E-15
GLRX5	4.50E-17	0.146037	0.935	0.854	9.42E-13
ATF4	1.82E-11	0.145179	0.995	0.987	3.81E-07
NPM1	8.63E-36	0.144966	1	1	1.81E-31
RPS2	7.46E-33	0.144837	1	1	1.56E-28
RBM26	5.91E-16	0.14482	0.713	0.539	1.24E-11
PPP2R5E	2.56E-11	0.144593	0.933	0.855	5.37E-07
CHAMP1	1.05E-19	0.144554	0.664	0.46	2.19E-15
PTGR1	1.95E-25	0.143626	0.521	0.275	4.08E-21
CPSF2	5.97E-15	0.143273	0.937	0.869	1.25E-10
ETS1	1.09E-15	0.143263	0.921	0.836	2.28E-11
N4BP2L2	6.15E-18	0.143193	0.763	0.579	1.29E-13
CCNK	7.84E-16	0.142703	0.836	0.71	1.64E-11
RPS27	7.24E-27	0.142482	1	1	1.52E-22
EIF4G1	3.35E-11	0.142413	0.864	0.778	7.01E-07
ZC3H14	4.38E-13	0.142228	0.906	0.827	9.18E-09
WDR43	8.87E-14	0.142142	0.961	0.898	1.86E-09
MICU2	5.16E-15	0.142129	0.89	0.793	1.08E-10
RASA3	4.28E-23	0.14104	0.552	0.318	8.97E-19
ESD	8.89E-16	0.140885	0.986	0.966	1.86E-11
CINP	7.27E-17	0.14047	0.926	0.849	1.52E-12
AJUBA	1.73E-12	0.14043	0.88	0.762	3.62E-08
CCND1	1.42E-10	0.139447	0.981	0.978	2.98E-06
SUPT20H	2.80E-19	0.139175	0.666	0.469	5.87E-15
NDUFAF3	2.89E-16	0.138681	0.855	0.728	6.05E-12
NUP58	2.74E-14	0.138418	0.812	0.667	5.73E-10
GPALPP1	2.80E-16	0.137726	0.735	0.555	5.86E-12
RPN2	1.24E-16	0.137693	0.997	0.987	2.61E-12
SUPT16H	1.73E-11	0.137044	0.969	0.945	3.62E-07
KCTD12	6.29E-16	0.136245	0.592	0.402	1.32E-11
PSPC1	8.06E-14	0.136121	0.867	0.763	1.69E-09

Supplementary table 2 (Continued)

Sep2	1.31E-19	0.135831	1	0.995	2.73E-15
GPAT3	6.32E-18	0.135592	0.704	0.496	1.32E-13
PLEC	2.72E-14	0.135435	0.761	0.593	5.70E-10
NEMF	1.11E-13	0.135408	0.831	0.675	2.32E-09
PSMC6	3.00E-13	0.13531	0.938	0.901	6.27E-09
FERMT2	1.58E-13	0.135261	0.873	0.785	3.32E-09
NOP56	1.31E-14	0.134749	0.997	0.991	2.75E-10
HMGCS1	5.06E-09	0.134447	0.471	0.346	0.000106
TNFRSF10D	5.66E-13	0.133947	0.695	0.55	1.19E-08
HNRNPA1	1.56E-17	0.132763	1	0.996	3.26E-13
ALCAM	9.76E-11	0.132515	0.981	0.966	2.04E-06
CAVIN1	3.61E-10	0.131815	0.996	0.995	7.56E-06
TLN1	1.60E-08	0.131518	0.915	0.865	0.000334
POLR2L	2.26E-18	0.131245	0.999	0.996	4.73E-14
EBPL	5.31E-16	0.131197	0.862	0.737	1.11E-11
CCDC57	1.22E-25	0.130808	0.488	0.236	2.56E-21
YY1	2.01E-12	0.130663	0.972	0.942	4.21E-08
ABCE1	1.39E-14	0.130624	0.996	0.982	2.91E-10
CAPN2	1.82E-12	0.130331	0.984	0.966	3.82E-08
SFPQ	5.97E-11	0.130251	0.992	0.985	1.25E-06
PYGL	3.93E-13	0.130189	0.644	0.486	8.23E-09
ACTN4	3.12E-13	0.130183	1	1	6.54E-09
BIRC2	2.01E-09	0.129156	0.964	0.937	4.21E-05
COL8A1	5.20E-12	0.128714	0.669	0.501	1.09E-07
OPN3	6.47E-17	0.128404	0.643	0.442	1.35E-12
PPP1R15A	2.82E-11	0.128109	0.962	0.936	5.90E-07
PDHA1	2.55E-10	0.127886	0.903	0.806	5.35E-06
PSMD2	4.21E-11	0.127094	0.997	0.993	8.82E-07
MCM6	9.32E-07	0.126999	0.745	0.675	0.019507
NEDD4L	1.04E-10	0.12658	0.886	0.771	2.17E-06
ZC3H13	9.42E-11	0.126374	0.669	0.545	1.97E-06
IGFBP6	5.69E-14	0.126365	0.699	0.52	1.19E-09
ATP6V1D	1.34E-11	0.125828	0.99	0.964	2.81E-07
ARF6	7.47E-11	0.125205	0.992	0.978	1.56E-06
PFN2	2.24E-11	0.125032	0.829	0.709	4.70E-07
PAICS	9.88E-15	0.124818	0.997	0.991	2.07E-10
NUMB	1.35E-13	0.124303	0.768	0.613	2.82E-09
LMNB1	2.40E-08	0.124047	0.859	0.794	0.000502
USP12	1.66E-13	0.123806	0.752	0.604	3.47E-09
AATF	1.04E-09	0.1229	0.806	0.709	2.18E-05

Supplementary table 2 (Continued)

DLST	7.90E-12	0.122772	0.899	0.823	1.65E-07
AXL	7.13E-13	0.122742	0.999	0.998	1.49E-08
ADAM9	4.98E-11	0.122158	0.903	0.825	1.04E-06
CAPZA1	1.44E-18	0.121976	0.999	0.999	3.02E-14
KPNB1	1.19E-12	0.121888	0.999	0.996	2.50E-08
CUL4A	8.63E-13	0.121884	0.743	0.599	1.81E-08
PLAUR	3.66E-07	0.121767	0.913	0.892	0.007664
RNASEH2B	2.75E-11	0.121592	0.858	0.775	5.75E-07
NPC2	1.59E-12	0.121016	1	0.994	3.34E-08
TNPO1	4.46E-10	0.11998	0.918	0.836	9.33E-06
NIP7	4.19E-12	0.119978	0.96	0.887	8.78E-08
WDHD1	2.26E-09	0.119892	0.737	0.607	4.72E-05
FDFT1	7.01E-09	0.119828	0.761	0.674	0.000147
SYNCRIP	2.29E-12	0.119811	0.992	0.99	4.79E-08
BAG5	6.92E-11	0.119741	0.74	0.612	1.45E-06
MARS	4.19E-10	0.119512	0.917	0.853	8.78E-06
EIF4G2	5.24E-15	0.117541	1	1	1.10E-10
USP22	1.95E-07	0.116958	0.925	0.88	0.00408
NAT10	5.31E-10	0.116948	0.763	0.652	1.11E-05
PCNX4	4.24E-09	0.116934	0.805	0.714	8.89E-05
MAP3K20	1.19E-08	0.116501	0.987	0.963	0.000249
NRK	1.68E-19	0.115853	0.414	0.206	3.52E-15
YWHAB	1.81E-27	0.115201	1	1	3.79E-23
SERBP1	1.58E-13	0.115032	0.999	0.999	3.32E-09
SP100	8.68E-11	0.114853	0.957	0.904	1.82E-06
PPA2	1.59E-12	0.114744	0.994	0.982	3.32E-08
MPHOSPH8	1.70E-10	0.114436	0.735	0.604	3.57E-06
WDR1	6.77E-11	0.114097	0.99	0.969	1.42E-06
RDH11	1.38E-08	0.113737	0.994	0.987	0.000289
IARS	7.22E-10	0.113568	0.814	0.718	1.51E-05
RWDD1	6.16E-10	0.113378	0.981	0.956	1.29E-05
VRK1	1.07E-08	0.113352	0.887	0.818	0.000224
SDCBP	2.87E-08	0.11328	0.987	0.98	0.000602
ENO1	6.58E-29	0.113184	1	1	1.38E-24
PRRC2C	2.63E-07	0.111835	0.851	0.788	0.005511
DNAJC3	1.74E-10	0.111601	0.607	0.467	3.64E-06
EIF3D	1.04E-11	0.111408	0.986	0.974	2.18E-07
GLRX	2.03E-08	0.111313	0.894	0.805	0.000426
SMAP1	5.72E-13	0.111078	0.749	0.578	1.20E-08
MED6	6.03E-11	0.111075	0.849	0.745	1.26E-06

Supplementary table 2 (Continued)

FBXL3	5.02E-14	0.110745	0.701	0.53	1.05E-09
ID3	2.65E-08	0.109698	0.7	0.573	0.000555
HMGN2	4.32E-17	0.109579	1	1	9.04E-13
EEF1D	6.21E-16	0.109543	1	1	1.30E-11
CARS2	1.48E-13	0.109083	0.655	0.481	3.09E-09
ERO1A	6.91E-09	0.108763	0.869	0.833	0.000145
NUFIP1	2.33E-12	0.108335	0.679	0.503	4.88E-08
CDH4	1.10E-09	0.108245	0.658	0.507	2.30E-05
FLRT2	4.74E-13	0.108227	0.519	0.34	9.93E-09
FAH	9.50E-14	0.108164	0.718	0.556	1.99E-09
MNAT1	6.64E-10	0.108009	0.96	0.907	1.39E-05
HNRNPR	6.02E-09	0.107172	0.994	0.988	0.000126
DMKN	2.77E-33	0.107118	0.263	0.048	5.79E-29
PURA	1.45E-08	0.1071	0.849	0.753	0.000304
SMARCA5	6.47E-09	0.106944	0.846	0.746	0.000135
MRPL3	7.17E-12	0.106739	0.978	0.952	1.50E-07
SPTLC2	4.47E-11	0.106069	0.609	0.458	9.36E-07
MYH9	2.19E-06	0.106018	0.962	0.901	0.045772
ACTR3	1.43E-11	0.105475	1	0.996	2.99E-07
EPS8L2	3.13E-12	0.105369	0.633	0.477	6.55E-08
NAXD	1.14E-14	0.105341	0.523	0.335	2.38E-10
SARS	9.15E-07	0.105319	0.982	0.963	0.019158
MATR3	6.94E-10	0.105228	0.994	0.991	1.45E-05
CLIC4	1.73E-07	0.104776	0.986	0.969	0.003616
METRN	9.39E-14	0.104204	0.59	0.404	1.97E-09
CDK4	1.46E-07	0.103809	0.944	0.888	0.003052
ILF3	2.79E-08	0.102829	0.966	0.936	0.000584
SSRP1	1.76E-10	0.102571	0.994	0.987	3.68E-06
SNAI2	4.15E-13	0.102362	0.336	0.185	8.69E-09
SDAD1	2.96E-07	0.10184	0.946	0.896	0.00619
TFAP2C	5.50E-10	0.101727	0.732	0.579	1.15E-05
ZDHHC20	9.23E-10	0.101621	0.69	0.564	1.93E-05
CLTB	1.05E-09	0.101069	0.906	0.823	2.19E-05
DLEU2	1.59E-08	0.101046	0.624	0.515	0.000332
TRMT5	1.26E-08	0.100941	0.928	0.882	0.000263
EIF2B2	1.43E-09	0.100705	0.921	0.838	2.99E-05
PCID2	2.51E-09	0.100574	0.781	0.655	5.26E-05
PARP1	7.04E-08	0.100566	0.95	0.901	0.001475
TRIP11	3.48E-07	0.100509	0.625	0.509	0.007279
LPAR1	2.55E-08	0.100493	0.73	0.617	0.000534

Supplementary table 2 (Continued)

HNRNPM	1.37E-08	0.100433	0.996	0.99	0.000286
CORO1C	3.08E-08	0.100349	0.987	0.95	0.000644
ZNF326	3.05E-09	0.100187	0.64	0.496	6.38E-05
CTNNAL1	6.85E-08	0.100181	0.997	0.987	0.001434
IFRD1	1.54E-12	0.100111	0.587	0.421	3.23E-08
HNRNPK	7.95E-13	0.100068	1	0.999	1.67E-08

Supplementary Table 3. DEGs identified in MDAMB231-S cells which showed overlap with ExoCarta dataset

	ExoCarta_mRNA	ExoCarta_Protein	MDAMB231-S
FTL	1	1	1
TIMP3	1	1	1
TPT1	1	1	1
HSP90AA1	1	1	1
EEF1A1	1	1	1
ACTG1	1	1	1
CAV1	1	1	1
HMGA1	1	1	1
FTH1	1	1	1
CALM1	1	1	1
DBN1	1	1	1
TXN	1	1	1
NQO1	1	1	1
HNRNPA3	1	1	1
SEC22B	1	1	1
PABPC1	1	1	1
PSMA3	1	1	1
KRT18	1	1	1
RPS2	1	1	1
RPSA	1	1	1
TPM4	1	1	1
ITM2B	1	1	1
ENO1	1	1	1
SLC7A1	1	1	1
TFRC	1	1	1
CTSD	1	1	1
UBR4	1	1	1
HNRNPD	1	1	1
KRT8	1	1	1
IRS2	1	1	1
AKT1	1	1	1
EFHD2	1	1	1
POLR2L	1	1	1
LASP1	1	1	1
DYNC1H1	1	1	1
N4BP2L2	1	1	1
TARS	1	1	1
RPN2	1	1	1

Supplementary table 3 (Continued)

SPRY4	1	1	1
PARP4	1	1	1
NOP56	1	1	1
TNFRSF10D	1	1	1
AXL	1	1	1
TOP1	1	1	1
CUL4A	1	1	1
KPNB1	1	1	1
EPS8L2	1	1	1
RFC3	1	1	1
DLST	1	1	1
LBR	1	1	1
SLC1A5	1	1	1
EIF3D	1	1	1
CD55	1	1	1
SUPT16H	1	1	1
SFPQ	1	1	1
WDR1	1	1	1
BAG5	1	1	1
MARS	1	1	1
ZNF326	1	1	1
SMARCA5	1	1	1
VRK1	1	1	1
TLN1	1	1	1
ILF3	1	1	1
CORO1C	1	1	1
PARP1	1	1	1
CLIC4	1	1	1
SARS	1	1	1
MCM6	1	1	1
MYH9	1	1	1
GTF3A	1	0	1
ERH	1	0	1
ADM	1	0	1
KPNA3	1	0	1
CCDC57	1	0	1
NDUFB1	1	0	1
IRS1	1	0	1
CDCA4	1	0	1
RB1	1	0	1

Supplementary table 3 (Continued)

DDX24	1	0	1
CPSF2	1	0	1
METRN	1	0	1
OAF	1	0	1
YY1	1	0	1
COL8A1	1	0	1
SPTLC2	1	0	1
ZC3H13	1	0	1
CCND1	1	0	1
TFAP2C	1	0	1
USP22	1	0	1
HMGB1	0	1	1
RPL21	0	1	1
ACTN1	0	1	1
LCP1	0	1	1
SAP18	0	1	1
PHGDH	0	1	1
TPP2	0	1	1
STXBP6	0	1	1
UCHL3	0	1	1
IPO5	0	1	1
PTMA	0	1	1
EIF5	0	1	1
RPS29	0	1	1
HSPH1	0	1	1
UBL3	0	1	1
EIF2S1	0	1	1
SET	0	1	1
MDK	0	1	1
NPM1	0	1	1
ZYX	0	1	1
PSMC1	0	1	1
XRCC5	0	1	1
NCL	0	1	1
BZW1	0	1	1
SLC9A3R2	0	1	1
ACAT2	0	1	1
STK24	0	1	1
PDLIM7	0	1	1
YWHAB	0	1	1

Supplementary table 3 (Continued)

PDS5B	0	1	1
SRSF5	0	1	1
RPS27	0	1	1
TMED10	0	1	1
DIAPH3	0	1	1
PTGR1	0	1	1
PLS3	0	1	1
HNRNPH1	0	1	1
SUGT1	0	1	1
DIS3	0	1	1
RASA3	0	1	1
TM9SF2	0	1	1
C4BPB	0	1	1
CNN2	0	1	1
DKC1	0	1	1
RAB4A	0	1	1
TMX1	0	1	1
NAMPT	0	1	1
FUS	0	1	1
Sep2	0	1	1
WDR77	0	1	1
SUPT20H	0	1	1
COPS6	0	1	1
ARHGDIB	0	1	1
POLR1D	0	1	1
KTN1	0	1	1
ANP32A	0	1	1
CAPZA1	0	1	1
GNPNAT1	0	1	1
FBP1	0	1	1
EIF4H	0	1	1
HNRNPA1	0	1	1
EEF1D	0	1	1
KCTD12	0	1	1
ESD	0	1	1
PPP2R5C	0	1	1
FLNA	0	1	1
LAMP1	0	1	1
PAICS	0	1	1
MTHFD1	0	1	1

Supplementary table 3 (Continued)

ABCE1	0	1	1
MPP5	0	1	1
PLEC	0	1	1
IGFBP6	0	1	1
PSPC1	0	1	1
FAH	0	1	1
NUMB	0	1	1
SERBP1	0	1	1
FERMT2	0	1	1
IL11	0	1	1
WARS	0	1	1
PSMC6	0	1	1
ACTN4	0	1	1
PYGL	0	1	1
HNRNPK	0	1	1
IFRD1	0	1	1
PPA2	0	1	1
CAPN2	0	1	1
SYNCRIP	0	1	1
ATP6V1D	0	1	1
ACTR3	0	1	1
PFN2	0	1	1
PPP2R5E	0	1	1
EIF4G1	0	1	1
PSMD2	0	1	1
ADAM9	0	1	1
ARF6	0	1	1
ALCAM	0	1	1
NEDD4L	0	1	1
DNAJC3	0	1	1
SSRP1	0	1	1
PDHA1	0	1	1
TNPO1	0	1	1
NAT10	0	1	1
MATR3	0	1	1
IARS	0	1	1
ZDHHC20	0	1	1
CLTB	0	1	1
ASNS	0	1	1
EIF2B2	0	1	1

Supplementary table 3 (Continued)

PCID2	0	1	1
HMGCS1	0	1	1
HNRNPR	0	1	1
FDFT1	0	1	1
HNRNPM	0	1	1
RDH11	0	1	1
PURA	0	1	1
GLRX	0	1	1
LMNB1	0	1	1
SDCBP	0	1	1
CDK4	0	1	1
TRIP11	0	1	1
PLAUR	0	1	1

References

[1] M.P. Zaborowski, L. Balaj, X.O. Breakefield, C.P. Lai, “Extracellular Vesicles: Composition, Biological Relevance, and Methods of Study,” *Bioscience*. (2015). https://doi.org/10.1093/biosci/biv084.

[2] M. Yáñez-Mó, P.R.M. Siljander, Z. Andreu, A.B. Zavec, F.E. Borràs, E.I. Buzas, K. Buzas, E. Casal, F. Cappello, J. Carvalho, E. Colás, A. Cordeiro-Da Silva, S. Fais, J.M. Falcon-Perez, I.M. Ghobrial, B. Giebel, M. Gimona, M. Graner, I. Gursel, M. Gursel, N.H.H. Heegaard, A. Hendrix, P. Kierulf, K. Kokubun, M. Kosanovic, V. Kralj-Iglic, E.M. Krämer-Albers, S. Laitinen, C. Lässer, T. Lener, E. Ligeti, A. Line, G. Lipps, A. Llorente, J. Lötvall, M. Manček-Keber, A. Marcilla, M. Mittelbrunn, I. Nazarenko, E.N.M. Nolte-’t Hoen, T.A. Nyman, L. O’Driscoll, M. Olivan, C. Oliveira, É. Pállinger, H.A. Del Portillo, J. Reventós, M. Rigau, E. Rohde, M. Sammar, F. Sánchez-Madrid, N. Santarém, K. Schallmoser, M.S. Ostenfeld, W. Stoorvogel, R. Stukelj, S.G. Van Der Grein, M. Helena Vasconcelos, M.H.M. Wauben, O. De Wever, “Biological properties of extracellular vesicles and their physiological functions,” *J. Extracell. Vesicles*. (2015). https://doi.org/10.3402/jev.v4.27066.

[3] G. Raposo, W. Stoorvogel, “Extracellular vesicles: Exosomes, microvesicles, and friends,” *J. Cell Biol.* (2013). https://doi.org/10.1083/jcb.201211138.

[4] H. Sonoda, N. Yokota-Ikeda, S. Oshikawa, Y. Kanno, K. Yoshinaga, K. Uchida, Y. Ueda, K. Kimiya, S. Uezono, A. Ueda, K. Ito, M. Ikeda,

“Decreased abundance of urinary exosomal aquaporin-1 in renal ischemia-reperfusion injury,” *Am. J. Physiol. - Ren. Physiol.* (2009). https://doi.org/10.1152/ajprenal.00200.2009.

[5] A. Bobrie, M. Colombo, G. Raposo, C. Théry, “Exosome Secretion: Molecular Mechanisms and Roles in Immune Responses,” *Traffic*. (2011). https://doi.org/10.1111/j.1600-0854.2011.01225.x.

[6] M.P. Bebelman, M.J. Smit, D.M. Pegtel, S.R. Baglio, “Biogenesis and function of extracellular vesicles in cancer,” *Pharmacol. Ther.* (2018). https://doi.org/10.1016/j.pharmthera.2018.02.013.

[7] L. Christ, C. Raiborg, E.M. Wenzel, C. Campsteijn, H. Stenmark, “Cellular Functions and Molecular Mechanisms of the ESCRT Membrane-Scission Machinery,” *Trends Biochem. Sci.* (2017). https://doi.org/10.1016/j.tibs.2016.08.016.

[8] K. Trajkovic, C. Hsu, S. Chiantia, L. Rajendran, D. Wenzel, F. Wieland, P. Schwille, B. Brügger, M. Simons, “Ceramide triggers budding of exosome vesicles into multivesicular endosomes,” *Science (80-.).* (2008). https://doi.org/10.1126/science.1153124.

[9] T. Kajimoto, T. Okada, S. Miya, L. Zhang, S.I. Nakamura, “Ongoing activation of sphingosine 1-phosphate receptors mediates maturation of exosomal multivesicular endosomes,” *Nat. Commun.* (2013). https://doi.org/10.1038/ncomms3712.

[10] R. Ghossoub, F. Lembo, A. Rubio, C.B. Gaillard, J. Bouchet, N. Vitale, J.

Slavík, M. Machala, P. Zimmermann, “Syntenin-ALIX exosome biogenesis and budding into multivesicular bodies are controlled by ARF6 and PLD2,” *Nat. Commun.* (2014). https://doi.org/10.1038/ncomms4477.

[11] G. Van Niel, G. D’Angelo, G. Raposo, “Shedding light on the cell biology of extracellular vesicles,” *Nat. Rev. Mol. Cell Biol.* (2018). https://doi.org/10.1038/nrm.2017.125.

[12] D.J. Gibbings, C. Ciaudo, M. Erhardt, O. Voinnet, “Multivesicular bodies associate with components of miRNA effector complexes and modulate miRNA activity,” *Nat. Cell Biol.* (2009). https://doi.org/10.1038/ncb1929.

[13] M.F. Baietti, Z. Zhang, E. Mortier, A. Melchior, G. Degeest, A. Geeraerts, Y. Ivarsson, F. Depoortere, C. Coomans, E. Vermeiren, P. Zimmermann, G. David, “Syndecan-syntenin-ALIX regulates the biogenesis of exosomes,” *Nat. Cell Biol.* (2012). https://doi.org/10.1038/ncb2502.

[14] C. Hsu, Y. Morohashi, S.I. Yoshimura, N. Manrique-Hoyos, S.Y. Jung, M.A. Lauterbach, M. Bakhti, M. Grønborg, W. Möbius, J.S. Rhee, F.A. Barr, M. Simons, “Regulation of exosome secretion by Rab35 and its GTPase-activating proteins TBC1D10A-C,” *J. Cell Biol.* (2010). https://doi.org/10.1083/jcb.200911018.

[15] A. Savina, M. Vidal, M.I. Colombo, “The exosome pathway in K562 cells is regulated by Rab11,” *J. Cell Sci.* (2002).

[16] D. Hoshino, K.C. Kirkbride, K. Costello, E.S. Clark, S. Sinha, N. Grega-Larson, M.J. Tyska, A.M. Weaver, “Exosome secretion is enhanced by

invadopodia and drives invasive behavior," *Cell Rep.* (2013). https://doi.org/10.1016/j.celrep.2013.10.050.

[17] M. Ostrowski, N.B. Carmo, S. Krumeich, I. Fanget, G. Raposo, A. Savina, C.F. Moita, K. Schauer, A.N. Hume, R.P. Freitas, B. Goud, P. Benaroch, N. Hacohen, M. Fukuda, C. Desnos, M.C. Seabra, F. Darchen, S. Amigorena, L.F. Moita, C. Thery, "Rab27a and Rab27b control different steps of the exosome secretion pathway," *Nat. Cell Biol.* (2010). https://doi.org/10.1038/ncb2000.

[18] C. Villarroya-Beltri, F. Baixauli, M. Mittelbrunn, I. Fernández-Delgado, D. Torralba, O. Moreno-Gonzalo, S. Baldanta, C. Enrich, S. Guerra, F. Sánchez-Madrid, "ISGylation controls exosome secretion by promoting lysosomal degradation of MVB proteins," *Nat. Commun.* (2016). https://doi.org/10.1038/ncomms13588.

[19] J.R. Edgar, P.T. Manna, S. Nishimura, G. Banting, M.S. Robinson, "Tetherin is an exosomal tether," *Elife*. (2016). https://doi.org/10.7554/eLife.17180.

[20] M.V.S. Dias, B.L. Teixeira, B.R. Rodrigues, R. Sinigaglia-Coimbra, I. Porto-Carreiro, M. Roffé, G.N.M. Hajj, V.R. Martins, "PRNP/prion protein regulates the secretion of exosomes modulating CAV1/caveolin-1-suppressed autophagy," *Autophagy*. (2016). https://doi.org/10.1080/15548627.2016.1226735.

[21] W.J. Hong, S. Lev, "Tethering the assembly of SNARE complexes," *Trends*

Cell Biol. (2014). https://doi.org/10.1016/j.tcb.2013.09.006.

[22] T.C. Südhof, J.E. Rothman, “Membrane fusion: Grappling with SNARE and SM proteins,” *Science (80-.).* (2009). https://doi.org/10.1126/science.1161748.

[23] C.M. Fader, D. Sánchez, M. Furlán, M.I. Colombo, “Induction of autophagy promotes fusion of multivesicular bodies with autophagic vacuoles in K562 cells,” *Traffic*. (2008). https://doi.org/10.1111/j.1600-0854.2007.00677.x.

[24] Y. Wei, D. Wang, F. Jin, Z. Bian, L. Li, H. Liang, M. Li, L. Shi, C. Pan, D. Zhu, X. Chen, G. Hu, Y. Liu, C.Y. Zhang, K. Zen, “Pyruvate kinase type M2 promotes tumour cell exosome release via phosphorylating synaptosome-associated protein 23,” *Nat. Commun.* (2017). https://doi.org/10.1038/ncomms14041.

[25] F.J. Verweij, M.A.J. Van Eijndhoven, E.S. Hopmans, T. Vendrig, T. Wurdinger, E. Cahir-Mcfarland, E. Kieff, D. Geerts, R. Van Der Kant, J. Neefjes, J.M. Middeldorp, D.M. Pegtel, “LMP1 association with CD63 in endosomes and secretion via exosomes limits constitutive NF-κB activation,” *EMBO J.* (2011). https://doi.org/10.1038/emboj.2011.123.

[26] V. Hyenne, A. Apaydin, D. Rodriguez, C. Spiegelhalter, S. Hoff-Yoessle, M. Diem, S. Tak, O. Lefebvre, Y. Schwab, J.G. Goetz, M. Labouesse, “RAL-1 controls multivesicular body biogenesis and exosome secretion,” *J. Cell Biol.* (2015). https://doi.org/10.1083/jcb.201504136.

[27] K. Koles, V. Budnik, “Exosomes go with the Wnt,” *Cell. Logist.* (2012).

https://doi.org/10.4161/cl.21981.

[28] J.C. Gross, V. Chaudhary, K. Bartscherer, M. Boutros, “Active Wnt proteins are secreted on exosomes,” *Nat. Cell Biol.* (2012). https://doi.org/10.1038/ncb2574.

[29] S. Raimondo, L. Saieva, C. Corrado, S. Fontana, A. Flugy, A. Rizzo, G. De Leo, R. Alessandro, “Chronic myeloid leukemia-derived exosomes promote tumor growth through an autocrine mechanism,” *Cell Commun. Signal.* (2015). https://doi.org/10.1186/s12964-015-0086-x.

[30] A. Takahashi, R. Okada, K. Nagao, Y. Kawamata, A. Hanyu, S. Yoshimoto, M. Takasugi, S. Watanabe, M.T. Kanemaki, C. Obuse, E. Hara, “Exosomes maintain cellular homeostasis by excreting harmful DNA from cells,” *Nat. Commun.* (2017). https://doi.org/10.1038/ncomms15287.

[31] L. Zhang, D. Yu, “Exosomes in cancer development, metastasis, and immunity,” *Biochim. Biophys. Acta - Rev. Cancer*. (2019). https://doi.org/10.1016/j.bbcan.2019.04.004.

[32] K. Al-Nedawi, B. Meehan, J. Micallef, V. Lhotak, L. May, A. Guha, J. Rak, “Intercellular transfer of the oncogenic receptor EGFRvIII by microvesicles derived from tumour cells,” *Nat. Cell Biol.* (2008). https://doi.org/10.1038/ncb1725.

[33] Y. Yang, C.W. Li, L.C. Chan, Y. Wei, J.M. Hsu, W. Xia, J.H. Cha, J. Hou, J.L. Hsu, L. Sun, M.C. Hung, “Exosomal PD-L1 harbors active defense function to suppress t cell killing of breast cancer cells and promote tumor

growth," *Cell Res.* (2018). https://doi.org/10.1038/s41422-018-0060-4.

[34] M.D. Beckler, J.N. Higginbotham, J.L. Franklin, A.J. Ham, P.J. Halvey, I.E. Imasuen, C. Whitwell, M. Li, D.C. Liebler, R.J. Coffey, "Proteomic analysis of exosomes from mutant KRAS colon cancer cells identifies intercellular transfer of mutant KRAS," *Mol. Cell. Proteomics*. (2013). https://doi.org/10.1074/mcp.M112.022806.

[35] A. Hendrix, D. Maynard, P. Pauwels, G. Braems, H. Denys, R. Van Den Broecke, J. Lambert, S. Van Belle, V. Cocquyt, C. Gespach, M. Bracke, M.C. Seabra, W.A. Gahl, O. De Wever, W. Westbroek, "Effect of the secretory small GTPase Rab27B on breast cancer growth, invasion, and metastasis," *J. Natl. Cancer Inst.* (2010). https://doi.org/10.1093/jnci/djq153.

[36] S. Yue, W. Mu, U. Erb, M. Zöller, "The tetraspanins CD151 and Tspan8 are essential exosome components for the crosstalk between cancer initiating cells and their surrounding," *Oncotarget*. (2015). https://doi.org/10.18632/oncotarget.2958.

[37] M. Aga, G.L. Bentz, S. Raffa, M.R. Torrisi, S. Kondo, N. Wakisaka, T. Yoshizaki, J.S. Pagano, J. Shackelford, "Exosomal HIF1α supports invasive potential of nasopharyngeal carcinoma-associated LMP1-positive exosomes," *Oncogene*. (2014). https://doi.org/10.1038/onc.2014.66.

[38] D.K. Jeppesen, A. Nawrocki, S.G. Jensen, K. Thorsen, B. Whitehead, K.A. Howard, L. Dyrskjøt, T.F. Ørntoft, M.R. Larsen, M.S. Ostenfeld,

"Quantitative proteomics of fractionated membrane and lumen exosome proteins from isogenic metastatic and nonmetastatic bladder cancer cells reveal differential expression of EMT factors," *Proteomics*. (2014). https://doi.org/10.1002/pmic.201300452.

[39] Y. You, Y. Shan, J. Chen, H. Yue, B. You, S. Shi, X. Li, X. Cao, "Matrix metalloproteinase 13-containing exosomes promote nasopharyngeal carcinoma metastasis," *Cancer Sci.* (2015). https://doi.org/10.1111/cas.12818.

[40] T. Yoshizaki, S. Kondo, N. Wakisaka, S. Murono, K. Endo, H. Sugimoto, S. Nakanishi, A. Tsuji, M. Ito, "Pathogenic role of Epstein-Barr virus latent membrane protein-1 in the development of nasopharyngeal carcinoma," *Cancer Lett.* (2013). https://doi.org/10.1016/j.canlet.2013.05.018.

[41] W. Zhou, M.Y. Fong, Y. Min, G. Somlo, L. Liu, M.R. Palomares, Y. Yu, A. Chow, S.T.F. O'Connor, A.R. Chin, Y. Yen, Y. Wang, E.G. Marcusson, P. Chu, J. Wu, X. Wu, A.X. Li, Z. Li, H. Gao, X. Ren, M.P. Boldin, P.C. Lin, S.E. Wang, "Cancer-Secreted miR-105 destroys vascular endothelial barriers to promote metastasis," *Cancer Cell*. (2014). https://doi.org/10.1016/j.ccr.2014.03.007.

[42] M.S. Ostenfeld, D.K. Jeppesen, J.R. Laurberg, A.T. Boysen, J.B. Bramsen, B. Primdal-Bengtson, A. Hendrix, P. Lamy, F. Dagnaes-Hansen, M.H. Rasmussen, K.H. Bui, N. Fristrup, E.I. Christensen, I. Nordentoft, J.P. Morth, J.B. Jensen, J.S. Pedersen, M. Beck, D. Theodorescu, M. Borre,

K.A. Howard, L. Dyrskjøt, T.F. Ørntoft, “Cellular disposal of miR23b by RAB27-dependent exosome release is linked to acquisition of metastatic properties,” *Cancer Res.* (2014). https://doi.org/10.1158/0008-5472.CAN-13-3512.

[43] S. Rana, K. Malinowska, M. Zöller, “Exosomal tumor microRNA modulates premetastatic organ cells,” *Neoplasia (United States)*. (2013). https://doi.org/10.1593/neo.122010.

[44] J.L. Hood, S. San Roman, S.A. Wickline, “Exosomes released by melanoma cells prepare sentinel lymph nodes for tumor metastasis,” *Cancer Res.* (2011). https://doi.org/10.1158/0008-5472.CAN-10-4455.

[45] A. Hoshino, B. Costa-Silva, T.L. Shen, G. Rodrigues, A. Hashimoto, M. Tesic Mark, H. Molina, S. Kohsaka, A. Di Giannatale, S. Ceder, S. Singh, C. Williams, N. Soplop, K. Uryu, L. Pharmer, T. King, L. Bojmar, A.E. Davies, Y. Ararso, T. Zhang, H. Zhang, J. Hernandez, J.M. Weiss, V.D. Dumont-Cole, K. Kramer, L.H. Wexler, A. Narendran, G.K. Schwartz, J.H. Healey, P. Sandstrom, K. Jørgen Labori, E.H. Kure, P.M. Grandgenett, M.A. Hollingsworth, M. De Sousa, S. Kaur, M. Jain, K. Mallya, S.K. Batra, W.R. Jarnagin, M.S. Brady, O. Fodstad, V. Muller, K. Pantel, A.J. Minn, M.J. Bissell, B.A. Garcia, Y. Kang, V.K. Rajasekhar, C.M. Ghajar, I. Matei, H. Peinado, J. Bromberg, D. Lyden, “Tumour exosome integrins determine organotropic metastasis,” *Nature*. (2015). https://doi.org/10.1038/nature15756.

[46] Y. Liu, Y. Gu, Y. Han, Q. Zhang, Z. Jiang, X. Zhang, B. Huang, X. Xu, J. Zheng, X. Cao, “Tumor Exosomal RNAs Promote Lung Pre-metastatic Niche Formation by Activating Alveolar Epithelial TLR3 to Recruit Neutrophils,” *Cancer Cell*. (2016). https://doi.org/10.1016/j.ccell.2016.06.021.

[47] M.P. Plebanek, N.L. Angeloni, E. Vinokour, J. Li, A. Henkin, D. Martinez-Marin, S. Filleur, R. Bhowmick, J. Henkin, S.D. Miller, I. Ifergan, Y. Lee, I. Osman, C.S. Thaxton, O. V. Volpert, “Pre-metastatic cancer exosomes induce immune surveillance by patrolling monocytes at the metastatic niche,” *Nat. Commun.* (2017). https://doi.org/10.1038/s41467-017-01433-3.

[48] K. Valencia, D. Luis-Ravelo, N. Bovy, I. Antón, S. Martínez-Canarias, C. Zandueta, C. Ormazábal, I. Struman, S. Tabruyn, V. Rebmann, J. De Las Rivas, E. Guruceaga, E. Bandrés, F. Lecanda, “MiRNA cargo within exosome-like vesicle transfer influences metastatic bone colonization,” *Mol. Oncol.* (2014). https://doi.org/10.1016/j.molonc.2014.01.012.

[49] L. Muller, C.S. Hong, D.B. Stolz, S.C. Watkins, T.L. Whiteside, “Isolation of biologically-active exosomes from human plasma,” *J. Immunol. Methods*. (2014). https://doi.org/10.1016/j.jim.2014.06.007.

[50] N. Zarovni, A. Corrado, P. Guazzi, D. Zocco, E. Lari, G. Radano, J. Muhhina, C. Fondelli, J. Gavrilova, A. Chiesi, “Integrated isolation and quantitative analysis of exosome shuttled proteins and nucleic acids using immunocapture approaches,” *Methods*. (2015).

https://doi.org/10.1016/j.ymeth.2015.05.028.

[51] A. Cvjetkovic, J. Lötvall, C. Lässer, “The influence of rotor type and centrifugation time on the yield and purity of extracellular vesicles,” *J. Extracell. Vesicles*. (2014). https://doi.org/10.3402/jev.v3.23111.

[52] E. Zeringer, T. Barta, M. Li, A. V. Vlassov, “Strategies for isolation of exosomes,” *Cold Spring Harb. Protoc.* (2015). https://doi.org/10.1101/pdb.top074476.

[53] M. Zhang, K. Jin, L. Gao, Z. Zhang, F. Li, F. Zhou, L. Zhang, “Methods and Technologies for Exosome Isolation and Characterization,” *Small Methods*. (2018). https://doi.org/10.1002/smtd.201800021.

[54] P. Li, M. Kaslan, S.H. Lee, J. Yao, Z. Gao, “Progress in exosome isolation techniques,” *Theranostics*. (2017). https://doi.org/10.7150/thno.18133.

[55] J.M. Escola, M.J. Kleijmeer, W. Stoorvogel, J.M. Griffith, O. Yoshie, H.J. Geuze, “Selective enrichment of tetraspan proteins on the internal vesicles of multivesicular endosomes and on exosomes secreted by human B-lymphocytes,” *J. Biol. Chem.* (1998). https://doi.org/10.1074/jbc.273.32.20121.

[56] S. Runz, S. Keller, C. Rupp, A. Stoeck, Y. Issa, D. Koensgen, A. Mustea, J. Sehouli, G. Kristiansen, P. Altevogt, “Malignant ascites-derived exosomes of ovarian carcinoma patients contain CD24 and EpCAM,” *Gynecol. Oncol.* (2007). https://doi.org/10.1016/j.ygyno.2007.08.064.

[57] S. Mathivanan, J.W.E. Lim, B.J. Tauro, H. Ji, R.L. Moritz, R.J. Simpson, “Proteomics analysis of A33 immunoaffinity-purified exosomes released from the human colon tumor cell line LIM1215 reveals a tissue-specific protein signature,” *Mol. Cell. Proteomics*. (2010). https://doi.org/10.1074/mcp.M900152-MCP200.

[58] D.D. Taylor, C. Gercel-Taylor, “MicroRNA signatures of tumor-derived exosomes as diagnostic biomarkers of ovarian cancer,” *Gynecol. Oncol.* (2008). https://doi.org/10.1016/j.ygyno.2008.04.033.

[59] J. Conde-Vancells, E. Rodriguez-Suarez, N. Embade, D. Gil, R. Matthiesen, M. Valle, F. Elortza, S.C. Lu, J.M. Mato, J.M. Falcon-Perez, “Characterization and comprehensive proteome profiling of exosomes secreted by hepatocytes,” *J. Proteome Res.* (2008). https://doi.org/10.1021/pr8004887.

[60] E. V. Batrakova, M.S. Kim, “Using exosomes, naturally-equipped nanocarriers, for drug delivery,” *J. Control. Release*. (2015). https://doi.org/10.1016/j.jconrel.2015.07.030.

[61] S. Hosseini, P. Vázquez-Villegas, M. Rito-Palomares, S.O. Martinez-Chapa, General overviews on applications of ELISA, in: SpringerBriefs Appl. Sci. Technol., 2018. https://doi.org/10.1007/978-981-10-6766-2_2.

[62] R.T. Davies, J. Kim, S.C. Jang, E.J. Choi, Y.S. Gho, J. Park, “Microfluidic filtration system to isolate extracellular vesicles from blood,” *Lab Chip*. (2012). https://doi.org/10.1039/c2lc41006k.

[63] K. Lee, H. Shao, R. Weissleder, H. Lee, “Acoustic purification of extracellular microvesicles,” *ACS Nano*. (2015). https://doi.org/10.1021/nn506538f.

[64] Z. Zhao, Y. Yang, Y. Zeng, M. He, “A microfluidic ExoSearch chip for multiplexed exosome detection towards blood-based ovarian cancer diagnosis,” *Lab Chip*. (2016). https://doi.org/10.1039/c5lc01117e.

[65] M. He, J. Crow, M. Roth, Y. Zeng, A.K. Godwin, “Integrated immunoisolation and protein analysis of circulating exosomes using microfluidic technology,” *Lab Chip*. (2014). https://doi.org/10.1039/c4lc00662c.

[66] S.S. Kanwar, C.J. Dunlay, D.M. Simeone, S. Nagrath, “Microfluidic device (ExoChip) for on-chip isolation, quantification and characterization of circulating exosomes,” *Lab Chip*. (2014). https://doi.org/10.1039/c4lc00136b.

[67] P. Ziaei, C.E. Berkman, M.G. Norton, “Review: Isolation and Detection of Tumor-Derived Extracellular Vesicles,” *ACS Appl. Nano Mater.* (2018). https://doi.org/10.1021/acsanm.8b00267.

[68] R.A. Dragovic, C. Gardiner, A.S. Brooks, D.S. Tannetta, D.J.P. Ferguson, P. Hole, B. Carr, C.W.G. Redman, A.L. Harris, P.J. Dobson, P. Harrison, I.L. Sargent, “Sizing and phenotyping of cellular vesicles using Nanoparticle Tracking Analysis,” *Nanomedicine Nanotechnology, Biol. Med.* (2011). https://doi.org/10.1016/j.nano.2011.04.003.

[69] C.Y. Soo, Y. Song, Y. Zheng, E.C. Campbell, A.C. Riches, F. Gunn-Moore, S.J. Powis, “Nanoparticle tracking analysis monitors microvesicle and exosome secretion from immune cells,” *Immunology*. (2012). https://doi.org/10.1111/j.1365-2567.2012.03569.x.

[70] V. Filipe, A. Hawe, W. Jiskoot, “Critical evaluation of nanoparticle tracking analysis (NTA) by NanoSight for the measurement of nanoparticles and protein aggregates,” *Pharm. Res.* (2010). https://doi.org/10.1007/s11095-010-0073-2.

[71] D. a Skoog, F.J. Holler, T. a Nieman, Principles of Instrumental Analysis, Brooks/Cole, 1998.

[72] H.W. King, M.Z. Michael, J.M. Gleadle, “Hypoxic enhancement of exosome release by breast cancer cells,” *BMC Cancer*. (2012). https://doi.org/10.1186/1471-2407-12-421.

[73] A. Delfarah, D. Zheng, J.H. Joly, J. Yang, N.A. Graham, “Proteomic profiling enables prediction of novel senolytics from large-scale drug screens,” *BioRxiv Prepr. Serv. Biol.* (2020).

[74] S. Kita, N. Maeda, I. Shimomura, “Interorgan communication by exosomes, adipose tissue, and adiponectin in metabolic syndrome,” *J. Clin. Invest.* (2019). https://doi.org/10.1172/JCI129193.

[75] C. Ciardiello, L. Cavallini, C. Spinelli, J. Yang, M. Reis-Sobreiro, P. De Candia, V.R. Minciacchi, D. Di Vizio, “Focus on extracellular vesicles: New frontiers of cell-to-cell communication in cancer,” *Int. J. Mol. Sci.* (2016).

https://doi.org/10.3390/ijms17020175.

[76] J.R. Chevillet, Q. Kang, I.K. Ruf, H.A. Briggs, L.N. Vojtech, S.M. Hughes, H.H. Cheng, J.D. Arroyo, E.K. Meredith, E.N. Gallichotte, E.L. Pogosova-Agadjanyan, C. Morrissey, D.L. Stirewalt, F. Hladik, E.Y. Yu, C.S. Higano, M. Tewari, “Quantitative and stoichiometric analysis of the microRNA content of exosomes,” *Proc. Natl. Acad. Sci. U. S. A.* (2014). https://doi.org/10.1073/pnas.1408301111.

[77] R. Kalluri, V.S. LeBleu, “The biology, function, and biomedical applications of exosomes,” *Science (80-.).* (2020). https://doi.org/10.1126/science.aau6977.

[78] S.W. Wen, L.G. Lima, R.J. Lobb, E.L. Norris, M.L. Hastie, S. Krumeich, A. Möller, “Breast Cancer-Derived Exosomes Reflect the Cell-of-Origin Phenotype,” *Proteomics*. (2019). https://doi.org/10.1002/pmic.201800180.

[79] F.J. Verweij, M.P. Bebelman, C.R. Jimenez, J.J. Garcia-Vallejo, H. Janssen, J. Neefjes, J.C. Knol, R. de Goeij-de Haas, S.R. Piersma, S.R. Baglio, M. Verhage, J.M. Middeldorp, A. Zomer, J. van Rheenen, M.G. Coppolino, I. Hurbain, G. Raposo, M.J. Smit, R.F.G. Toonen, G. van Niel, D.M. Pegtel, “Quantifying exosome secretion from single cells reveals a modulatory role for GPCR signaling,” *J. Cell Biol.* (2018). https://doi.org/10.1083/jcb.201703206.

[80] Y.J. Chiu, W. Cai, Y.R. V. Shih, I. Lian, Y.H. Lo, “A single-cell assay for time lapse studies of exosome secretion and cell behaviors,” *Small*. (2016).

https://doi.org/10.1002/smll.201600725.

[81] K.J. Son, A. Rahimian, D.S. Shin, C. Siltanen, T. Patel, A. Revzin, “Microfluidic compartments with sensing microbeads for dynamic monitoring of cytokine and exosome release from single cells,” *Analyst*. (2016). https://doi.org/10.1039/c5an01648g.

[82] E. van der Pol, A.N. Böing, P. Harrison, A. Sturk, R. Nieuwland, “Classification, functions, and clinical relevance of extracellular vesicles,” *Pharmacol. Rev.* (2012). https://doi.org/10.1124/pr.112.005983.

[83] M. Simons, G. Raposo, “Exosomes - vesicular carriers for intercellular communication,” *Curr. Opin. Cell Biol.* (2009). https://doi.org/10.1016/j.ceb.2009.03.007.

[84] V. Muralidharan-Chari, J.W. Clancy, A. Sedgwick, C. D’Souza-Schorey, “Microvesicles: Mediators of extracellular communication during cancer progression,” *J. Cell Sci.* (2010). https://doi.org/10.1242/jcs.064386.

[85] J. Skog, T. Würdinger, S. van Rijn, D.H. Meijer, L. Gainche, W.T. Curry, B.S. Carter, A.M. Krichevsky, X.O. Breakefield, “Glioblastoma microvesicles transport RNA and proteins that promote tumour growth and provide diagnostic biomarkers,” *Nat. Cell Biol.* (2008). https://doi.org/10.1038/ncb1800.

[86] M. Wysoczynski, M.Z. Ratajczak, “Lung cancer secreted microvesicles: Underappreciated modulators of microenvironment in expanding tumors,” *Int. J. Cancer*. (2009). https://doi.org/10.1002/ijc.24479.

[87] V. Muralidharan-Chari, H. Hoover, J. Clancy, J. Schweitzer, M.A. Suckow, V. Schroeder, F.J. Castellino, J.S. Schorey, C. D'Souza-Schorey, "ADP-Ribosylation factor 6 regulates tumorigenic and invasive properties in vivo," *Cancer Res.* (2009). https://doi.org/10.1158/0008-5472.CAN-08-1301.

[88] R. Valenti, V. Huber, M. Iero, P. Filipazzi, G. Parmiani, L. Rivoltini, "Tumor-released microvesicles as vehicles of immunosuppression," *Cancer Res.* (2007). https://doi.org/10.1158/0008-5472.CAN-07-0520.

[89] G.P. Dunn, L.J. Old, R.D. Schreiber, "The immunobiology of cancer immunosurveillance and immunoediting," *Immunity*. (2004). https://doi.org/10.1016/j.immuni.2004.07.017.

[90] K. Shedden, X.T. Xie, P. Chandaroy, Y.T. Chang, G.R. Rosania, "Expulsion of small molecules in vesicles shed by cancer cells: Association with gene expression and chemosensitivity profiles," *Cancer Res.* (2003).

[91] H. Peinado, M. Alečković, S. Lavotshkin, I. Matei, B. Costa-Silva, G. Moreno-Bueno, M. Hergueta-Redondo, C. Williams, G. García-Santos, C.M. Ghajar, A. Nitadori-Hoshino, C. Hoffman, K. Badal, B.A. Garcia, M.K. Callahan, J. Yuan, V.R. Martins, J. Skog, R.N. Kaplan, M.S. Brady, J.D. Wolchok, P.B. Chapman, Y. Kang, J. Bromberg, D. Lyden, "Melanoma exosomes educate bone marrow progenitor cells toward a pro-metastatic phenotype through MET," *Nat. Med.* (2012). https://doi.org/10.1038/nm.2753.

[92] P.D. Robbins, A.E. Morelli, "Regulation of immune responses by

extracellular vesicles," *Nat. Rev. Immunol.* (2014). https://doi.org/10.1038/nri3622.

[93] K.S. Yang, H. Im, S. Hong, I. Pergolini, A.F. Del Castillo, R. Wang, S. Clardy, C.H. Huang, C. Pille, S. Ferrone, R. Yang, C.M. Castro, H. Lee, C.F. Del Castillo, R. Weissleder, "Multiparametric plasma EV profiling facilitates diagnosis of pancreatic malignancy," *Sci. Transl. Med.* (2017). https://doi.org/10.1126/scitranslmed.aal3226.

[94] H. Shao, J. Chung, L. Balaj, A. Charest, D.D. Bigner, B.S. Carter, F.H. Hochberg, X.O. Breakefield, R. Weissleder, H. Lee, "Protein typing of circulating microvesicles allows real-time monitoring of glioblastoma therapy," *Nat. Med.* (2012). https://doi.org/10.1038/nm.2994.

[95] S. El Andaloussi, I. Mäger, X.O. Breakefield, M.J.A. Wood, "Extracellular vesicles: Biology and emerging therapeutic opportunities," *Nat. Rev. Drug Discov.* (2013). https://doi.org/10.1038/nrd3978.

[96] V. Sokolova, A.K. Ludwig, S. Hornung, O. Rotan, P.A. Horn, M. Epple, B. Giebel, "Characterisation of exosomes derived from human cells by nanoparticle tracking analysis and scanning electron microscopy," *Colloids Surfaces B Biointerfaces*. (2011). https://doi.org/10.1016/j.colsurfb.2011.05.013.

[97] E. van der Pol, F.A.W. Coumans, A.E. Grootemaat, C. Gardiner, I.L. Sargent, P. Harrison, A. Sturk, T.G. van Leeuwen, R. Nieuwland, "Particle size distribution of exosomes and microvesicles determined by

transmission electron microscopy, flow cytometry, nanoparticle tracking analysis, and resistive pulse sensing," *J. Thromb. Haemost.* (2014). https://doi.org/10.1111/jth.12602.

[98] A. Clayton, J. Court, H. Navabi, M. Adams, M.D. Mason, J.A. Hobot, G.R. Newman, B. Jasani, "Analysis of antigen presenting cell derived exosomes, based on immuno-magnetic isolation and flow cytometry," *J. Immunol. Methods*. (2001). https://doi.org/10.1016/S0022-1759(00)00321-5.

[99] J.C. Contreras-Naranjo, H.J. Wu, V.M. Ugaz, "Microfluidics for exosome isolation and analysis: Enabling liquid biopsy for personalized medicine," *Lab Chip*. (2017). https://doi.org/10.1039/c7lc00592j.

[100] J.M. Street, P.E. Barran, C.L. Mackay, S. Weidt, C. Balmforth, T.S. Walsh, R.T.A. Chalmers, D.J. Webb, J.W. Dear, "Identification and proteomic profiling of exosomes in human cerebrospinal fluid," *J. Transl. Med.* (2012). https://doi.org/10.1186/1479-5876-10-5.

[101] C.J. Aslakson, F.R. Miller, "Selective Events in the Metastatic Process Defined by Analysis of the Sequential Dissemination of Subpopulations of a Mouse Mammary Tumor," *Cancer Res.* (1992).

[102] X. An, V.G. Sendra, I. Liadi, B. Ramesh, G. Romain, C. Haymaker, M. Martinez-Paniagua, Y. Lu, L.G. Radvanyi, B. Roysam, N. Varadarajan, "Single-cell profiling of dynamic cytokine secretion and the phenotype of immune cells," *PLoS One*. (2017). https://doi.org/10.1371/journal.pone.0181904.

[103] T. Gebäck, M.M.P. Schulz, P. Koumoutsakos, M. Detmar, “TScratch: A novel and simple software tool for automated analysis of monolayer wound healing assays,” *Biotechniques*. (2009). https://doi.org/10.2144/000113083.

[104] T. Stuart, A. Butler, P. Hoffman, C. Hafemeister, E. Papalexi, W.M. Mauck, Y. Hao, M. Stoeckius, P. Smibert, R. Satija, “Comprehensive Integration of Single-Cell Data,” *Cell*. (2019). https://doi.org/10.1016/j.cell.2019.05.031.

[105] S. Durinck, Y. Moreau, A. Kasprzyk, S. Davis, B. De Moor, A. Brazma, W. Huber, “BioMart and Bioconductor: A powerful link between biological databases and microarray data analysis,” *Bioinformatics*. (2005). https://doi.org/10.1093/bioinformatics/bti525.

[106] S. Durinck, P.T. Spellman, E. Birney, W. Huber, “Mapping identifiers for the integration of genomic datasets with the R/ Bioconductor package biomaRt,” *Nat. Protoc.* (2009). https://doi.org/10.1038/nprot.2009.97.

[107] A. Subramanian, P. Tamayo, V.K. Mootha, S. Mukherjee, B.L. Ebert, M.A. Gillette, A. Paulovich, S.L. Pomeroy, T.R. Golub, E.S. Lander, J.P. Mesirov, “Gene set enrichment analysis: A knowledge-based approach for interpreting genome-wide expression profiles,” *Proc. Natl. Acad. Sci. U. S. A.* (2005). https://doi.org/10.1073/pnas.0506580102.

[108] V.K. Mootha, C.M. Lindgren, K.F. Eriksson, A. Subramanian, S. Sihag, J. Lehar, P. Puigserver, E. Carlsson, M. Ridderstråle, E. Laurila, N. Houstis, M.J. Daly, N. Patterson, J.P. Mesirov, T.R. Golub, P. Tamayo, B. Spiegelman, E.S. Lander, J.N. Hirschhorn, D. Altshuler, L.C. Groop, “PGC-

1α-responsive genes involved in oxidative phosphorylation are coordinately downregulated in human diabetes," *Nat. Genet.* (2003). https://doi.org/10.1038/ng1180.

[109] I.S. Kim, Y. Gao, T. Welte, H. Wang, J. Liu, M. Janghorban, K. Sheng, Y. Niu, A. Goldstein, N. Zhao, I. Bado, H.C. Lo, M.J. Toneff, T. Nguyen, W. Bu, W. Jiang, J. Arnold, F. Gu, J. He, D. Jebakumar, K. Walker, Y. Li, Q. Mo, T.F. Westbrook, C. Zong, A. Rao, A. Sreekumar, J.M. Rosen, X.H.F. Zhang, "Immuno-subtyping of breast cancer reveals distinct myeloid cell profiles and immunotherapy resistance mechanisms," *Nat. Cell Biol.* (2019). https://doi.org/10.1038/s41556-019-0373-7.

[110] M.I. Love, W. Huber, S. Anders, "Moderated estimation of fold change and dispersion for RNA-seq data with DESeq2," *Genome Biol.* (2014). https://doi.org/10.1186/s13059-014-0550-8.

[111] M.S. Rooney, S.A. Shukla, C.J. Wu, G. Getz, N. Hacohen, "Molecular and genetic properties of tumors associated with local immune cytolytic activity," *Cell*. (2015). https://doi.org/10.1016/j.cell.2014.12.033.

[112] A.M. Newman, C.L. Liu, M.R. Green, A.J. Gentles, W. Feng, Y. Xu, C.D. Hoang, M. Diehn, A.A. Alizadeh, "Robust enumeration of cell subsets from tissue expression profiles," *Nat. Methods*. (2015). https://doi.org/10.1038/nmeth.3337.

[113] S. Hänzelmann, R. Castelo, J. Guinney, "GSVA: Gene set variation analysis for microarray and RNA-Seq data," *BMC Bioinformatics*. (2013).

https://doi.org/10.1186/1471-2105-14-7.

[114] G. Bindea, B. Mlecnik, M. Tosolini, A. Kirilovsky, M. Waldner, A.C. Obenauf, H. Angell, T. Fredriksen, L. Lafontaine, A. Berger, P. Bruneval, W.H. Fridman, C. Becker, F. Pagès, M.R. Speicher, Z. Trajanoski, J.Ô. Galon, “Spatiotemporal dynamics of intratumoral immune cells reveal the immune landscape in human cancer,” *Immunity*. (2013). https://doi.org/10.1016/j.immuni.2013.10.003.

[115] J. Kowal, G. Arras, M. Colombo, M. Jouve, J.P. Morath, B. Primdal-Bengtson, F. Dingli, D. Loew, M. Tkach, C. Théry, “Proteomic comparison defines novel markers to characterize heterogeneous populations of extracellular vesicle subtypes,” *Proc. Natl. Acad. Sci. U. S. A.* (2016). https://doi.org/10.1073/pnas.1521230113.

[116] N.A. Garcia, J. Moncayo-Arlandi, P. Sepulveda, A. Diez-Juan, “Cardiomyocyte exosomes regulate glycolytic flux in endothelium by direct transfer of GLUT transporters and glycolytic enzymes,” *Cardiovasc. Res.* (2016). https://doi.org/10.1093/cvr/cvv260.

[117] W. Gao, H. Liu, J. Yuan, C. Wu, D. Huang, Y. Ma, J. Zhu, L. Ma, J. Guo, H. Shi, Y. Zou, J. Ge, “Exosomes derived from mature dendritic cells increase endothelial inflammation and atherosclerosis via membrane TNF-α mediated NF-κB pathway,” *J. Cell. Mol. Med.* (2016). https://doi.org/10.1111/jcmm.12923.

[118] F.J. Verweij, M.A.J. Van Eijndhoven, J. Middeldorp, D.M. Pegtel, “Analysis

of viral microRNA exchange via exosomes in vitro and in vivo," *Methods Mol. Biol.* (2013). https://doi.org/10.1007/978-1-62703-453-1_5.

[119] N.P. Hessvik, A. Llorente, "Current knowledge on exosome biogenesis and release," *Cell. Mol. Life Sci.* (2018). https://doi.org/10.1007/s00018-017-2595-9.

[120] K. Tamai, N. Tanaka, T. Nakano, E. Kakazu, Y. Kondo, J. Inoue, M. Shiina, K. Fukushima, T. Hoshino, K. Sano, Y. Ueno, T. Shimosegawa, K. Sugamura, "Exosome secretion of dendritic cells is regulated by Hrs, an ESCRT-0 protein," *Biochem. Biophys. Res. Commun.* (2010). https://doi.org/10.1016/j.bbrc.2010.07.083.

[121] M. Colombo, C. Moita, G. Van Niel, J. Kowal, J. Vigneron, P. Benaroch, N. Manel, L.F. Moita, C. Théry, G. Raposo, "Analysis of ESCRT functions in exosome biogenesis, composition and secretion highlights the heterogeneity of extracellular vesicles," *J. Cell Sci.* (2013). https://doi.org/10.1242/jcs.128868.

[122] N. Jaé, D.G. McEwan, Y. Manavski, R.A. Boon, S. Dimmeler, "Rab7a and Rab27b control secretion of endothelial microRNA through extracellular vesicles," *FEBS Lett.* (2015). https://doi.org/10.1016/j.febslet.2015.08.040.

[123] A. Bobrie, S. Krumeich, F. Reyal, C. Recchi, L.F. Moita, M.C. Seabra, M. Ostrowski, C. Théry, "Rab27a supports exosome-dependent and -independent mechanisms that modify the tumor microenvironment and can promote tumor progression," *Cancer Res.* (2012).

https://doi.org/10.1158/0008-5472.CAN-12-0925.

[124] A. Chairoungdua, D.L. Smith, P. Pochard, M. Hull, M.J. Caplan, “Exosome release of β-catenin: A novel mechanism that antagonizes Wnt signaling,” *J. Cell Biol.* (2010). https://doi.org/10.1083/jcb.201002049.

[125] R.J. Loomis, D.A. Holmes, A. Elms, P.A. Solski, C.J. Der, L. Su, “Citron kinase, a RhoA effector, enhances HIV-1 virion production by modulating exocytosis,” *Traffic*. (2006). https://doi.org/10.1111/j.1600-0854.2006.00503.x.

[126] S. Sinha, D. Hoshino, N.H. Hong, K.C. Kirkbride, N.E. Grega-Larson, M. Seiki, M.J. Tyska, A.M. Weaver, “Cortactin promotes exosome secretion by controlling branched actin dynamics,” *J. Cell Biol.* (2016). https://doi.org/10.1083/jcb.201601025.

[127] S.N. Hurwitz, M.M. Conlon, M.A. Rider, N.C. Brownstein, D.G. Meckes, “Nanoparticle analysis sheds budding insights into genetic drivers of extracellular vesicle biogenesis,” *J. Extracell. Vesicles*. (2016). https://doi.org/10.3402/jev.v5.31295.

[128] S.N. Hurwitz, D. Nkosi, M.M. Conlon, S.B. York, X. Liu, D.C. Tremblay, D.G. Meckes, “CD63 Regulates Epstein-Barr Virus LMP1 Exosomal Packaging, Enhancement of Vesicle Production, and Noncanonical NF-κB Signaling,” *J. Virol.* (2017). https://doi.org/10.1128/jvi.02251-16.

[129] R. Alonso, C. Mazzeo, M.C. Rodriguez, M. Marsh, A. Fraile-Ramos, V. Calvo, A. Avila-Flores, I. Merida, M. Izquierdo, “Diacylglycerol kinase α

regulates the formation and polarisation of mature multivesicular bodies involved in the secretion of Fas ligand-containing exosomes in T lymphocytes," *Cell Death Differ.* (2011). https://doi.org/10.1038/cdd.2010.184.

[130] I. Nazarenko, S. Rana, A. Baumann, J. McAlear, A. Hellwig, M. Trendelenburg, G. Lochnit, K.T. Preissner, M. Zöller, "Cell surface tetraspanin Tspan8 contributes to molecular pathways of exosome-induced endothelial cell activation," *Cancer Res.* (2010). https://doi.org/10.1158/0008-5472.CAN-09-2470.

[131] K. Laulagnier, D. Grand, A. Dujardin, S. Hamdi, H. Vincent-Schneider, D. Lankar, J.P. Salles, C. Bonnerot, B. Perret, M. Record, "PLD2 is enriched on exosomes and its activity is correlated to the release of exosomes," *FEBS Lett.* (2004). https://doi.org/10.1016/j.febslet.2004.06.082.

[132] C.M. Fader, D.G. Sánchez, M.B. Mestre, M.I. Colombo, "TI-VAMP/VAMP7 and VAMP3/cellubrevin: two v-SNARE proteins involved in specific steps of the autophagy/multivesicular body pathways," *Biochim. Biophys. Acta - Mol. Cell Res.* (2009). https://doi.org/10.1016/j.bbamcr.2009.09.011.

[133] Y. Fu, L. Zhang, F. Zhang, T. Tang, Q. Zhou, C. Feng, Y. Jin, Z. Wu, "Exosome-mediated miR-146a transfer suppresses type I interferon response and facilitates EV71 infection," *PLoS Pathog.* (2017). https://doi.org/10.1371/journal.ppat.1006611.

[134] M. Ruiz-Martinez, A. Navarro, R.M. Marrades, N. Viñolas, S.

Santasusagna, C. Muñoz, J. Ramírez, L. Molins, M. Monzo, “YKT6 expression, exosome release, and survival in non-small cell lung cancer,” *Oncotarget*. (2016). https://doi.org/10.18632/oncotarget.9862.

[135] L. Murrow, R. Malhotra, J. Debnath, “ATG12-ATG3 interacts with Alix to promote basal autophagic flux and late endosome function,” *Nat. Cell Biol.* (2015). https://doi.org/10.1038/ncb3112.

[136] K. Koles, J. Nunnari, C. Korkut, R. Barria, C. Brewer, Y. Li, J. Leszyk, B. Zhang, V. Budnik, “Mechanism of evenness interrupted (Evi)-exosome release at synaptic boutons,” *J. Biol. Chem.* (2012). https://doi.org/10.1074/jbc.M112.342667.

[137] N.P. Hessvik, A. Øverbye, A. Brech, M.L. Torgersen, I.S. Jakobsen, K. Sandvig, A. Llorente, “PIKfyve inhibition increases exosome release and induces secretory autophagy,” *Cell. Mol. Life Sci.* (2016). https://doi.org/10.1007/s00018-016-2309-8.

[138] Y. Lou, O. Preobrazhenska, U. Auf Dem Keller, M. Sutcliffe, L. Barclay, P.C. McDonald, C. Roskelley, C.M. Overall, S. Dedhar, “Epithelial-Mesenchymal Transition (EMT) is not sufficient for spontaneous murine breast cancer metastasis,” *Dev. Dyn.* (2008). https://doi.org/10.1002/dvdy.21658.

[139] I. Wortzel, S. Dror, C.M. Kenific, D. Lyden, “Exosome-Mediated Metastasis: Communication from a Distance,” *Dev. Cell*. (2019). https://doi.org/10.1016/j.devcel.2019.04.011.

[140] R. Kalluri, “The biology and function of exosomes in cancer,” *J. Clin. Invest.* (2016). https://doi.org/10.1172/JCI81135.

[141] J. Wang, X. Guan, Y. Zhang, S. Ge, L. Zhang, H. Li, X. Wang, R. Liu, T. Ning, T. Deng, H. Zhang, X. Jiang, Y. Ba, D. Huang, “Exosomal miR-27a derived from gastric cancer cells regulates the transformation of fibroblasts into cancer-associated fibroblasts,” *Cell. Physiol. Biochem.* (2018). https://doi.org/10.1159/000493218.

[142] K. Lee, K. Fraser, B. Ghaddar, K. Yang, E. Kim, L. Balaj, E.A. Chiocca, X.O. Breakefield, H. Lee, R. Weissleder, “Multiplexed Profiling of Single Extracellular Vesicles,” *ACS Nano*. (2018). https://doi.org/10.1021/acsnano.7b07060.

[143] S.W. Wen, J. Sceneay, L.G. Lima, C.S.F. Wong, M. Becker, S. Krumeich, R.J. Lobb, V. Castillo, K.N. Wong, S. Ellis, B.S. Parker, A. Möller, “The biodistribution and immune suppressive effects of breast cancer-derived exosomes,” *Cancer Res.* (2016). https://doi.org/10.1158/0008-5472.CAN-16-0868.

[144] S. Ham, L.G. Lima, E.P.Z. Chai, A. Muller, R.J. Lobb, S. Krumeich, S.W. Wen, A.P. Wiegmans, A. Möller, “Breast cancer-derived exosomes alter macrophage polarization via gp130/STAT3 signaling,” *Front. Immunol.* (2018). https://doi.org/10.3389/fimmu.2018.00871.

[145] C. Kahlert, R. Kalluri, “Exosomes in tumor microenvironment influence cancer progression and metastasis,” *J. Mol. Med.* (2013).

https://doi.org/10.1007/s00109-013-1020-6.

[146] C. Théry, L. Zitvogel, S. Amigorena, “Exosomes: Composition, biogenesis and function,” *Nat. Rev. Immunol.* (2002). https://doi.org/10.1038/nri855.

[147] H. Valadi, K. Ekström, A. Bossios, M. Sjöstrand, J.J. Lee, J.O. Lötvall, “Exosome-mediated transfer of mRNAs and microRNAs is a novel mechanism of genetic exchange between cells,” *Nat. Cell Biol.* (2007). https://doi.org/10.1038/ncb1596.

[148] L. Balaj, R. Lessard, L. Dai, Y.J. Cho, S.L. Pomeroy, X.O. Breakefield, J. Skog, “Tumour microvesicles contain retrotransposon elements and amplified oncogene sequences,” *Nat. Commun.* (2011). https://doi.org/10.1038/ncomms1180.

[149] I. Salido-Guadarrama, S. Romero-Cordoba, O. Peralta-Zaragoza, A. Hidalgo-Miranda, M. Rodríguez-Dorantes, “MicroRNAs transported by exosomes in body fluids as mediators of intercellular communication in cancer,” *Onco. Targets. Ther.* (2014). https://doi.org/10.2147/OTT.S61562.

[150] H.G. Zhang, W.E. Grizzle, “Exosomes: A novel pathway of local and distant intercellular communication that facilitates the growth and metastasis of neoplastic lesions,” *Am. J. Pathol.* (2014). https://doi.org/10.1016/j.ajpath.2013.09.027.

[151] S. Gesierich, I. Berezovskiy, E. Ryschich, M. Zöller, “Systemic induction of the angiogenesis switch by the tetraspanin D6.1A/CO-029,” *Cancer Res.* (2006). https://doi.org/10.1158/0008-5472.CAN-06-0391.

[152] K.J. Svensson, P. Kucharzewska, H.C. Christianson, S. Sköld, T. Löfstedt, M.C. Johansson, M. Mörgelin, J. Bengzon, W. Ruf, M. Belting, “Hypoxia triggers a proangiogenic pathway involving cancer cell microvesicles and PAR-2-mediated heparin-binding EGF signaling in endothelial cells,” *Proc. Natl. Acad. Sci. U. S. A.* (2011). https://doi.org/10.1073/pnas.1104261108.

[153] R. Gastpar, M. Gehrmann, M.A. Bausero, A. Asea, C. Gross, J.A. Schroeder, G. Multhoff, “Heat shock protein 70 surface-positive tumor exosomes stimulate migratory and cytolytic activity of natural killer cells,” *Cancer Res.* (2005). https://doi.org/10.1158/0008-5472.CAN-04-3804.

[154] V.L. Vega, M. Rodríguez-Silva, T. Frey, M. Gehrmann, J.C. Diaz, C. Steinem, G. Multhoff, N. Arispe, A. De Maio, “Hsp70 Translocates into the Plasma Membrane after Stress and Is Released into the Extracellular Environment in a Membrane-Associated Form that Activates Macrophages,” *J. Immunol.* (2008). https://doi.org/10.4049/jimmunol.180.6.4299.

[155] J. ah Cho, Y.S. Lee, S.H. Kim, J.K. Ko, C.W. Kim, “MHC independent anti-tumor immune responses induced by Hsp70-enriched exosomes generate tumor regression in murine models,” *Cancer Lett.* (2009). https://doi.org/10.1016/j.canlet.2008.10.021.

[156] A. Campos, C. Salomon, R. Bustos, J. Díaz, S. Martínez, V. Silva, C. Reyes, N. Díaz-Valdivia, M. Varas-Godoy, L. Lobos-González, A.F. Quest, “Caveolin-1-containing extracellular vesicles transport adhesion proteins

and promote malignancy in breast cancer cell lines," *Nanomedicine*. (2018). https://doi.org/10.2217/nnm-2018-0094.

[157] D.J. Katzmann, M. Babst, S.D. Emr, "Ubiquitin-dependent sorting into the multivesicular body pathway requires the function of a conserved endosomal protein sorting complex, ESCRT-I," *Cell*. (2001). https://doi.org/10.1016/S0092-8674(01)00434-2.

[158] W.M. Henne, H. Stenmark, S.D. Emr, "Molecular mechanisms of the membrane sculpting ESCRT pathway," *Cold Spring Harb. Perspect. Biol.* (2013). https://doi.org/10.1101/cshperspect.a016766.

[159] G. van Niel, S. Charrin, S. Simoes, M. Romao, L. Rochin, P. Saftig, M.S. Marks, E. Rubinstein, G. Raposo, "The Tetraspanin CD63 Regulates ESCRT-Independent and -Dependent Endosomal Sorting during Melanogenesis," *Dev. Cell*. (2011). https://doi.org/10.1016/j.devcel.2011.08.019.

[160] K. Zylbersztejn, T. Galli, "Vesicular traffic in cell navigation," *FEBS J.* (2011). https://doi.org/10.1111/j.1742-4658.2011.08168.x.

[161] B.Y. Chen, C.W.H. Sung, C. Chen, C.M. Cheng, D.P.C. Lin, C. Te Huang, M.Y. Hsu, "Advances in exosomes technology," *Clin. Chim. Acta*. (2019). https://doi.org/10.1016/j.cca.2019.02.021.

[162] T. Baslan, J. Hicks, "Unravelling biology and shifting paradigms in cancer with single-cell sequencing," *Nat. Rev. Cancer*. (2017). https://doi.org/10.1038/nrc.2017.58.

[163] W. Chung, H.H. Eum, H.O. Lee, K.M. Lee, H.B. Lee, K.T. Kim, H.S. Ryu, S. Kim, J.E. Lee, Y.H. Park, Z. Kan, W. Han, W.Y. Park, “Single-cell RNA-seq enables comprehensive tumour and immune cell profiling in primary breast cancer,” *Nat. Commun.* (2017). https://doi.org/10.1038/ncomms15081.

[164] S.S. Yang, S. Ma, H. Dou, F. Liu, S.Y. Zhang, C. Jiang, M. Xiao, Y.X. Huang, “Breast cancer-derived exosomes regulate cell invasion and metastasis in breast cancer via miR-146a to activate cancer associated fibroblasts in tumor microenvironment,” *Exp. Cell Res.* (2020). https://doi.org/10.1016/j.yexcr.2020.111983.

[165] R. Suzuki, H. Shimodaira, “Pvclust: An R package for assessing the uncertainty in hierarchical clustering,” *Bioinformatics*. (2006). https://doi.org/10.1093/bioinformatics/btl117.

[166] G. Csardi, T. Nepusz, “The igraph software package for complex network research,” *InterJournal Complex Syst.* (2006).

[167] S. Keerthikumar, D. Chisanga, D. Ariyaratne, H. Al Saffar, S. Anand, K. Zhao, M. Samuel, M. Pathan, M. Jois, N. Chilamkurti, L. Gangoda, S. Mathivanan, “ExoCarta: A Web-Based Compendium of Exosomal Cargo,” *J. Mol. Biol.* (2016). https://doi.org/10.1016/j.jmb.2015.09.019.

[168] S. Mathivanan, C.J. Fahner, G.E. Reid, R.J. Simpson, “ExoCarta 2012: Database of exosomal proteins, RNA and lipids,” *Nucleic Acids Res.* (2012). https://doi.org/10.1093/nar/gkr828.

[169] S. Mathivanan, R.J. Simpson, “ExoCarta: A compendium of exosomal proteins and RNA,” *Proteomics*. (2009). https://doi.org/10.1002/pmic.200900351.

[170] X. Lu, Y. Kang, “Chemokine (C-C Motif) ligand 2 engages CCR2+ stromal cells of monocytic origin to promote breast cancer metastasis to lung and bone,” *J. Biol. Chem.* (2009). https://doi.org/10.1074/jbc.M109.035899.

[171] X. Jiao, S.D. Hooper, T. Djureinovic, C. Larsson, F. Wärnberg, C. Tellgren-Roth, J. Botling, T. Sjöblom, “Gene rearrangements in hormone receptor negative breast cancers revealed by mate pair sequencing,” *BMC Genomics*. (2013). https://doi.org/10.1186/1471-2164-14-165.

[172] D. Tang, X. Zhao, L. Zhang, Z. Wang, C. Wang, “Identification of hub genes to regulate breast cancer metastasis to brain by bioinformatics analyses,” *J. Cell. Biochem.* (2019). https://doi.org/10.1002/jcb.28228.

[173] L. Dong, Z. Li, L. Xue, G. Li, C. Zhang, Z. Cai, H. Li, R. Guo, “DIAPH3 promoted the growth, migration and metastasis of hepatocellular carcinoma cells by activating beta-catenin/TCF signaling,” *Mol. Cell. Biochem.* (2018). https://doi.org/10.1007/s11010-017-3125-7.

[174] X. Dai, H. Cheng, Z. Bai, J. Li, “Breast cancer cell line classification and Its relevance with breast tumor subtyping,” *J. Cancer*. (2017). https://doi.org/10.7150/jca.18457.

[175] A.M. Marleau, C.S. Chen, J.A. Joyce, R.H. Tullis, “Exosome removal as a therapeutic adjuvant in cancer,” *J. Transl. Med.* (2012).

https://doi.org/10.1186/1479-5876-10-134.

[176] S.I. Ohno, M. Takanashi, K. Sudo, S. Ueda, A. Ishikawa, N. Matsuyama, K. Fujita, T. Mizutani, T. Ohgi, T. Ochiya, N. Gotoh, M. Kuroda, “Systemically injected exosomes targeted to EGFR deliver antitumor microrna to breast cancer cells,” *Mol. Ther.* (2013). https://doi.org/10.1038/mt.2012.180.

[177] A. Campos, R. Burgos-Ravanal, M.F. González, R. Huilcaman, L.L. González, A.F.G. Quest, “Cell intrinsic and extrinsic mechanisms of caveolin-1-enhanced metastasis,” *Biomolecules*. (2019). https://doi.org/10.3390/biom9080314.

[178] H. Ageta, N. Ageta-Ishihara, K. Hitachi, O. Karayel, T. Onouchi, H. Yamaguchi, T. Kahyo, K. Hatanaka, K. Ikegami, Y. Yoshioka, K. Nakamura, N. Kosaka, M. Nakatani, A. Uezumi, T. Ide, Y. Tsutsumi, H. Sugimura, M. Kinoshita, T. Ochiya, M. Mann, M. Setou, K. Tsuchida, “UBL3 modification influences protein sorting to small extracellular vesicles,” *Nat. Commun.* (2018). https://doi.org/10.1038/s41467-018-06197-y.

[179] P. Jenjaroenpun, Y. Kremenska, V.M. Nair, M. Kremenskoy, B. Joseph, I. V. Kurochkin, “Characterization of RNA in exosomes secreted by human breast cancer cell lines using next-generation sequencing,” *PeerJ*. (2013). https://doi.org/10.7717/peerj.201.

[180] K. Kalishwaralal, W.Y. Kwon, K.S. Park, “Exosomes for Non-Invasive Cancer Monitoring,” *Biotechnol. J.* (2019).

https://doi.org/10.1002/biot.201800430.

[181] K. Tiedemann, G. Sadvakassova, N. Mikolajewicz, M. Juhas, Z. Sabirova, S. Tabariès, J. Gettemans, P.M. Siegel, S. V. Komarova, “Exosomal Release of L-Plastin by Breast Cancer Cells Facilitates Metastatic Bone Osteolysis,” *Transl. Oncol.* (2019). https://doi.org/10.1016/j.tranon.2018.11.014.

[182] J.A. Dubovsky, D.L. Chappell, B.K. Harrington, K. Agrawal, L.A. Andritsos, J.M. Flynn, J.A. Jones, M.E. Paulaitis, B. Bolon, A.J. Johnson, J.C. Byrd, N. Muthusamy, “Lymphocyte cytosolic protein 1 is a chronic lymphocytic leukemia membrane-associated antigen critical to niche homing,” *Blood*. (2013). https://doi.org/10.1182/blood-2013-05-504597.

[183] T.G. Santos, V.R. Martins, G.N.M. Hajj, “Unconventional secretion of heat shock proteins in cancer,” *Int. J. Mol. Sci.* (2017). https://doi.org/10.3390/ijms18050946.

[184] J. McCready, J.D. Sims, D. Chan, D.G. Jay, “Secretion of extracellular hsp90α via exosomes increases cancer cell motility: A role for plasminogen activation,” *BMC Cancer*. (2010). https://doi.org/10.1186/1471-2407-10-294.

[185] A. Hoshino, H.S. Kim, L. Bojmar, K.E. Gyan, M. Cioffi, J. Hernandez, C.P. Zambirinis, G. Rodrigues, H. Molina, S. Heissel, M.T. Mark, L. Steiner, A. Benito-Martin, S. Lucotti, A. Di Giannatale, K. Offer, M. Nakajima, C. Williams, L. Nogués, F.A. Pelissier Vatter, A. Hashimoto, A.E. Davies, D.

Freitas, C.M. Kenific, Y. Ararso, W. Buehring, P. Lauritzen, Y. Ogitani, K. Sugiura, N. Takahashi, M. Alečković, K.A. Bailey, J.S. Jolissant, H. Wang, A. Harris, L.M. Schaeffer, G. García-Santos, Z. Posner, V.P. Balachandran, Y. Khakoo, G.P. Raju, A. Scherz, I. Sagi, R. Scherz-Shouval, Y. Yarden, M. Oren, M. Malladi, M. Petriccione, K.C. De Braganca, M. Donzelli, C. Fischer, S. Vitolano, G.P. Wright, L. Ganshaw, M. Marrano, A. Ahmed, J. DeStefano, E. Danzer, M.H.A. Roehrl, N.J. Lacayo, T.C. Vincent, M.R. Weiser, M.S. Brady, P.A. Meyers, L.H. Wexler, S.R. Ambati, A.J. Chou, E.K. Slotkin, S. Modak, S.S. Roberts, E.M. Basu, D. Diolaiti, B.A. Krantz, F. Cardoso, A.L. Simpson, M. Berger, C.M. Rudin, D.M. Simeone, M. Jain, C.M. Ghajar, S.K. Batra, B.Z. Stanger, J. Bui, K.A. Brown, V.K. Rajasekhar, J.H. Healey, M. de Sousa, K. Kramer, S. Sheth, J. Baisch, V. Pascual, T.E. Heaton, M.P. La Quaglia, D.J. Pisapia, R. Schwartz, H. Zhang, Y. Liu, A. Shukla, L. Blavier, Y.A. DeClerck, M. LaBarge, M.J. Bissell, T.C. Caffrey, P.M. Grandgenett, M.A. Hollingsworth, J. Bromberg, B. Costa-Silva, H. Peinado, Y. Kang, B.A. Garcia, E.M. O'Reilly, D. Kelsen, T.M. Trippett, D.R. Jones, I.R. Matei, W.R. Jarnagin, D. Lyden, "Extracellular Vesicle and Particle Biomarkers Define Multiple Human Cancers," *Cell*. (2020). https://doi.org/10.1016/j.cell.2020.07.009.

[186] I. Lazar, E. Clement, M. Ducoux-Petit, L. Denat, V. Soldan, S. Dauvillier, S. Balor, O. Burlet-Schiltz, L. Larue, C. Muller, L. Nieto, "Proteome characterization of melanoma exosomes reveals a specific signature for metastatic cell lines," *Pigment Cell Melanoma Res.* (2015).

https://doi.org/10.1111/pcmr.12380.

[187] B. Liang, P. Peng, S. Chen, L. Li, M. Zhang, D. Cao, J. Yang, H. Li, T. Gui, X. Li, K. Shen, “Characterization and proteomic analysis of ovarian cancer-derived exosomes,” *J. Proteomics*. (2013). https://doi.org/10.1016/j.jprot.2012.12.029.

[188] R. Xu, D.W. Greening, A. Rai, H. Ji, R.J. Simpson, “Highly-purified exosomes and shed microvesicles isolated from the human colon cancer cell line LIM1863 by sequential centrifugal ultrafiltration are biochemically and functionally distinct,” *Methods*. (2015). https://doi.org/10.1016/j.ymeth.2015.04.008.

[189] M. He, H. Qin, T.C.W. Poon, S.C. Sze, X. Ding, N.N. Co, S.M. Ngai, T.F. Chan, N. Wong, “Hepatocellular carcinoma-derived exosomes promote motility of immortalized hepatocyte through transfer of oncogenic proteins and RNAs,” *Carcinogenesis*. (2015). https://doi.org/10.1093/carcin/bgv081.

[190] L.G. Fulford, J.S. Reis-Filho, K. Ryder, C. Jones, C.E. Gillett, A. Hanby, D. Easton, S.R. Lakhani, “Basal-like grade III invasive ductal carcinoma of the breast: Patterns of metastasis and long-term survival,” *Breast Cancer Res.* (2007). https://doi.org/10.1186/bcr1636.